PREDICTION OF PLASTIC DEFORMATION IN ALUMINUM SOFTBALL BATS USING FINITE ELEMENT ANALYSIS

By

ERIC DAVID BIESEN

A thesis submitted in partial fulfillment of
the requirements for the degree of

MASTER OF SCIENCE IN MECHANICAL ENGINEERING

WASHINGTON STATE UNIVERSITY
Department of Mechanical and Materials Engineering

AUGUST 2006

To the Faculty of Washington State University:

The members of the Committee appointed to examine the thesis of Eric David Biesen find it satisfactory and recommend that it be accepted.

_____
Chair

_____

_____

ACKNOWLEGEMENTS

First and foremost, I would like to thank my family for the continuous emotional and financial support. Without them, getting this far would not have been as easy as it has been. By example, my family members have shown me that hard work does pay off and those that strive for something better will eventually achieve it. I would like to give particular thanks to my parents, Chris and Carla, for instilling in me at a young age a strong sense of responsibility. This has been an important part of my success, both during my education and my working career.

Secondly, I would like to thank Dr. Lloyd Smith for allowing me to research under his supervision at the Sports Science Laboratory at Washington State University. This has to be one of the most unique research opportunities one could take part in. I still look forward to the response I get from people who I describe the lab to and the work we perform. I hope to see it thrive for many more years to come.

Louisville Slugger has graciously provided me with the bats used for the experimental testing and any relevant information I needed, and for that I am truly grateful. Particularly John Suchy, who took time out of his busy day many times to answer any and all questions I may have concerning the work I was performing. I hope this work will help with any future attempts at finite element modeling at Louisville Slugger.

I would also like to thank my friends and teammates I had over the two years I attended WSU. You know who you are. (And chances are most of you will never read this.) Constantly nagging me about the rules of the game and which bats were banned from ASA play kept me sharp and up to date on the latest happenings in the world of softball. To my roommates Dan and Drew, if my day at the Bat Lab consisted of staring at a computer screen, I could always count on you two to make me laugh…and then shake my head in disgust.

Last but not least, I would like to thank my coworkers. Matt, Terry, Amanda, Craig, Jeff, Greg, and Tom, I enjoyed working with you all. For those of you that will be continuing to work in the Bat Lab, I am confident that the quality of work will continue to be high. Regardless if you choose to use your experience to pursue a career in sports science, I wish you all the best of luck.

PREDICTION OF PLASTIC DEFORMATION IN ALUMINUM SOFTBALL BATS USING FINITE ELEMENT ANALYSIS

Abstract

by Eric David Biesen, M.S.
Washington State University
AUGUST 2006

Chair: Lloyd V. Smith

Since the introduction of the first aluminum bat, durability has been a great concern. Some work has been performed in the area of predicting bat performance, but little has been done in the way of quantifying their durability or longevity. The work performed here sets out to predict the durability of a single wall aluminum softball bat by modeling a bat-ball collision using finite element analysis and correlating the predicted bat deformation to that which was created experimentally using a high speed ball cannon.

Multiple numerical bat models were generated based on the same make and model of softball bat and the resulting model deformations were compared. Model variables such as the material hardening law, type of elements used, and inclusion of strain rate effects were explored.

A viscoelastic ball model was developed for use in the numerical bat-ball collision models. The performance of the ball model was tuned to experimental results and showed good correlation based on its dynamic stiffness and COR values at the desired impact speeds. Additionally, a low-speed impact study was performed with a bat instrumented with strain gages to further verify the ball tuning technique based on the strain response of the bat during impact.

High-speed bat-ball collision simulations were performed and the resulting deformations were compared to measured experimental values. The numerical model that generated the most

accurate results was within ±0.004 inches of the experimental deformations at the various relative impact speeds.

A simple strain rate model was used to take into account the high strain rates generated during impact. The inclusion of strain rate effects was shown to have a significant effect on the bat deformations produced in the finite element simulations.

TABLE OF CONTENTS

LIST OF TABLES

LIST OF FIGURES

CHAPTER ONE

- INTRODUCTION -

The first aluminum bats were introduced in the late 1960's. These bats immediately became popular among players because of the increased durability they offered over their predecessors, wood bats. Prior to any knowledge of what is now known as the trampoline effect, which is present in thin-walled hollow bats, the performance of the first aluminum bats were not near what they are today. (Ironically, the performance of the first aluminum bats was comparable to that of wood bats.) As more was discovered about how the performance of a hollow aluminum bat can be changed by using different alloys or wall thicknesses, the performance eventually went up. But the tradeoff to this increased performance was decreased durability. To counteract this problem, manufacturers began to introduce bats with stronger aluminum alloys, added strengthening alloys such as scandium, or used entirely different metals such as titanium. Due to the cost of the raw material, aluminum has become the choice material for metal bats. Titanium is still being used today, but not on the same scale as that of aluminum.

Currently, there are multiple measures of bat performance, but there is no minimum requirement on a bat's level or durability or lifespan. Durability, as well as performance, can be very subjective based on how fast the bat is swung, the hardness of the ball that is used, and the temperature of the environment. Typically, a bat is designed to withstand the wear and tear of a year's worth of use [1.1], but unless first hand knowledge is known about how the bat will hold up for a player of comparable skill and strength, there isn't any indication of how long the bat will go without denting for the person that is purchasing it. With that in mind, manufacturers typically offer one year (one time) warranties that allow for a full replacement if the bat dents excessively under normal use. Organizations such as the Amateur Softball Association (ASA)

have regulations [1.2] on barrel diameter and how out of round the bat can be if it has dented or started to dent. If an umpire thinks that a bat is too deformed to be considered safe or that it may provide some sort of advantage to the hitter, he or she could then test the diameter of the bat with a go/no-go gauge and have it removed from the field of play if it doesn't pass. So, potentially, a player could purchase a bat and have it dent the next day during a game and not be able to use it in competitive play again. This is a problem that all metal barreled bats face, and the gamble one takes when buying one.

As mentioned previously, performance and durability seem to be the complement of one another for single wall aluminum bats. When designing a bat for durability, to ensure the maximum lifespan all one can do is design it for the extremes, i.e. hardest ball, fastest pitch and swing speed, etc. For a company that has been making bats for a long time, this may be a simple task based on previous testing they have performed on bats of varying wall thickness and alloy. If this ability isn't available to the bat designer, then another method by which a bat could go through development is by the use of finite element analysis (FEA). With this method, the bat and ball are modeled using a computer and relevant information is input, such as material properties and velocities, and the computer performs calculations to describe the movement and interaction of the bat and ball. To perform such an analysis, the operator must have a reasonable amount of training and experience to achieve accurate results. If the designer is capable and the computer resources are available to him or her, then FEA can be a powerful tool to predict the performance and durability of a bat without ever having to produce a prototype.

In general, the goal of FEA is to model reality as completely and accurately as possible. Of the work performed in FEA for the bat-ball impact, much of it has been in area of characterizing the performance of a softball or baseball bat, but little has been done on the side of durability.

The work presented here aims to more completely model the bat-ball impact by including the ability to describe plastic deformation, or denting, in the bat. With the capacity for plasticity to occur in the model, not only will its effects on performance be shown, but the bat's level of durability can then be quantified.

Building on the work of previous researchers, the explicit finite element software package LS-DYNA was used to model the bat-ball impact of a single wall aluminum softball bat. Prior to any modeling of the bat, experimental characterization of the performance of a polyurethane core softball was performed at various speeds. Utilizing this experimental data, the ball was then modeled and the material properties adjusted to "tune" the ball to match the experimental values for that speed. A bat model was then developed based on an actual bat on the market today. Utilizing this model, a strain comparison was made for a low speed impact of a bat that was instrumented with strain gages at specific locations. Multiple elements and integration formulations were then used and their durability and performance effects were noted. Plasticity was included in the model of this bat using different hardening laws. Strain rate effects were also included with the use of a simple strain rate formulation model. The deformation and strain data calculated within the finite element model was then compared to experimental values taken from impact tests performed using an air cannon to fire the ball at the bat. Multiple impact speeds were used experimentally and modeled.

REFERENCES

1.1 Cruz, C.M. Rawlings Sporting Goods. *Private Communication*. January, 2006.

1.2 Official Rules of Softball Team Edition. 2005 Edition. Oklahoma City, OK: Amateur Softball Association of America, 2005.

CHAPTER TWO

- LITERATURE REVIEW -

2.1 General bat constructions and history

The evolution of bats used in either baseball or softball has a long storied past, but it can all be attributed to the introduction of the wood baseball bat. There are conflicting reports of who or when the first wood bat was manufactured, but the most common theory [2.1] is that John Andrew "Bud" Hillerich created the first white ash bat for Pete Browning in 1884. Though wood bats had been used prior to this event, this was the first time that it was noted that a bat was made with a specific player in mind. The demand for these bats eventually grew to the point that Bud Hillerich allocated a portion of his existing business to the production of bats. As the popularity of his bats increased in the following years, he eventually focused his attention to bats alone and developed the company which is now known as Hillerich & Bradsbury/Louisville Slugger.

As with any competitive sport, there is always the desire to have equipment that is higher performing and/or more durable than the competition's. So of course, it was only a matter of time before the wood bat became a thing of the past. The earliest known record of a metal bat, or plans for a metal bat, is from a US patent [2.2] issued to William Shroyer Jr. on June 24, 1924. Within this patent, Shroyer outlines the method of construction of the bat, the suggested material of either brass or steel, and even an integral weighting system in the barrel. Although no record could be found of any bats made by Shroyer, the intent and design was well ahead of its time. It wasn't until the late 1960s when aluminum single wall bats were being manufactured. Easton claims to have developed the first aluminum bat in 1969 [2.5] but Worth also claims to be the first to do the same in 1970 [2.3]. Regardless, as more and more people realized how much more durable aluminum bats were over wood, other manufactures began to produce them as well.

Within a decade other manufacturers such as Louisville Slugger began producing their own aluminum bats [2.4].

In 1993, Worth and Easton both introduced bats made of titanium [2.4, 2.3]. There wasn't anything particularly novel about these bats other than their material; they just offered lighter weight and higher performance. Because of this increased performance, certain softball organizations banned their use [2.3].

Also in the 1990's, companies started to experiment with composite materials such as graphite, carbon fiber, fiberglass, and Kevlar. Manufacturers realized the versatility of these orthotropic materials because of the flexibility they offered when making a bat. The designer had the ability to 'tune' the bat's performance, feel, and durability simply by changing the combination of materials used and/or the fiber angles between layers. The only drawback to this type of bat construction is that it is very labor intensive. The most common method for manufacturing a composite bat is by applying the layers of material to a mandrel and then curing the fiber/resin composite in an autoclave. Filament winding is another method of manufacturing bats, but is not used nearly as much as the mandrel lay-up method just mentioned. Because of the amount of work that goes into making a bat out of composite materials, it is common that today one would pay between $200 and $400 whereas one could expect to pay between $100 and $200 for a single wall aluminum bat.

Composite bats have become extremely popular in the last decade. A majority of the high performing bats on the market today are of composite construction. Companies such as Louisville Slugger, Easton, Miken, Mizuno, and Rawlings have developed their own lines of composite bats that are easily recognizable to those that play baseball or softball.

One of the most significant developments in the bat industry was the invention of the multi-wall bat. In1993, DeMarini developed the first double-wall aluminum bat [2.6]. This bat was constructed of an inner and outer aluminum shell that offered increased performance without increased swing weight or moment of inertia (MOI). Double wall bats are still extremely popular today and other companies have been producing their own for many years. Some have even gone as far as to produce multi-wall bats out of more exotic alloys such as scandium, or have modified the design to include an external barrel sleeve instead of the full-length inner shell.

Taking it one step further, companies began combining the technologies of composite materials and the multi-wall bat to produce hybrids. Currently, there are multiple bats on the market that utilize a composite handle attached to an aluminum barrel using a rubber connection. The performance claim with this type of construction is that the connection allows for increased flex or 'whip' of the barrel, much like a golf club, to increase the energy transfer to the ball [2.7]. Similarly, the same connection type of bat has been made with a composite barrel and composite handle.

Contrary to the composite handle/metal barrel construction, another common type of bat is a full length metal handle with a composite sleeve adhered to the outside. Worth currently makes a line of softball and baseball bats based on this principle. In Figure 2.1 is an example of a connection type bat where the handle is attached to the barrel by a rubber plug, and Figure 2.2 shows a bat manufactured by Worth that uses an external composite shell.

Figure 2.1 - 2004 Easton Z-Core Connection

Figure 2.2 - 2004 Worth Wicked Insanity

Hybrid bats are not limited only to composite/aluminum combinations, but more exotic alloys have been introduced as well. Recently, DeMarini introduced their DXWHI-6 White Steel model with the claim that it is the first ever steel barreled bat [2.8]. It is a composite handled bat with a steel barrel that is supposedly more durable than that of aluminum. Similarly, Worth has made bats in the past that utilize a titanium barrel over a full length aluminum handle. Again, the titanium was used for increased performance and durability.

2.2 Methods to determine performance and durability

2.2.1 Field use

The easiest, yet least scientific, method for determining the performance and/or durability of a bat is simply by using it for batting practice or a in a game. Player testimonials can give some insight as to how a bat performs or feels if it is used by someone that has experience swinging a bat. The internet is a valuable source for information, and for softball bats it is no different. Certain websites [2.9, 2.12] offer online forums where individuals can share their opinion about a specific bat or bats and can post formal reviews using a ranking system that considers both performance and durability. Again, this isn't the most scientific method of describing a bat, but it is a valuable resource to manufacturers and others that play the game. Information on tangible items, such as feel and sound, which a laboratory test cannot gage, is readily available from the person(s) hitting with the bat. Some manufacturers even go as far as to hire professional players or to sponsor teams to use their equipment exclusively in exchange for their opinion of the product and/or the ideas they may have about making improvements. Often, this 'advisory staff' is the first to use bats that are to be manufactured or are in development.

One step beyond the player testimonial is the field study. Typically with the field study, bats are compared in a more controlled fashion. With player testimonials, there can be many things

that come into question, such as the balls used, the swing speed of the player, the pitch speed, and the temperature of the environment. Whereas with a field study, these variables are usually documented and an effort is made to minimize their variation from player to player for the duration of the field study. When bats are compared in a field study, there is a more structured approach to the testing and players are usually assigned bats to use, rather than choosing what they would prefer to use. So it is essentially a more thorough approach to getting the testimonials from the players in addition to collecting experimental data if they so choose to. Depending on those that conduct the field study, it may be the intent to compare a variety of bats or skill levels, or both. For instance, the batting cage study [2.10] conducted by Greenwald, Penna, and Crisco set out to compare the performance of metal baseball bats to wood bats using professional, collegiate, and high school athletes. They concluded that metal bats had an average batted-ball speed 9mph faster than wood bats and that the batted ball speed increased with increasing experience level. More recently, a field study conducted by Smith, Broker, and Nathan [2.11] set out to see what effect bat mass and moment of inertia (MOI) had on a softball player's swing speed. The batters used in this study were of two different skill levels and swing speeds were measured through the use of high speed cameras and a light trap on the ground.

Similarly, there are individuals [2.12] that field test bats and post their reviews online for the public to view in exchange for an annual fee. The service provided is analogous to the controlled field study just described, with specific batters and protocols used such that bats are compared with minimal bias.

2.2.2 Direct methods

A more scientific means of testing a bat for its performance and durability is to have it tested in a laboratory setting. Facilities such as the Baseball Research Center [2.13] at the University of

Massachusetts-Lowell and the Sports Science Laboratory [2.14] at Washington State University provide independent testing services for manufacturers and sports organizations such as the National Collegiate Athletic Association (NCAA) and the Amateur Softball Association (ASA). These associations use standardized test protocols to certify bats for use in their respective leagues. If a bat manufacturer wishes to have their bat certified, it is sent to a certified testing facility where it is tested under these test protocols and the results are reported to the manufacturer and the association. If it passes the test, i.e. it doesn't exceed some performance limit dictated by the association rules, it can then be certified if the manufacturer so chooses and a certification label can be printed on any subsequent bat of that model. Examples of some of these certification labels can be seen below in Figure 2.3.

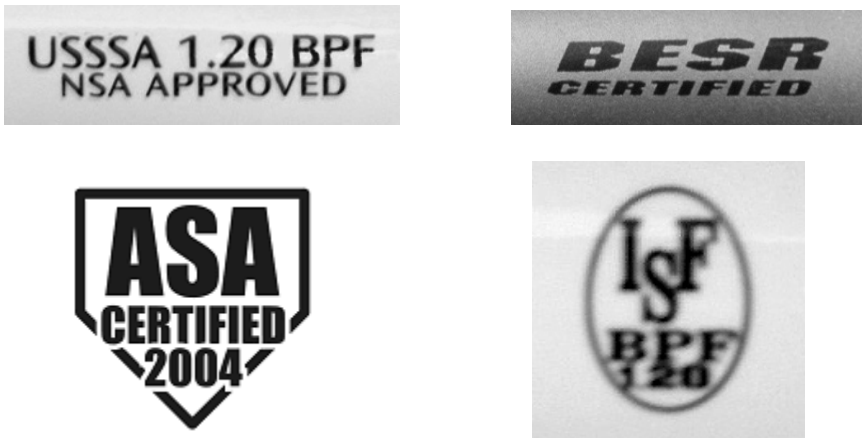

Figure 2.3 - Baseball and softball bat certification logos.

The performance metric that the NCAA requires to certify a baseball bat is called the Ball Exit Speed Ratio (BESR). The NCAA BESR limits are dictated by their own test protocol [2.15] which is based on the American Society for Testing and Materials (ASTM) standard F2219-05 [2.16]. The testing apparatus is an air cannon that fires a ball at the bat which is mounted in a pivot. Both the inbound and rebound velocities of the ball are recorded and used to calculate the BESR according to

$$\text{BESR} = \frac{V_R - \delta v}{V_I + \delta v} + 0.5 + < \varepsilon >, \tag{2.1}$$

where V_R is the rebound velocity, V_I is the inbound velocity, ε is a correction factor, and δv is defined below as

$$\delta v = 136\text{mph} - V_{contact} \tag{2.2}$$

and $V_{contact}$ is given by

$$V_{contact} = (66\text{mph})\left(\frac{L - 6 - z}{L - 12}\right) + 70\text{mph}\,. \tag{2.3}$$

Similarly, the National Federation of State High School Associations (NFHS) has adopted the BESR certification standard for baseball.

Other organizations, including Little League Baseball, the United States Slow-Pitch Softball Association (USSSA), the National Softball Association (NSA), and the International Softball Federation (ISF), have adopted a different method of certifying their bats. Their certification is determined by the Bat Performance Factor (BPF). The test protocol, ASTM F1890-05 [2.17], for determining BPF is similar to that of the BESR because it utilizes an air cannon to fire the ball at a stationary bat mounted in a pivot, the only difference being that the ball is fired at the bat at 60mph and the bat speed after impact is measured and used in the computations. As defined in the ASTM standard [2.17], BPF is calculated using the following equation,

$$BPF = \left(\frac{\text{Bat - Ball COR}}{\text{Ball COR}}\right). \tag{2.4}$$

The Ball COR referenced in the above equation is the ball coefficient of restitution (COR) and is defined in ASTM F 1887-02 [2.16] as the ratio of the rebound velocity to the impact velocity of a ball fired at a rigid surface at 60mph. The Bat-Ball COR, as defined in ASTM F 1890-05, is a measure of the collision efficiency and is calculated as the relative speed of the objects after

impact divided by the relative speed of the objects before impact. This value is a function of the moment of inertia (MOI) of the bat, the weight of the ball, the center of gravity of the bat, the velocity of the ball before impact, and of course the velocity of the bat after impact. The previously mentioned organizations that use this as their standard have set forth an upper limit to the BPF of 1.20. Little league baseball also uses the BPF test method for certification of baseball bats, but limits BPF to 1.15 [2.47].

A third laboratory method of determining a bat's performance, and is used by both the ASA and NCAA softball, is the batted ball speed (BBS) measure. (Unlike NCAA baseball bat certification, NCAA softball has adopted the ASA bat certification test and standard) Like the BESR and BBS measure, it too utilizes a high speed ball cannon to impact a stationary bat mounted in a pivot but requires further numerical calculations. In addition, it also is based on the ASTM F 2219-05 standard.

To calculate BBS, one must first compute the bat-ball COR (BBCOR) or e_{BB}. This value is given by

$$e_{BB} = \frac{v_r}{v_i} + \frac{mQ^2}{v_i I_p}\left(v_i + v_r\right) \quad , \tag{2.5}$$

where v_R and v_I are the rebound and inbound velocities of the ball (in/s), respectively, Q (in) is the distance from the pivot to the impact location on the bat, m is the weight of the ball (oz), and I_p (oz-in^2) is the combined moment of inertia of the bat and pivot.

In addition, two more parameters, the bat recoil factor (r) and the bat-ball collision efficiency (e_a) are required to complete the BBS calculations. The bat recoil factor is a function of the inertial properties of the bat and ball and is given by

$$r = \frac{m_n Q^2}{I_p} \tag{2.6}$$

where m_n is the nominal ball weight (oz). The collision efficiency is a model-independent relationship that can be derived using conservation laws [2.19], and is defined as

$$e_a = \left(\frac{e_{BB} - r}{1 + r} \right) \tag{2.7}$$

or

$$e_a = \frac{V_R}{V_I}. \tag{2.8}$$

The BBS is based on the bat-ball collision efficiency and also accounts for the pitch and swing speed of a player. It is written as

$$BBS = (ve_a) + V(1 + e_a), \tag{2.9}$$

where v is the pitch speed and V is the bat swing speed at the impact location. The ASA assumes a pitch speed of 25 *mph*, and the bat swing speed is found from

$$V = 85\left(\frac{Q + 8.5}{30.5} \right)\left(\frac{9000}{I_p} \right)^{\frac{1}{4}}. \tag{2.10}$$

The 85mph average swing speed used in the above equation was generated from the field study [2.11] by Smith, Broker, and Nathan.

The current ASA BBS limit for any bat, and any impact location on that bat, is 98mph.

2.2.3 Indirect methods

The aforementioned tests are a direct approach to determining a bat's performance, but there are also ways to describe a bat's performance indirectly. One of those methods is barrel compression. This is a rather simple test that consists of compressing the barrel of the bat .070" between two solid cylindrical surfaces with radii equivalent to that of a softball with a 12 inch circumference, and recording the load required to reach that deflection. A stiffness value (lb/in)

is computed for that displacement and the measurement is repeated at a second circumferential location 90° away from the first and the average of the two values is taken. The relevance of this test is that bats tend to have higher performance with lower barrel compression because of the trampoline effect. The trampoline effect, as described by Nathan, Russell, and Smith [2.20], is a mechanism by which a thin-walled hollow bat stores kinetic energy and can efficiently return that energy to the ball during impact, creating higher rebound velocities. This trend is evident when comparisons are made between different construction types of bats. For a low performing single wall aluminum bat, the stiffness values are around 8700-9700 lb/in, whereas a newer high performing multi-wall aluminum or composite bat can have a barrel stiffness as low as 6500 lb/in [2.21].

The concept of barrel stiffness and its performance effects has been known to softball players for many years, and a popular bat doctoring technique is to decrease the wall thickness, or "shave" the bat [2.29]. This is done to lower the bat's effective barrel stiffness, and it isn't uncommon to see a doctored bat's barrel stiffness below 5000 lb/in. Figure 2.4 shows performance values for a series of bats with differing barrel compressions.

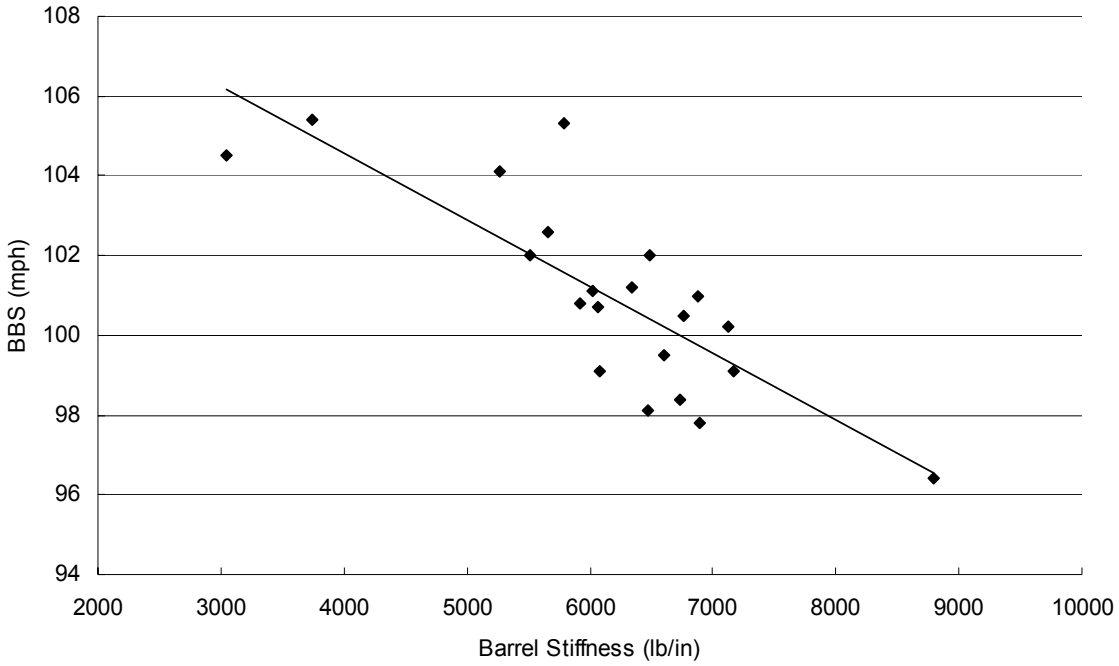

Figure 2.4 - Bat Performance vs. Barrel Stiffness [2.21]

The vibrational response of the bat during impact plays a large role in how it performs. The vibrations that take place in the barrel that are of particular interest are called the hoop modes. As described by Russell [2.22], the hoop modes of a hollow bat describe the radial vibration of the barrel and are responsible for the sound the bat makes upon impact, as a well as the trampoline effect. Depending on the construction of the bat, these hoop modes can be different from bat to bat, and can also be another indirect method of determining performance. The method used to measure a bats dynamic frequency response is called modal analysis [2.21]. Here, an accelerometer is adhered to the bat and an impact hammer with a load cell on the tip is used to strike the bat at incremental locations. Similarly, one could impact the bat at one location and move the accelerometer in increments along the length of the bat and accomplish the same thing. Through high speed data acquisition and computational software such as LabVIEW, one is able to determine the frequency response function (frf) for any given bat and

determine the hoop modes as well as the bending modes. Russell showed that the first hoop mode was the greatest contributor to bat performance, and that the lower the first hoop mode/frequency, the higher the performance tended to be. There appears to be a lower bound to the first hoop mode though. Below 900Hz the barrel becomes too compliant and will either dent or crack under normal use, or the overall performance would be low. Typical hoop frequencies for a single wall bat are between 1650 and 2400 Hz, whereas multi-wall bats are between 1200 to 1700 Hz. In contrast, the best composite bats on the market have hoop frequencies below 1200 Hz. Figure 2.5 below shows a comparison between different types of bat constructions, their hoop frequencies, and batted ball speeds.

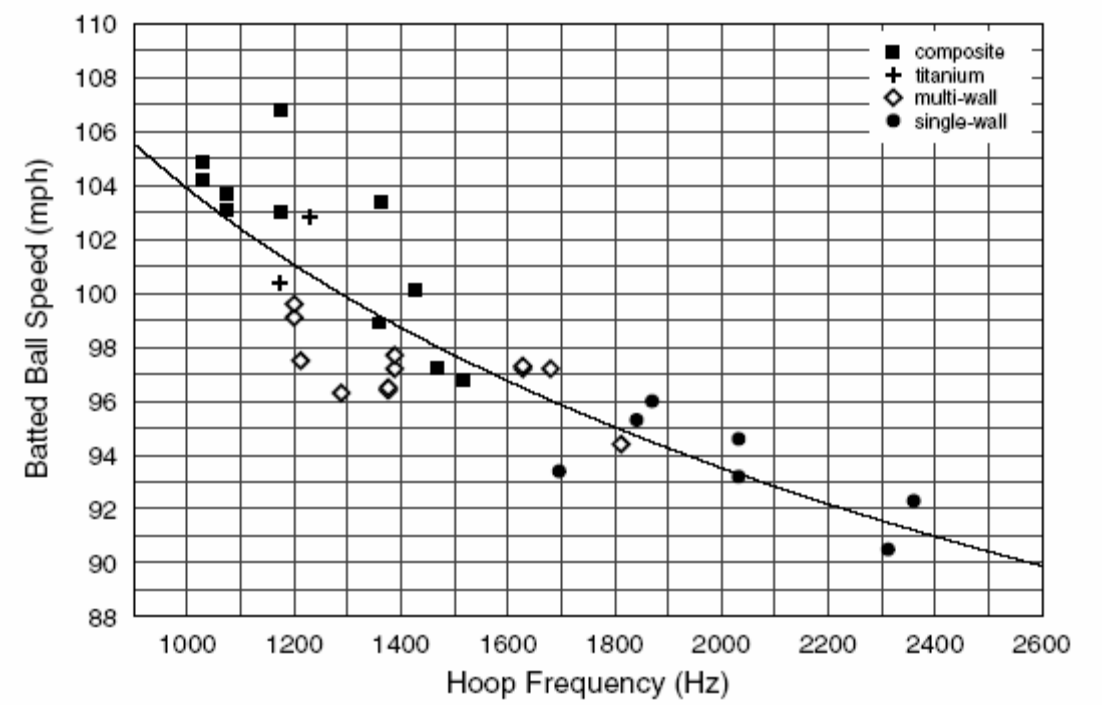

Figure 2.5 - Batted Ball Speed (BBS) vs. Hoop Frequency [2.22]

Again, as with barrel compression, the hoop mode/frequency measurement has proven to be another method to gauge the performance of a bat without having to subject it to direct testing as with the BBS or BESR measures.

2.2.4 Fatigue testing

Often times, the highest performing bats are the least durable and the most durable are the lowest performing. Every bat manufacturer has to weigh the benefits of one against the other when designing a bat. Field studies or player testimonials are the easiest method of determining a bat's level of durability, but again these methods may or may not regulate what balls are used, what temperature the environment is, or who is swinging the bat, so again they can be the least scientific of the methods available. Steps have been taken by both research facilities and manufacturers to approach durability testing in a more scientific manner. The Baseball Research Center at the University of Massachusetts - Lowell has acquired a machine [2.23] that is used test the durability of baseball bats. The machine has the capability of firing a baseball at the bat at speeds from 50 to 200 mph every five seconds. Similarly, Rawlings sporting goods has developed a mechanical batter [2.24] that swings a bat at a ball that is positioned on a tee and records the ball out speed for every impact. These machines are automated enough that the operator can set up the test and walk away for however long they desire to test the bat. Typically, a bat is designed to withstand the abuse of one season of play, so a bat may be tested for up to 750-1000 impacts [2.34]. Although not everyone has access to machines like the ones just described, these are just examples of how researchers and/or manufacturers are taking steps to further improve how bats are tested.

2.2.5 Finite element analysis

The last and probably most scientifically rigorous method to determine a bat's performance and durability is through the use of finite element analysis (FEA). Of the previous finite element work performed by other researchers, the focus seems to have been on performance, rather than durability. As will be seen below, some works have included information in their models that

allow for the quantification of durability or denting, but results are not reported. In contrast, durability is the focus of the work presented here after.

If performed by a properly trained person, FEA can be a powerful design tool that can significantly reduce the design to market times. Unfortunately, it appears that this method has largely been used by researchers and not by bat manufacturers because of the prerequisite knowledge, material characterization, and the cost of the program(s) [2.24]. With FEA, one has the ability to design the bat and test it without ever seeing a final production model. But the downside to this approach is that a great deal of knowledge must be known about material properties of the bat, as well as the ball with which the bat model will be impacted within the finite element model. Laboratories such as the Sports Science Lab at Washington State University and the Baseball Research Center at the University of Massachusetts – Lowell have the ability to test for how a softball or baseball performs at various impact speeds, but a manufacturer may not have the resources or time to explore these unknowns and would rather rely on knowledge from previous research and design to produce their next generation of bats.

A relatively little amount of work has been performed in the area of finite element modeling of a bat ball collision, An early work by Mustone and Sherwood [2.26] describes the development of an unrefined bat-ball finite element model. Their work produced a very preliminary model of the bat-ball impact with the intention of comparing it to experimental values. The numerical results were higher than the experimental values for both the wood and aluminum bats, yet there was no mention of an attempt to converge the model results to the experimental results. The ball model they developed utilized the Mooney-Rivlin material model to account for the nonlinear properties of a real baseball. A load curve was generated by compressing a ball in a load frame at various rates and then loading it into LS-DYNA for use

with the Mooney-Rivlin material formulation. The wood and aluminum bat models were created using shell elements of uniform thickness and 8-node brick elements, respectively. The ball model was calibrated by modeling a COR test against a fixed wood block at 60 mph and then comparing it to known experimental values. No calibration of the bat was mentioned in this work. The finite element model results for performance were higher than the experimental values for both the aluminum and wood bats, and that may be attributed to the fact that the bat model was so unrefined and the load curve generated for the deformation of a baseball was done at a rate that is significantly slower than that of an actual bat-ball impact.

In another work, Shenoy, Smith, and Axtell [2.28] developed a bat-ball model in LS-DYNA for a wood, aluminum, and composite reinforced wood baseball bat using a viscoelastic ball model. The ball model consisted of 2048 8-noded solid elements. The wood bat model was generated using 9696 8-noded solid elements and the aluminum bat was meshed using 2496 4-noded Hughes-Liu shell elements. The composite sleeve on the reinforced wood bat was meshed with 4-noded Hughes-Liu shell elements as well. Comparisons between exit velocities for both the FE models and the experimental values showed good correlation.

In Vedula's thesis work [2.25], a bat model was developed for both an aluminum and wood bat using LS-DYNA as the finite element program. To calibrate these models to the actual bats, the mass, MOI, center of gravity (CG), and center of percussion (COP) were calculated and compared to the values taken off the actual bats. In addition, a modal analysis was performed using an eigen-analysis and the bending and hoop modes/frequencies were compared. The aluminum bat was generated using thin-shell elements and the wood bat was created using solid hexagonal elements. Properties of C405 alloy aluminum were used as the isotropic-elastic material for the aluminum bat, and the wood bat model used the orthotropic elastic material type,

but the type of wood these properties were based on was not mentioned. Calibration results for both the wood and aluminum bats showed good correlation for mass, MOI, CG, COP, and the bending and hoop frequencies. A baseball model was also generated and calibrated. The ball was generated using solid hexagonal elements and the material type was assumed to be viscoelastic. Vedula provides the material properties used for the viscoelastic ball model but doesn't reference how they were generated or why they were used. The ball model was calibrated by comparing COR values to experimental data taken between 30 to 100 mph. The calibrated ball was subsequently used to impact the calibrated bat models and the performance values were then compared to experimental values. The experimental values used were taken from a machine that swings the bat horizontally in opposition to a ball that is mounted in similar rotating assembly. The relative collision speed and impact locations can be changed independently and the exit velocity of the ball was measured. For both the wood and aluminum bat models, the performance values generated by the models overestimated the experimental values. It is important to note that no information was provided on the number of elements used in any of the modeling or that any convergence study was performed.

A similar but more comprehensive work by Nicholls [2.32] uses both the Mooney-Rivlin and viscoelastic material properties to model a baseball. The Mooney-Rivlin and viscoelastic models were employed in ANSYS to simulate the ASTM F 1888-02 standard [2.33] for measuring the compression-displacement of softballs and baseballs. The load-displacement plots generated with the use of the Mooney-Rivlin model in ANSYS most closely matched that of an actual baseball and it was decided that this model was superior to the viscoelastic model. Nicholls' intent was to use these Mooney-Rivlin material properties in LS-DYNA to model actual bat-ball impacts, but there was no material card for that at the time and the viscoelastic ball model was

then utilized. A wood and aluminum bat was modeled and had 9800 and 12974 elements, respectively. 8-node solid elements were used for both. A linear elastic isotropic material was assigned to both the wood and aluminum bats, despite the fact that a wood bat is clearly anisotropic. An interesting note with Nicholls' work is the inclusion of friction in the bat-ball simulations. Within LS-DYNA, the friction during impact can be calculated by providing values for both static and dynamic friction. Nicholls' chose to use the default values of 0.1 and 0.2 for the dynamic and static friction coefficients, respectively. The code then makes a calculation based on these coefficients and assigns an overall friction value to the impact based on the velocities of the colliding surfaces. Nicholls reports that a friction coefficient of 0.2 was calculated for the impacts she modeled. No comparison was made to known friction coefficients or what effect, if any, it had on the performance of the bat models. Although a significant amount of FE work is presented, the focus of Nicholls' work was not on determining bat performance or durability, but how advances in bat technology have increased the threat of injury to players on the field.

A more recent work with FE modeling was done by Cruz [2.29]. The FE work presented in his thesis didn't include bat-ball impacts but focused on using LS-DYNA to determine the dynamic characteristics of a wood bat and a single and double wall aluminum bat. All the bat models used 8-node solid brick elements. A convergence study was conducted with the single wall aluminum bat and the flexural and hoop modes were compared for a variety of mesh densities. To reduce computation time, a 95% convergence threshold was decided upon. The mesh density that resulted from this threshold was 102 elements longitudinally, 180 elements circumferentially, and 2 elements through the thickness which equates to a total of 36720 elements. The results generated by the numerical analysis for the first two flexural and first hoop

modes compared well to the measured values taken from the modal analysis performed on each bat. It is worth mentioning that Cruz suggests the use of a different element if this work were to be carried over to modeling of impacts because of the excessive number of elements used.

Work that parallels what Cruz performed has been presented for cricket bats as well. Penrose and Hose [2.30] developed cricket bat models using Matlab 4 (The Mathworks, Inc) and LS-DYNA and calculated flexural modes as well as performance values. Matlab is a mathematical programming software package and was used by Penrose and Hose to model the cricket bat as an idealized free 1-dimensional uniform beam. A total of 41 equally sized beam elements were used and an iterative method was used to solve for the motion of the bat for small time steps. This simulation was simplified by modeling the ball as a single point mass that contacts the bat, and the material property of the bat was assumed isotropic even though typical cricket bats are made of anisotropic materials such as willow. For the models generated in LS-DYNA, two bat designs were used and both were created with 7968 8-node brick elements. Unlike the model in Matlab, these models used orthotropic material properties similar to that of willow. A cricket ball's construction is similar to that of a baseball, so one would expect similar nonlinear properties, but Penrose and Hose chose to model the ball using elastic material properties. Results of their work basically compared two cricket bat designs and they concluded that the utilization of a finite element program could be a powerful tool when it comes to design of a new bat. No comparisons were made between the models and experimental values, so the accuracy of their models is unknown.

Grant and Nixon [2.31] conducted very similar work with the dynamic properties of cricket bats and showed that their models correlated well with experimental values. An optimized design was modeled with the intent of raising the third flexural mode, which is responsible for

the sting a batter feels upon impact, without raising the bat mass. They were successful in doing this and showed that using finite element analysis for modal analysis is an effective design tool. No mention was made of the program used or any other details relating to the models themselves.

A work of more interest, because it pertains more closely to the work presented here, is by Mustone and Sherwood [2.27]. It builds on their earlier work [2.26] with the inclusion of kinematic hardening in the model of the aluminum bat, but models the bat with a constant wall thickness and still uses the Mooney-Rivlin material property for the ball model. As before, the bat models were calibrated using modal analysis, and the ball was calibrated by simulating a COR test against a stationary wood block. The performance results of this work correlated very well with experimental values, but unfortunately no particulars were given about the inclusion of the kinematic hardening in the aluminum bat model. Also, there was no mention of how the addition of the hardening in the bat model affected the performance values.

Mustone's thesis [2.35] provides more modeling detail than given previously. Within this work, a wood and aluminum bat is again modeled using LS-DYNA, but this time the bats were calibrated using their MOI in addition to modal analysis. The aluminum bat, consisting of 4840 solid shell elements, was modeled with the addition of plasticity and kinematic hardening. This type of hardening was recommended for use with solid elements, but Mustone doesn't provide his source for the values (σ_{yield}, tangent modulus, and hardening parameter (β')) that are required for input into the MAT_PLASTIC_KINEMATIC material card, nor is mention made of the performance effect this has on the bat model. Also, the bat was modeled as being made only of aluminum, but the actual bat has carbon and fiberglass reinforcement inside the barrel. The weight, CG, and MOI were calibrated to this bat, but it is unknown if this composite

reinforcement would have any effect if it were modeled as well in the bat. Something of great interest to this work, but was not mentioned, is the amount of deformation that was predicted with the addition of the plasticity in the aluminum bat model. No such information was provided.

Mustone's ball model was calibrated in a similar fashion using the Mooney-Rivlin material model. Comparisons of the numerical and experimental results showed that the exit velocities of the ball in the finite element models were significantly higher than experimental values. Mustone concluded that the ball model was to blame for this lack of correlation based on the irregular shape during and after impact with the bat model, as can be seen in Figure 2.6. These deformations were not seen when verification was sought by viewing high-speed camera video of an actual bat-ball collision.

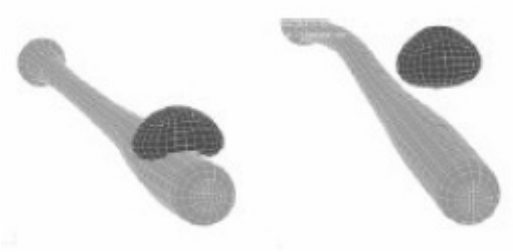

Figure 2.6 - Mooney-Rivlin baseball deformations during and after impact [2.35].

He concludes that the Mooney-Rivlin ball model does not accurately describe the nonlinear behavior of a baseball during impact and suggests that an alternative material model be used in the future for similar work.

Accurately modeling the behavior of a softball was of primary concern to Duris [2.36]. His work compared the Power Law and Prony series viscoelastic models. The Power Law viscoelastic material used in LS-DYNA is based on the time-dependent shear modulus, G(t),

$$G(t) = G_{\infty} + (G_0 - G_{\infty})e^{(-\beta t)} \tag{2.11}$$

where G_∞ is the long term shear modulus, G_0 is the short term shear modulus, and β is the decay constant. The formulation of the time-dependent shear modulus is based on a spring/damper system, shown in Fig. 2.7.

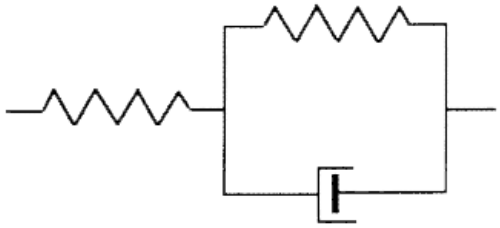

Figure 2.7 - Viscoelastic model representation

Symbolically, the springs shown here represent either G_∞ or G_0, and the damper represents β. A fourth parameter is also needed for use with this material model in LS-DYNA and that is the bulk modulus, *k*. The Poisson ratio, υ, is a function of both the shear and bulk modulii according to

$$\upsilon = \frac{3G - 2k}{6G - 2k} \tag{2.12}$$

where *G* is either the long or short term shear modulus. Equation 2.12 is of particular importance to the modeling of the ball because if at any time either the shear or bulk modulus causes the Poisson ratio to be negative or greater than 0.5, it can create instabilities and errors in the model [2.36].

The Prony series viscoelastic model formulation is based on a series of N spring and dashpot sets in parallel, called Voigt elements.

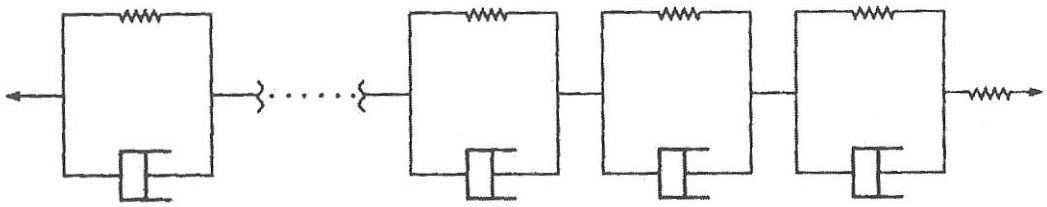

Figure 2.8 - Prony series viscoelastic model represented by a series of Voigt elements.

The shear relaxation modulus for this model is given by the equation,

$$G(t) = \sum_{i=1}^{N} g_i e^{-\beta_i t} \tag{2.13}$$

where g_i is the shear modulus and β_i is the decay constant for the *i*th Voigt element. Like the Mooney-Rivlin material model, the Prony series material card in LS-DYNA allows for the input of actual test data from mechanical testing of a sample of the material. Duris conducted such mechanical testing on a sample of polyurethane foam taken from the core of a softball and determined the shear modulii and decay constants for a series of six Voigt elements.

Both viscoelastic models were then compared to experimental values for COR and hardness. The measure of hardness was done in a similar fashion to that of COR except that the ball impacts a rigid cylindrical surface rather than a flat surface. The half cylinder impacted was 2.25 inches in diameter and approximately 4 inches long. Load cells were mounted directly behind the half cylinder and a load vs. time plot was generated. Duris used this setup to compare contact time, COR, and ball hardness to that of the numerical simulations for velocities of 60, 90, and 110mph. His findings showed that the Prony series representation of the ball didn't accurately describe the dynamics of the impact with the rigid cylinder at different speeds, whereas the Power law model was better at modeling ball hardness if the correct combination of

k, G_∞, G_0, and β was used. Because of that, a parametric study was conducted to determine the effect of each of these variables on the ball's COR, hardness, impulse COR, and contact time.

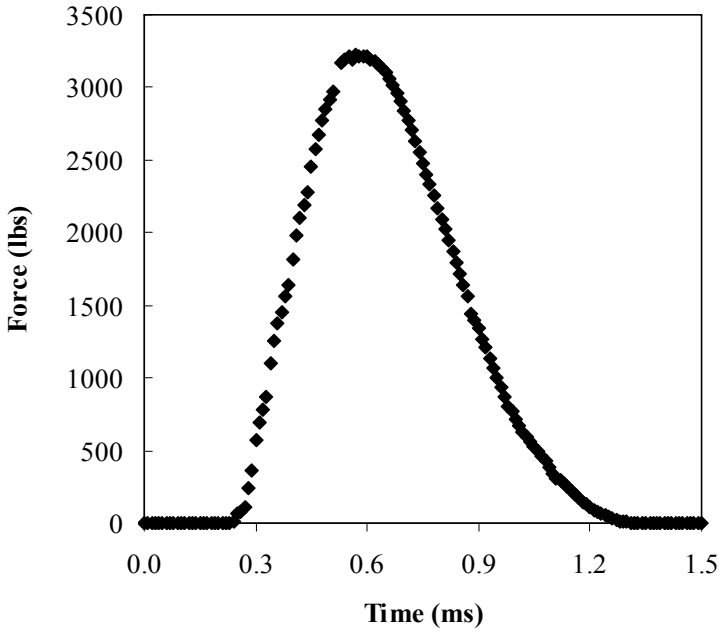

Figure 2.9 - Dynamic compression data generated in LS-DYNA for a 60mph impact [2.36].

Duris concluded that the Power Law viscoelastic model was the superior of the two and it should be used in future bat-ball models only after being calibrated on a cylindrical impact surface. As will be seen later, his parametric study serves as a valuable source of information for further development of a Power law viscoelastic softball model used in bat-ball impacts.

2.3 Typical aluminum bat alloys and mechanical properties.

2.3.1 Alloys and their properties.

When speaking of an "aluminum" bat, there are many more aluminum alloys being used in bat construction than one would first assume, and not all are created equal. When the aluminum bat was first introduced, alloys such as 6061, 6063, and 7005 were used [2.37]. By today's standards, these alloys are inferior. Prior to 1996, the majority of aluminum bats made were of 7050 alloy, commonly known as Cu31. The Cu31 designation implies the addition of copper

[2.39] to the composition as well as it was supplied by Alcoa. Most of the alloys listed here have a special designation that was developed in conjunction with a bat or sporting goods manufacturer to be used for marketing purposes.

In 1996, Alcoa introduced its C405 (7055) alloy. Worth was the first to introduce this alloy to the bat market, and since then most manufacturers have used this alloy in their better bats.

C555 was introduced by Alcoa in 2000. With the addition of Scandium, a rare and expensive metal found only in Scandinavia [2.38], C555 was stronger than its predecessor which allowed for bats to be made with thinner walls and added durability. Supposedly, C555 is 8-10% stronger than C405 because of the inclusion of Scandium [2.37]. Similarly, Kaiser Aluminum developed an alloy called Sc777 for Easton that has Scandium in its composition as well. Although there is no official 7XXX designation, this material is most like 7055 [2.37]. There have been additional variations to the Sc777 introduced to the market in the past few years, such as Sc888 and Sc900, but they are essentially the same alloy with small improvements on durability and performance.

Additionally, C805 is a modification to 7055/C405. Comparing the properties of C805 and 7055/C405 in Table 2.1, one can see that the strength properties for these alloys are very similar. Like that of Sc777, the addition of Scandium to C805 produces C855 which is slightly stronger. Even though the addition of Scandium does contribute to the durability and performance of a bat, there tends to be a competition between manufacturers as to who has the most Scandium in their bat so they can use it as a marketing tool. The average player may not even notice the difference between the Sc777 and C855 alloys.

Table 2.1 - Typical bat material properties [2.34, 40].

	Ultimate Tensile Strength (ksi)	Yield Strength (ksi)
6061*	18-45	8-40
6063*	13-42	7-39
7005*	28-57	12-50
7046-T6	65	60
7050/Cu31	27 O Temper 86 T6 Temper	12 O Temper 81 T6 Temper
7055/C405	27 O Temper 91 T6 Temper	10 O Temper 88 T6 Temper
C555	32	24
C805	28 O Temper 98 T6 Temper	17 O Temper 93 T6 Temper
C855	29.6 O Temper 99.4 T6 Temper	20.8 O Temper 96.3 T6 Temper
Pure Scandium	37	25
Carbon Steel[#]	40-273	27-110
6-4 Titanium	140	130

**Temper dependent*
[#]*Grade/class dependent*

As seen above, titanium has superior material properties to that of any of the common aluminum alloys used in bats, but its use has been limited in recent years because of increasing cost. The 7046 alloy is standard grade aircraft aluminum [2.39] and is of particular interest to this work. As will be seen later, bats made of this alloy tend to be lower performing and require thicker walls for durability.

2.3.2 Stress-strain behavior

The main focus of this work revolves around durability and predicting deformation, so it is important to know the behavior of the material in both the elastic and plastic regions of its stress-strain curve. A common method for generating a stress-strain curve is through a simple tensile test, as depicted in Fig. 2.10. In this test, a material test specimen is placed in a machine that applies a tension force and the amount of elongation is measured as the tension force increases until the specimen fails. The data generated by this test forms a stress-strain curve that is

characteristic of that material. Figure 2.11a shows a typical stress-strain curve as well as the regions of elastic and plastic deformation. The elastic region is defined by the linear relationship of the stress and strain, and the slope of that line is called E, the modulus of elasticity.

$$\mathrm{E} = \frac{\mathrm{S}}{e} \tag{2.14}$$

Where S is the engineering stress (psi) and e is the engineering strain.

Engineering strain is defined as

$$\mathrm{S} = \frac{\mathrm{F}}{\mathrm{A}} \tag{2.15}$$

where F is the force (lb) applied and A (in^2) is the cross-sectional area of the specimen.

Engineering strain is a measure of the specimen's elongation due to the applied load and is calculated by

$$e = \frac{L - L_0}{L_0} \tag{2.16}$$

where L_0 is the original or gauge length of the specimen and L is the length of the specimen at any time during the tensile test [2.42].

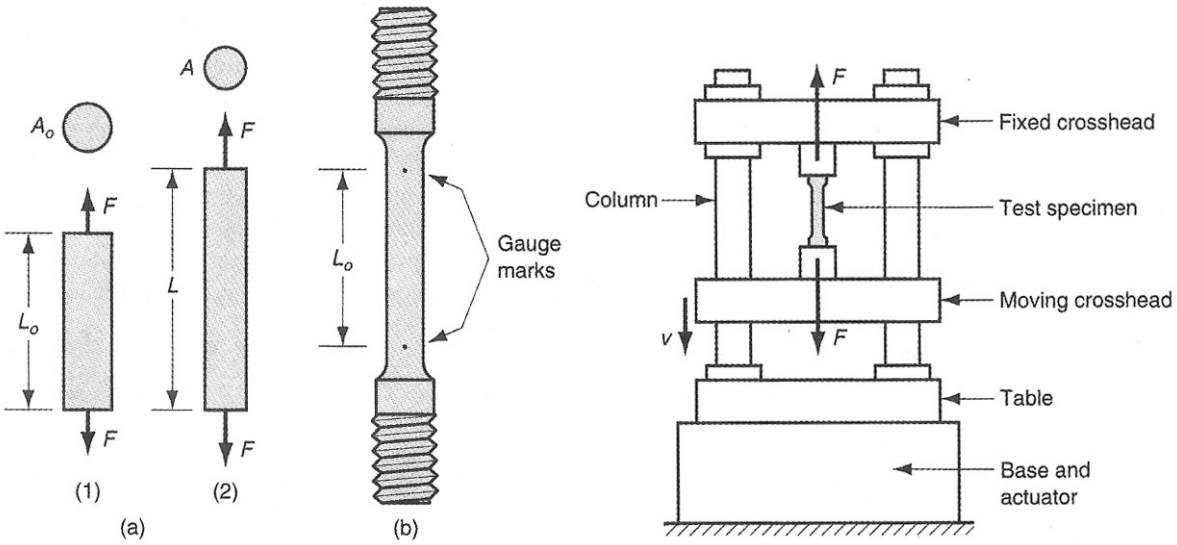

Figure 2.10 - Typical tensile specimen and testing apparatus [2.42].

If the specimen is not strained to the point that it exceeds its elastic limit, the specimen will return to it original, undeformed, length. If it does exceed its elastic limit, the specimen will perform plastically, permanently deform, and not be able to return to its original gauge length, L_0. When thinking of an aluminum bat during impact with a ball, the same principle applies. As the barrel deforms upon impact, the amount of deformation it undergoes will determine if it springs back elastically to its original shape, or will behave plastically and dent. An important phenomenon that occurs in the plastic region for most metals is called strain or work hardening. Strain hardening implies that the material is actually getting stronger as the strain increases. The measure of this hardening is usually done by transforming the engineering stress-strain curve to a true stress-strain curve where the engineering stress is related to the true stress by

$$\sigma = \mathrm{S}(1+e) \tag{2.17}$$

where σ is the true stress, S is the engineering stress, and e is the engineering strain. For this relationship to be valid, the material is assumed incompressible.

Similarly, the true strain is calculated as follows;

$$\varepsilon = \ln(1+e) \tag{2.18}$$

Once calculated, the true stress-strain curve gives a better representation of the behavior of the material because it takes into account the instantaneous reduction of the cross-sectional area of the specimen due to elongation [2.42]. Figure 2.11 shows both an engineering and true stress-strain curve, and is important to note that both curves show linear behavior in the elastic region. The region of hardening in the plastic region starts at the yield point and ends as the ultimate tensile strength. For aluminum, the yield point isn't always easy to identify because the stress keeps increasing (although not linearly) until the ultimate tensile strength is reached. Because of this, a 0.2% offset is employed to identify the yield point [2.43]. A parallel line, the slope defined by the elastic modulus, E, is offset 0.2% to the right of the linear/elastic portion of the engineering stress-strain curve and where that line intersects the curve defines the yield point or "yield strength". This is point B in Figure 2.11a. Table 2.1 lists common yield strengths for various bat materials.

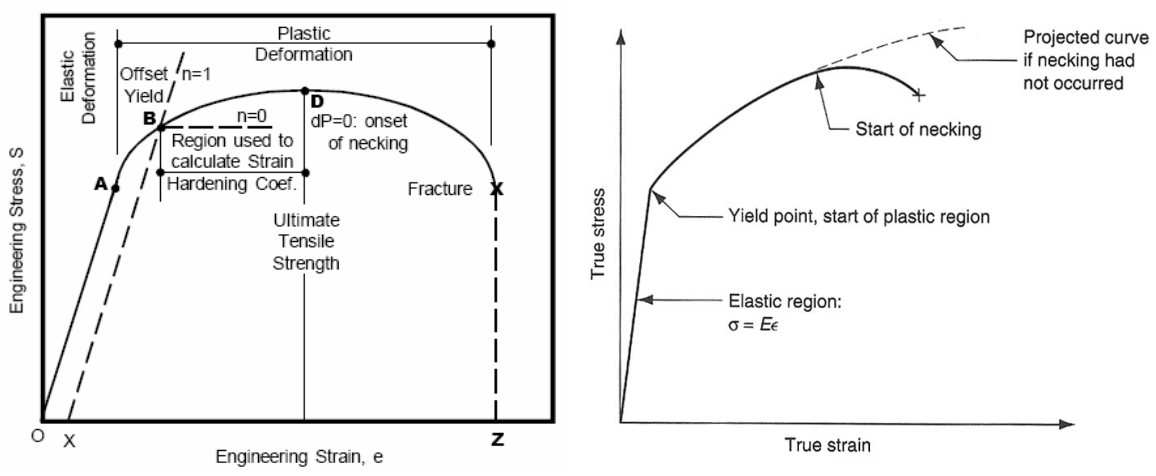

(a) (b)

Figure 2.11 - Typical Engineering and True Stress-Strain Curves [2.41, 42].

2.3.3 Isotropic and kinematic hardening

There are two types of hardening that can describe the material behavior between the yielding point and the ultimate tensile strength, isotropic hardening and kinematic hardening. To understand both of these hardening methods, it is important to first know what is meant by a "yield surface". The yield surface is a graphical representation of the strength of the material based on its compressive, tensile, and shear strengths. If the specimen is loaded, either in compression, shear, tension, or a combination of the three, the calculated principle stresses will locate a point on a stress plot. If that point is within the yield surface for that material, it will behave elastically, whereas if that point falls outside of the yield surface the material will behave plastically and hardening can occur. The yield surface is generated through a series of these measurements and usually forms an oval shape on the principle stress plot.

The principle strains mentioned are calculated based on the general stress state. Where $\sigma_{\#}$ signifies a normal stress in the # direction, and τ_{ab} represents a shearing stress in the *ab* plane.

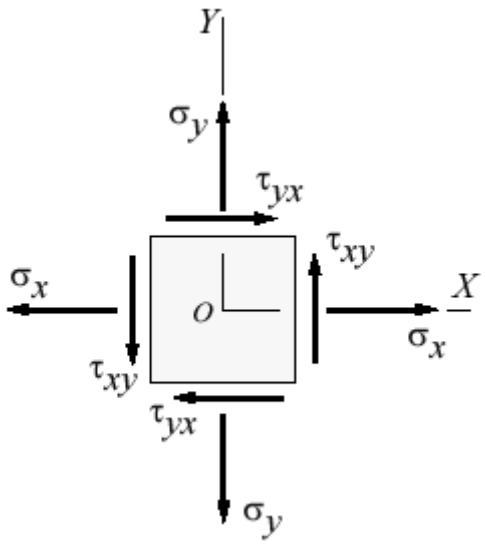

Figure 2.12 - General 2-D Stress State

For a 2-D plane stress state as shown in Figure 2.12, the principle stresses, σ_1 and σ_2, are calculated using the following equation(s) [2.43]

$$\sigma_{1,2} = \frac{\sigma_x + \sigma_y}{2} \pm \sqrt{\left(\frac{\sigma_x - \sigma_y}{2}\right)^2 + \tau_{xy}^2} \quad . \tag{2.19}$$

As mentioned previously, the material is actually getting stronger when it is hardened. With isotropic hardening, this strengthening is accounted for by uniformly increasing the size of the yield surface. If the specimen is loaded in tension beyond its yield point and then unloaded and reloaded in compression, the new yield stress in compression will be equal in magnitude to the new yield stress in tension, therefore showing that the yield surface has expanded [2.44]. This unloading and reloading is represented in Figure 2.13a.

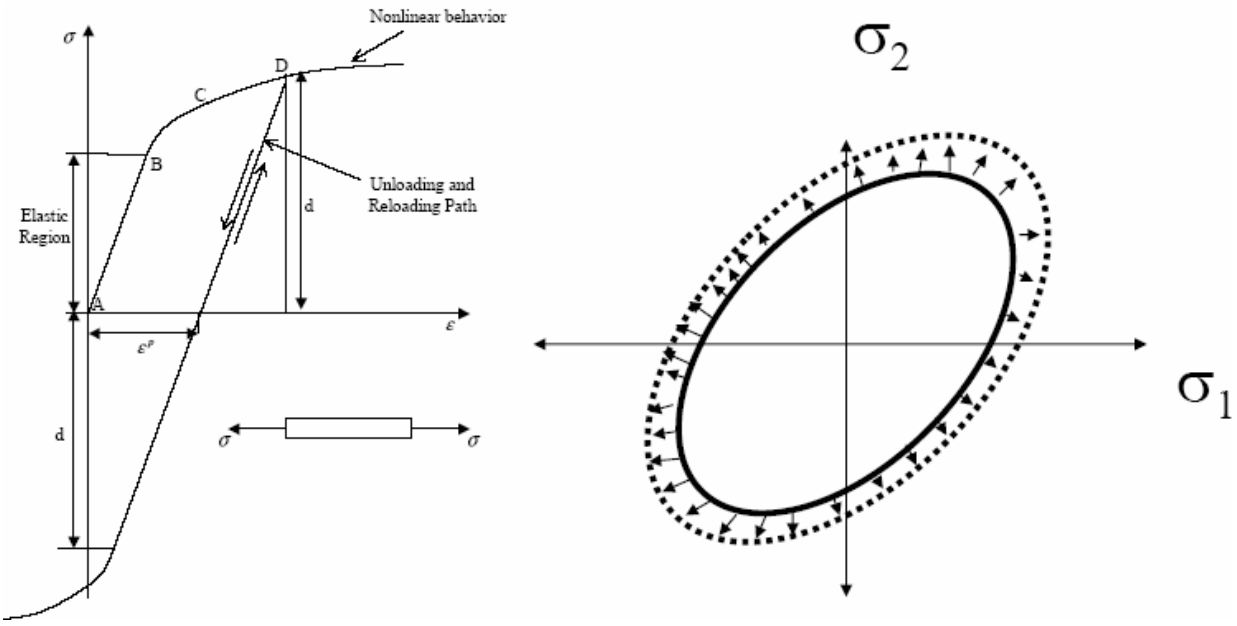

(a) (b)

Figure 2.13 - Loading cycle (a) and yield surface expansion (b) due to isotropic hardening [2.44].

A common method of using isotropic hardening is with what is called the Power law hardening rule. To describe the hardening that takes place beyond the yield point, the Power law hardening rule basically fits a curve to the true stress-strain curve between the yield point and

ultimate tensile strength, and the coefficients that are used to fit this curve are the hardening parameters. The equation used to fit this data, equation 2.20, is called the flow curve [2.42].

$$\sigma = K\varepsilon^n \tag{2.20}$$

In the above equation, K represents the strength coefficient, and n is the strain hardening exponent. Again, K and n are curve fitting parameters, but are characteristic of the metal specimen that is being tested. This hardening rule is only applicable to isotropic materials. Some common values for K and n are listed in Table 2.2 for various metals.

If experimental data is known, the values of K and n are rather simple to calculate. Plotting the true stress-strain curve on a log-log scale forms a straight line, of which the slope is n, the strain hardening exponent. Where the true strain value of 1.0 intersects the stress-strain curve defines the strength coefficient K.

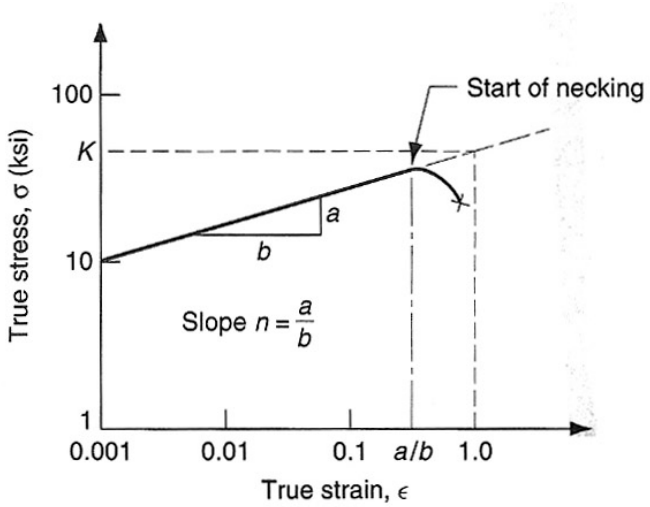

Figure 2.14 - Log-log plot of a true stress-strain curve [2.42].

Table 2.2 - Power law strength coefficients and hardening exponents for common materials [2.42].

	Strength Coefficient, K (lb/in^2)	Strain Hardening Exponent, n
Aluminum, pure, annealed	25,000	0.20
Aluminum alloy, annealed	35,000	0.15
Aluminum alloy, heat treated	60,000	0.10
Copper, pure, annealed	45,000	0.50
Copper alloy: brass	100,000	0.35
Steel, low C, annealed	75,000	0.25
Steel, high C, annealed	125,000	0.15
Steel, alloy, annealed	100,000	0.15
Steel, stainless, austenitic, annealed	175,000	0.40

In the case of kinematic hardening, rather than the yield surface increasing in size, it remains the same throughout the loading cycle, but translates in the stress space, as shown in Fig. 2.15. If one were to load, unload, and then reload a specimen in the same fashion as what was described for isotropic hardening, one would see that the compressive yield strength would no longer be equivalent in magnitude to the tensile yield strength, but would actually be less. This is known as the Bauschinger effect, and causes plastic anisotropy in the material behavior. During multiple cycles, this causes an accumulation of permanent deformation called "ratcheting". As loading is repeated, each consecutive hysteresis loop will translate forward due to the failure of closure of each loop [2.44]. This is of great concern in fatigue testing where cyclic loading is present, but for the experiments presented here, ratcheting is not an issue.

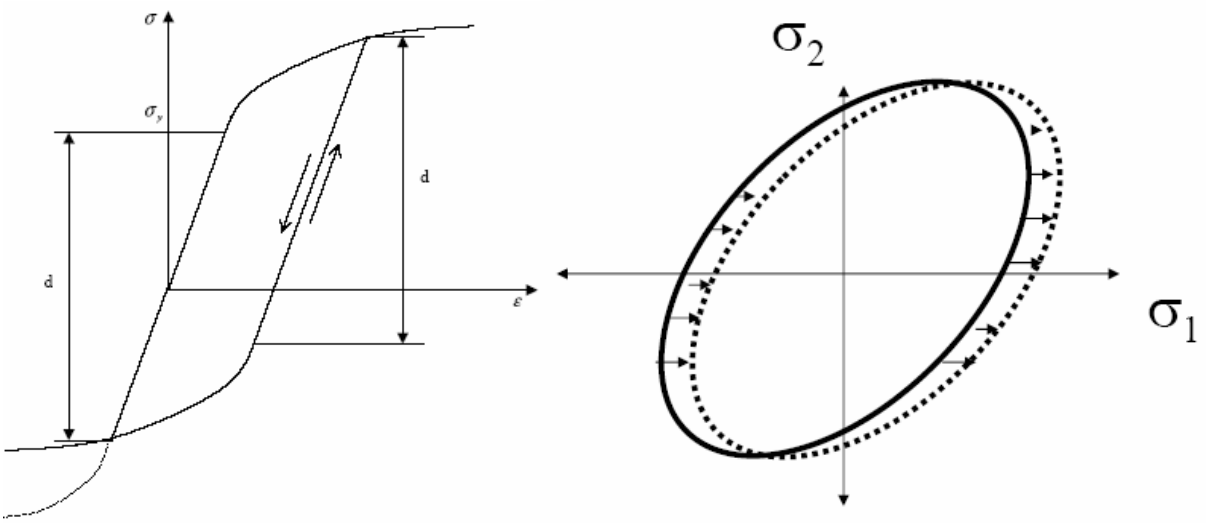

(a) (b)

Figure 2.15 - Loading cycle (a) demonstrating the Bauschinger effect and yield surface translation (b) during kinematic hardening [2.44].

Depending on the material, one or both of the hardening types presented here may accurately describe the material behavior in the plastic region. Other models have been developed in an attempt to further describe plastic behavior, and are known as coupled models. Mentioned earlier, Mustone used a material type in LS-DYNA that coupled the effects of isotropic and kinematic hardening. This model represents the stress-strain curve as being bilinear and shows the plastic region as being a straight line defined by the slope E_T, or tangent modulus [2.46]. A hardening parameter, β', is also required for input, and ranges from 0 for kinematic hardening to 1 for isotropic hardening, so the effect of the each of the hardening types can be adjusted simply by varying β'.

Similar work by Holmberg and Nejabat [2.45] used ABAQUS/Standard to predict dent sizes in steel exterior automotive door panels. They assumed isotropic hardening and soon realized that isotropic hardening alone overestimates the yield stress of the material after it has been stamped. They concluded that a mixed isotropic and kinematic hardening model would best describe the dent formation in future simulations.

2.4 Strain Rate Effects

In certain situations, such as high speed machining, impacts, and metal forming, strain rate can have a dramatic effect on material strength. For the work presented here, this is no different. Of the research performed in this area over a wide range of different materials, three different rate controlling mechanisms have been found; athermal flow, thermally activated flow, and phonon drag [2.48]. At high temperatures and low strain rates, a rate independent flow may be observed, attributed to athermal friction stress. Also, an increase in the amount of alloying elements will create an increase of the athermal friction stress. As a result, highly alloyed aluminum will show less strain rate sensitivity [2.48].

At higher strain rates and lower temperatures, a linear dependence of flow stress on the logarithm of strain rate is seen. The flow stress of pure aluminum demonstrates this behavior at room temperature, and the strain rate sensitivity increases at rates above 1000 strain/s [2.50]. For materials which are sensitive to thermally activated flow, dislocations within the material and their interactions dominate its sensitivity to strain rate. Plastic deformation in metallic materials is now generally accepted as the result of the movement of dislocations through the barriers that may exist in the crystalline structure of the material [2.49].

At very high strain rates, for some metals, a linear dependence of the flow stress on the strain rate is observed, called the influence of phonon drag. The flow stress in this situation is often considered viscous in nature because of the saturation of the mobile dislocation's average velocity [2.48].

2.5 Summary

The purpose of this chapter is to provide relevant historical and research related information towards the work that will be presented hereafter. In doing so, bat evolution was

outlined and different types of bat construction were explained. The various methods of bat testing, from field testing to finite element modeling, were discussed and the pros and cons of each method were presented. In addition, the different bat certification methods were presented along with the equations used to formulate the performance value on which the certification is based. Similarly, indirect performance measures such as barrel compression and modal analysis were introduced.

Because a significant amount of work presented here revolves around finite element analysis, multiple works performed by previous researchers on the subject of modeling the bat-ball impact were discussed along with any shortcomings that were observed. Ball material models were described and the mathematical models for each were provided.

An introduction to aluminum used in bats is also provided and brief comparisons were made amongst the different alloys. Plasticity was reviewed and isotropic and kinematic hardening was discussed. Strain rate effects were also introduced and discussed.

Ultimately, the goal of the work presented here is to develop the most realistic numerical model of a bat-ball impact as possible. Previous works have produced models that can accurately describe the performance of a bat or the behavior of the ball at various speeds, but little or no work has been done with bat durability or the prediction of denting in aluminum bats. This work will attempt to fill that void.

Extensive bat and ball modeling will be presented and the experiments used to verify the numerical results will also be detailed. Finally, durability of a single wall aluminum bat will be simulated using LS-DYNA and a comparison will be made using experimental results taken from impacts using a high–speed ball cannon.

REFERENCES

2.1 Louisville Slugger Historical Timeline. 1/5/2006 *http://www.sluggermuseum.org/timeline.aspx*

2.2 Shroyer, Jr., W.A. U.S. Patent 1 499 128, 1924, *Baseball Bat*

2.3 Worth Historical Timeline. 1/5/2006 *http://worthsports.com/about/history.php*

2.4 The History of Baseball Bats. 1/5/2006 *http://www.baseball-bats.net/baseball-bats/baseball-bat-history/index.html*

2.5 Easton Company Overview. 3/13/06. *http://www.eastonsports.com/corporate/about/history.php*

2.6 DeMarini Company History. 1/5/2006 *http://www.demarini.com/cas/company_history.html*

2.7 Easton Slow-Pitch Bats. 3/14/06. *http://baseball.eastonsports.com/slowpitch/details.php?scid=22&d=sst3&t=Bat*

2.8 DeMarini Steel Bat. 3/14/06. http://www.demarini.com/cas/slowpitch_steel.html

2.9 Softball Fans Online Bat Reviews. 3/15/06. http://www.softballfans.com/reviews

2.10 Greenwald, R.M., Penna, L.H., and Crisco, J.J. *Differences in Batted Ball Speed with Wood and Aluminum Baseball Bats: A Batting Cage Study.* Journal of Applied Biomechanics. 17(3) 2001 : 241-252.

2.11 Smith, L., Broker, J., and Nathan, A. *A Study of Softball Player Swing Speed.* Sports Dynamic Discovery and Application. Edited by A. Subic, P. Trivailo, and F. Alam, RMIT University, Melbourne Australia. (2003): 12-17.

2.12 Bomani Sports Research Inc. 3/15/06. http://www.bomani.com/BSRI/

2.13 University of Massachusetts – Lowell Baseball Research Center Homepage. 3/16/06. http://m-5.eng.uml.edu/umlbrc/

2.14 Washington State University Sports Science Laboratory Homepage. 3/16/06. http://www.ssl.wsu.edu

2.15 National Collegiate Athletic Association Standard for Testing Baseball Bat Performance. 3/16/06. http://www.ncaa.org/champadmin/baseball/bat_standards/2006_certification_protocol.pdf

2.16 ASTM F 2219-05. *Standard Test Methods for Measuring High-Speed Bat Performance*. West Conshohocken, Pa. 2005.

2.17 ASTM F 1890-05. *Standard Test Method for Measuring Softball Bat Performance Factor*. West Conshohocken, Pa. 2005.

2.18 ASTM F 1887-02. *Standard Test Method for Measuring the Coefficient of Restitution of Baseballs and Softballs*. West Conshohocken, Pa. 2003.

2.19 Nathan, A. *Characterizing the performance of baseball bats*. American Journal of Physics. Vol. 71 (2002) : 134-143.

2.20 Nathan, A., D. Russell, and L. Smith. *The Physics of the Trampoline Effect in Baseball and Softball bats*. Proceedings of ISEA 2005. Davis, CA. September 2004.

2.21 Cruz, C.M. *Characterizing Softball Bat Modifications and Their Resulting Performance Effects*. Unpublished MS Thesis, Washington State University, May 2005.

2.22 Russell, D.A. *Hoop Frequency as a Predictor of Performance for Softball Bats.* Engineering of Sport 5. Vol. 2 (2004) : 641-647.

2.23 UMass-Lowell Baseball Research Center durability testing machine. 3/23/06. http://m-5.eng.uml.edu/umlbrc/testing.htm

2.24 Cruz, C.M. Rawlings Sporting Goods. *Private communication.* January, 2006.

2.25 Vedula, G. *Experimental and Finite Element Study of the Design Parameters of an Aluminum Baseball Bat.* MS Thesis, University of Massachusetts Lowell, 2004.

2.26 Mustone, T.J. and J. Sherwood. *Using LS-DYNA to Characterize the Performance of Baseball Bats.* Proceedings of the 5th International LS-DYNA Users Conference. Southfield, MI. September 1998.

2.27 Mustone, T.J. and J. Sherwood. *Using LS-DYNA to develop a baseball bat performance and design tool*. Proceedings of 6th international LS-DYNA Users Conference. Detroit, MI. April 2000.

2.28 Shenoy, M.M., L.V. Smith, and J.T. Axtell. *Performance Assessment of Wood, Metal, and Composite Baseball Bats.* Composite Structures Vol. 52 (2001) : 397-404.

2.29 Cruz, C.M. *Characterizing Softball Bat Modifications and Their Resulting Performance Effects*. Unpublished MS Thesis, Washington State University, May 2005.

2.30 Penrose, J.M.T., and D.R. Hose. *Finite element impact analysis of a flexible cricket bat for design optimization.* Proceedings of the 2nd International Conference on the Engineering of Sport. Sheffield, England. July, 1998.

2.31 Grant, G. and S.A. Nixon. *Parametric modeling of the dynamic performance of a cricket bat.* The Engineering of Sport, Haake (ed.). Balkema, Rotterdam. 1996.

2.32 Nicholls, R.L. *Mathematical Modeling of Bat-Ball Impact in Baseball*. PhD Thesis, University of Western Australia, 2003.

2.33 ASTM F 1888-02. *Test method for compression-displacement of baseballs and softballs*. West Conshohocken, Pa. 2003.

2.34 Cruz, C.M. Rawlings Sporting Goods. *Private communication.* March, 2006.

2.35 Mustone, T.J. *A Method to Evaluate and Predict the Performance of Baseball Bats Using Finite Elements.* MS Thesis, University of Massachusetts Lowell, 2003.

2.36 Duris, J. *Experimental and numerical characterization of softballs*. Unpublished MS Thesis, Washington State University, December 2004.

2.37 What is and aluminum bat, anyway? 3/30/06 http://www.aluminumbats.com/index.asp?PageAction=Custom&ID=4

2.38 Scandium. 4/1/06. http://en.wikipedia.org/wiki/Scandium

2.39 Bat buying guide. 4/2/06 http://www.baseballcorner.com/batguide.asp

2.40 ASM International Handbooks Online. 4/3/06. http://products.asminternational.org/hbk/index.jsp

2.41 Gedney, R. *Tensile Testing for Determining the Formability of Sheet Metals.* Online Posting. ADMET, Inc. 3/4/06. http://www.admet.com/assets/Formabilityofsheetmetal.pdf

2.42 Groover, M.P. Fundamentals of Modern Manufacturing. Second Edition. John Wiley & Sons: New York. 2002. ISBN: 0-471-40051-3.

2.43 Beer, Johnston, DeWolf. Mechanics of Materials. Third Edition. McGraw-Hill: San Francisco. 2001. ISBN: 0-07-365935-5

2.44 Araujo, M.C. *Non-Linear Kinematic Hardening Model for Multiaxial Cyclic Plasticity*. Unpublished MS Thesis, Louisiana State University, August 2002. http://etd.lsu.edu/docs/available/etd-0708102-185912/

2.45 Holmbert, S and B. Nejabat. *Numerical Assessment of Stiffness and Dent Properties of Automotive Exterior Panels.* Materials and Design. Vol. 25 (2004) : 361-368.

2.46 *LS-DYNA Theoretical manual.* Version 970 Re5434a. Livermore Software Technology Corporation. May 1998.

2.47 Russell, D.A. *Physics and Acoustics of Baseball & Softball Bats* 4/17/06. http://www.kettering.edu/~drussell/bats-new/cop.html

2.48 Oosterkamp, L.D., A. Ivankovic, and G. Venizelos. *High strain rate properties of selected aluminum alloys.* Materials Science and Engineering Vol. A278 (2000) : 225-235.

2.49 Iswaran, C.V., R. Reed-Hill, V. Levit, and M. Kaufman. *Modeling Flow Stresses and Strain Rate Sensitivities Using Low Temperature Deformation Data.* Scripta Metallurgica *et* Materialia Vol. 32 No. 7 (1995) : 941-947.

2.50 Smerd, R., S. Winkler, C. Salisbury, M. Worsick, D. Lloyd, and M. Finn. *High strain rate tensile testing of automotive aluminum alloy sheet.* International Journal of Impact Engineering Vol. 32 (2005) : 541-560.

CHAPTER THREE

- BALL CHARACTERIZATION AND MODELING -

3.1 High speed cannon apparatus and test equipment

3.1.1 Ball cannon

Because the focus of this work was on durability and denting, an apparatus was needed that could create a relative impact velocity high enough between the test bat and ball to achieve some sort of deformation in the bat. Not only that, but it needed to do it in an accurate and repeatable manner. The high speed ball cannon originally developed at the Washington State University Sports Science Lab for use with bat and ball performance testing, as seen in Figure 3.1, lent itself well to this work and was the primary test fixture used.

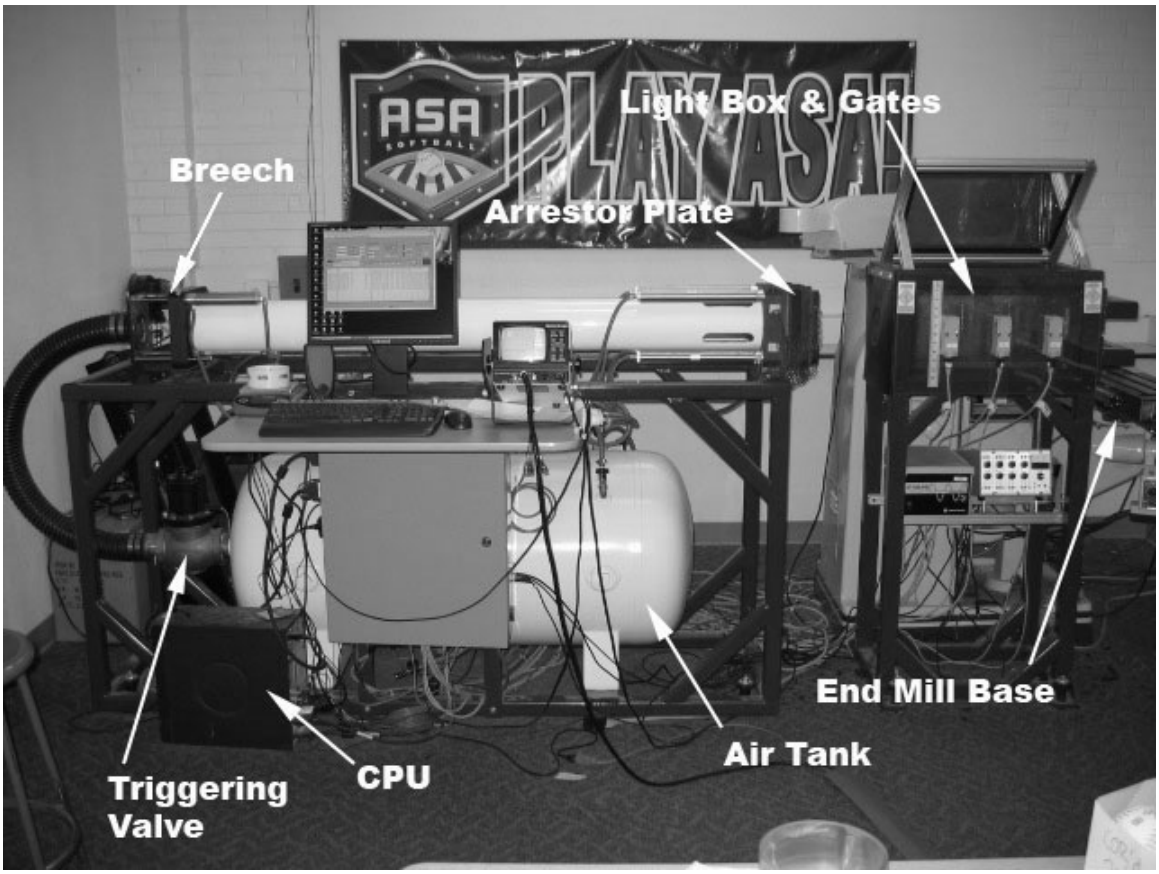

Figure 3.1 - Ball cannon.

The cannon setup consisted of a large air tank, a triggering valve, a barrel, a light box, and a large mounting fixture for the placement of the bat, and a desktop computer. The ball cannon operated on compressed air and the pressure within accumulation tank was controlled by an electronic regulating valve connected to the computer. The triggering valve, also controlled by the computer, was located between the air tank and the "breach" end of the cannon. The breach end of the barrel is where the ball was loaded and a breach plate was held tight against the end of the barrel by pneumatic cylinders prior to firing. The ball was loaded in what is called a sabot and placed within that barrel at the breach end. The sabot ensured proper centering of the ball within the barrel for accuracy reasons, and also assured that the ball was not spinning once it was fired. The sabot used for this work can be seen in Figure 3.2. On the exit side of the barrel, there was a series of leather and foam pads and an aluminum plate that made up what was called the arrestor plate. The arrestor plate prevented the sabot from traveling into the region where the ball velocity was measured, but still allowed the ball to travel at its intended velocity without any rotation. This too was connected to pneumatic cylinders that, once the cannon was fired, extended out and lessened the impact from the sabot as it struck the arrestor pads and plate. Beyond the arrestor plate at the exit end of the barrel was what was referred to as the light box. The light box was constructed of tubular steel with polycarbonate windows on the top, bottom, and sides to prevent the ball from escaping after impact. Attached to these windows on the sides of the light box was a series of three pair of Banner High-Speed Multi-Beam LS10 Infrared Light Screens (Banner Engineering Corp, Minneapolis, MN.) (hence the term light box) that were used to measure both the inbound and rebound velocities of the ball. On one side of the light box were the infrared emitters, and on the other were the receivers. These pairs of emitters and receivers were positioned six inches apart from one another between the barrel and where the bat

was positioned, and the time at which they were tripped by the ball was recorded by the computer, thus allowing a velocity to be calculated.

Figure 3.2 - Softball loaded in a sabot.

Most of the functions of the ball cannon were computer controlled, with the exception of the loading of the ball and the resetting of the bat. LabVIEW version 7.1 (National Instruments Austin, TX) was used to operate the cannon as well as record the desired experimental information. LabVIEW is a graphical programming platform that allowed for easy measurement and data acquisition as well as management and manipulation of the data once recorded.

The ball cannon was originally developed to do ball and bat performance testing, so the experimental testing was done primarily in accordance with ASTM F2219 [3.1] with the exception of the balls used and the velocity at which the ball was fired.

3.1.2 Ball dynamic stiffness

To accurately describe the performance of a softball at different speeds, the cylindrical impact surface ball test developed by Duris [3.2] was utilized for this work. This test used the same ball cannon just described, but instead of impacting a freely swinging bat, the ball was fired

at a four inch long solid steel half cylinder 2.25 inches in diameter (same as that of a softball bat) which was rigidly mounted by an angle bracket to the end mill. Between the cylindrical impact surface and the rigid wall was a group of four PCB 208C05 piezoelectric load cells (PCB Piezotronics, Depew, NY), three of which were oriented in an equilateral triangle and the fourth located at the geometric center of the triangle. The impact surface and the load cells behind it can be seen below in Figure 3.3.

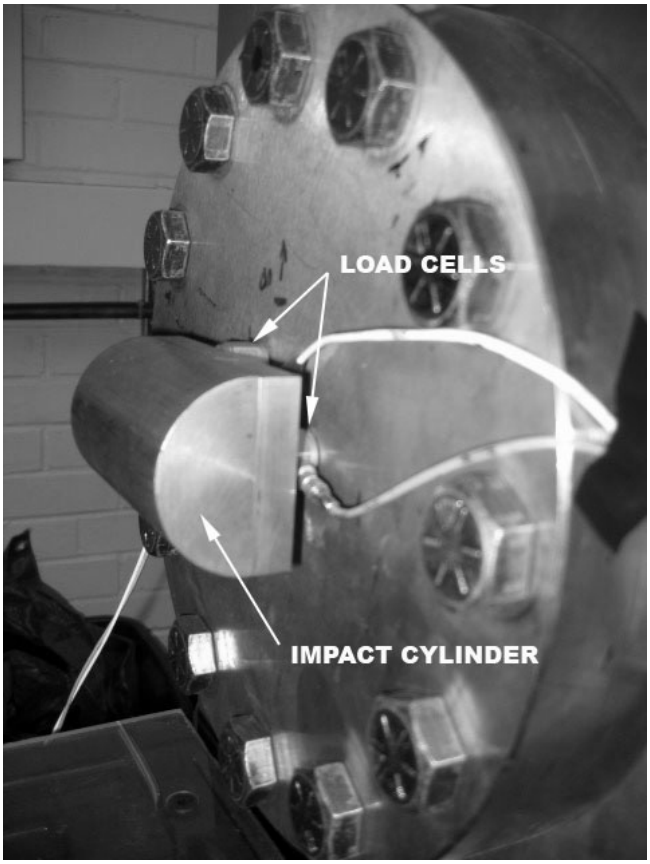

Figure 3.3 - Impact cylinder and load cells used for dynamic stiffness testing.

During impact, each of these load cells output a voltage that was proportional to the load that it was undergoing. A summation box was connected to all four of the load cells and the readings from each were summed and an individual signal was sent to the computer to be recorded. This experimental setup allowed a force vs. time plot to be generated and the duration

of impact and peak force can then be calculated. A typical force versus time plot can be seen in Figure 3.4 [3.6].

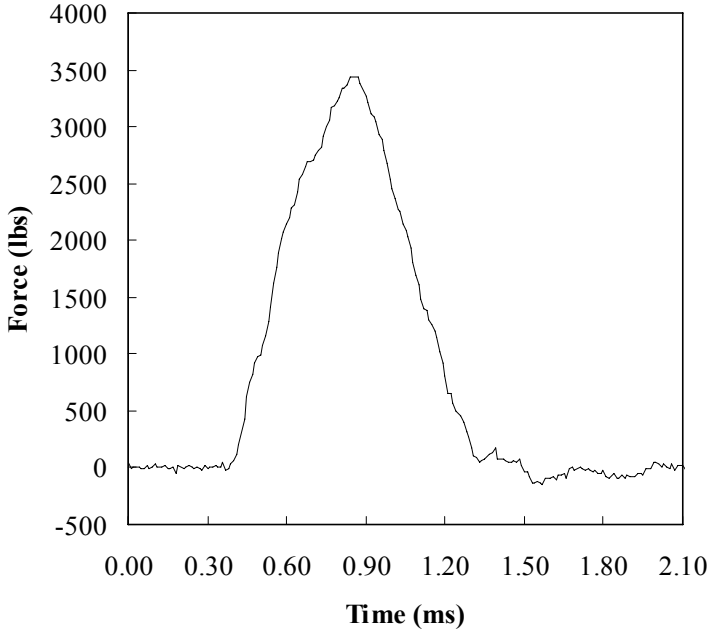

Figure 3.4 - Load cell force vs. time plot.

Of particular interest was the peak impact force. The numerical ball modeling that will be presented later uses a dynamic stiffness measure for calibration which is a function of peak impact force. The ball dynamic stiffness formulation, developed by Smith, Duris, and Nathan [3.3], assumes the ball to behave as a linear spring. Equating the initial ball kinetic energy, given by,

$$KE = \frac{1}{2} m v_p^{\,2} \tag{3.1}$$

to the ball's potential energy at maximum deformation,

$$PE = \frac{1}{2} k x^2 \tag{3.2}$$

and utilizing the spring force equation, $F=kx$, the peak displacement value x is eliminated and a the stiffness value, k, can then be calculated as .

$$k = \frac{1}{m}\left(\frac{F}{v_p}\right)^2 \tag{3.3}$$

where m is the ball mass, F is the peak impact force, and v_p is the pitch speed.

3.2 Test balls

Two different brands of softballs were used in this work, one was manufactured by Diamond and the other manufactured by Worth, pictured in Figure 3.5. Both balls were ASA certified as having a COR of 0.44 or less and a compression value of 375 lbs or less. The static compression [3.9] and COR [3.5] was not experimentally verified for these balls prior to conducting the experimental testing described in the next section. The Diamond ball was Flyer model 12RSC 44, and the Worth ball was a Super Gold Dot model SX44RLA3. The Worth brand ball was used for the dynamic stiffness experimentation, whereas the Diamond brand ball was used for the low-speed strain testing as will be discussed in the next chapter.

Figure 3.5 - Softball models used for the dynamic stiffness testing.

3.3 Finite element modeling and tuning of the ball model.

3.3.1 Experimental data collection

Prior to doing any modeling of the bat-ball collision, or even impacting a bat experimentally, a series of dynamic stiffness measurements were undertaken to characterize the performance of the test balls at various velocities. The speeds chosen to perform these tests were 60, 80, 95, 105, 110, 120, and 130 mph. The standard test [3.1] velocity at which bats are tested at for ASA certification purposes is 110 mph. The speeds of 110, 120, and 130 mph were chosen in reference to this velocity because it is known from previous experience that some aluminum bats will dent when impacted at this velocity, and the higher velocities of 120 and 130 mph should produce more pronounced deformations. The lower speeds of 60, 80, 95, and 105 mph were additionally chosen with the hope that a consistent trend could be seen and an appropriate curve could be fit to the data.

Forty two of the Worth balls were selected and randomly separated into seven groups of six balls and each of these groups was assigned to an impact speed. Each ball was then weighed prior to use. It is worth noting that these balls were not conditioned as one would do per ASTM F2219 or F1887 [3.5]. These balls were stored and tested in a laboratory space that was held to 72° F ± 4° and 40% R.H. ± 10%.

The dynamic stiffness experiments were carried out at the speeds mentioned above with the six balls selected to be tested at that speed, and the impact force as well as the COR was calculated and recorded. (The COR for the cylindrical impact surface was calculated in the same manner as is done for a flat surface impact [3.5], but shall be referred to as dynamic COR or DYN. COR from here on.) The firing or impact speed was held to within ± 20 in/s (± 1.136 mph) of the target speed, and if it fell outside this range it was deemed too fast or slow and the

experiment was repeated with the same ball until the speed fell within range. One good impact for each of the six balls in a group was used. A "good" impact meant that the inbound speed of the ball was within range of the target speed, and the rebound of the ball went back directly through the light gates on the same plane as it did prior to impact. This was verified for every impact by the use of a high speed video camera operating at 250 frames per second. Only one good impact per ball was used so as to reduce the chances of the ball being permanently damaged, especially at the higher speeds of 120 and 130 mph.

With the peak force, pitch speed, rebound speed, and ball mass now known, a dynamic COR and stiffness for every impact could be calculated. The average dynamic COR and stiffness was taken for the six good impacts at every speed. The plot of these results can be seen in Figures 3.6 and 3.7.

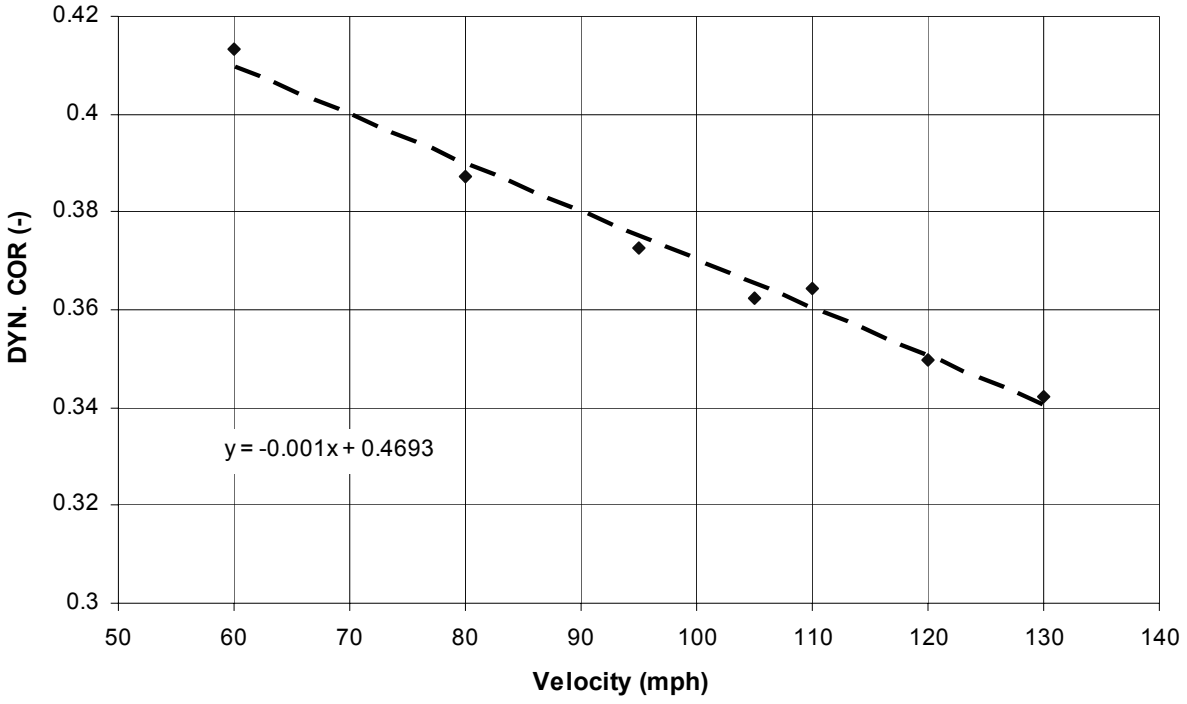

Figure 3.6 - Average dynamic COR vs. velocity results.

The dynamic COR results of the testing over the range from 60 to 130 mph proved to be very linear. From previous COR work done against a rigid flat plate [3.2, 3.6], the downward trend of a ball's COR with increasing velocity was observed and thus was expected here even though the impact surface was now cylindrical.

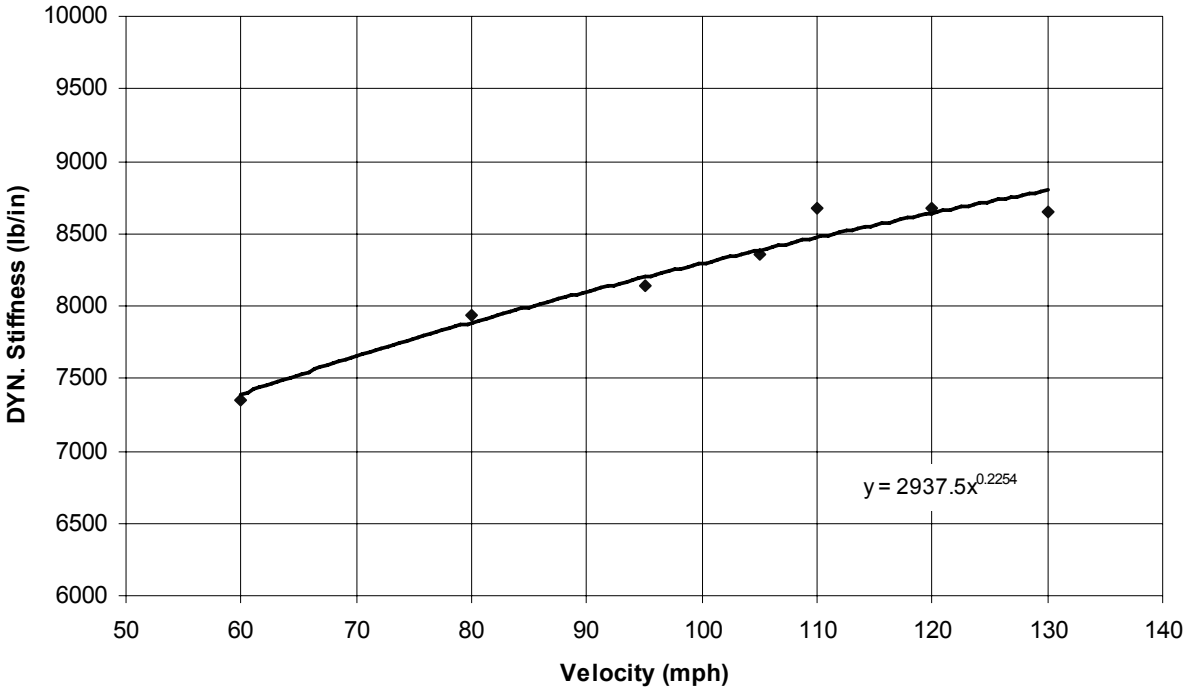

Figure 3.7 - Average dynamic stiffness vs. velocity results.

With the dynamic stiffness formulation based on a linear spring model, one would assume that the stiffness value would be constant for the entire range of speeds at which they were tested, but the upward trend presented in Figure 3.6 obviously shows that this isn't the case. Additional testing with different ball makes and models may prove differently, but for this specific Worth ball, the dynamic stiffness increased with impact speed.

Although the dynamic stiffness does increase with speed, a linear trend should still be seen. Unfortunately, it didn't prove to be as linear as expected. There was a reasonable amount of scatter in the dynamic stiffness from ball to ball in any speed group even though the dynamic

COR values for the same set of balls were very consistent from ball to ball. This scatter may be the reason for the lack of linearity over the range of test speeds.

There was concern that the polyurethane core of the softballs used at 130 mph could be damaged at that speed, so that same group of balls was tested again at 80 mph as a check to see if their resulting average dynamic COR and stiffness would match that of the balls in the 80 mph group. Any significant difference between the two sets of balls would be a good indicator of damage induced in the ball simply from testing it at the higher speed. The average dynamic COR of the original 80 mph test group and the 130 mph balls tested again at 80 mph were 0.38705 and 0.38708, respectively. Additionally, the dynamic stiffness values were compared and the average dynamic stiffness for the original 80 mph test group and the 130 mph balls tested again at 80 mph were 7939.5 lb/in and 7621.8 lb/in, respectively. With the difference in dynamic COR being negligible, and the difference in dynamic stiffness being only 4% between these two sets of balls tested at 80 mph, it was presumed that the balls used at 130 mph were not appreciably damaged during the course of their testing.

3.3.2 Finite element modeling and calibration of ball model

Physically, a ball impacting a rigid cylinder is not equivalent to a ball impacting a hollow cylinder that is allowed to recoil, so a correlation was needed to allow for the application of the dynamic stiffness data to the bat-ball simulations that were to be run. Smith, Duris, and Nathan [3.3] developed such a relationship by comparing the force of impact on a rigid and recoiling cylinder. By assuming the ball had undergone the same deformation for both situations, a formula was developed to relate the impact speeds of a rigid cylinder and one that was allowed to recoil as

$$v_r = v_f \left(1 + \frac{m_b r^2}{I} \right)^{\frac{1}{2}} \qquad 3.4$$

where v_r and v_f are the incoming ball speeds for the recoiling and fixed impact conditions, respectively, m_b is the mass of the ball, r is the distance from the pivot to the impact location on a bat, and I is the MOI of the bat about that same pivot point. For this work it seemed most appropriate to rearrange equation 3.4 because v_r was chosen in advance for the bat testing and v_f was needed for the finite element ball calibration. Rearranging equation 3.4 for v_r yields,

$$v_f = \frac{v_r}{\left(1 + \frac{m_b r^2}{I} \right)^{\frac{1}{2}}} \quad . \qquad 3.5$$

A bat with an MOI of 8500 oz-in^2, for example, impacted at 21 inches from the pivot point with a seven ounce ball fired at 110 mph should produce the same ball deformation as if the ball was fired at a rigid cylinder at 94 mph.

With this relationship in hand, the actual modeling and calibration of the ball model could then be undertaken.

LS-DYNA (Livermore Software Technology Corporation, Livermore, CA) version 970 release 5434a was used as the finite element program to carry out all the simulations in this work. It is a general purpose finite element code used for analyzing the large deformation dynamic response of structures including structures coupled to fluids [3.7]. Many elements and element options are available for use within this program. Only a few elements types were used within this work, and will be described in more detail as they are presented.

Coupled with this finite element code was the eta/FEMB-PC version 28 (Engineering Technology Associates, Inc., Troy. MI) pre- and post-processor. The pre- and post-processor was used for all the geometric modeling and meshing of the ball and/or bat simulations, as well

as the analysis of the results produced by LS-DYNA. This pre- and post-processor allowed for models of up to 250,000 nodes and elements [3.8].

The desktop computer used to carry out the finite element modeling operated using a single 3.00 GHz Intel Pentium 4 CPU, and 3.00 GB of available RAM.

The ball model, its subsequent mesh geometry, material type, and element formulation used in this work was developed by Duris for his thesis work [3.6]. The ball itself was modeled as a solid isotropic sphere having a radius of 1.91 inches, equivalent to that of a slow-pitch softball with a cover. The cover was not included in this model for simplification purposes, and as will be seen later, the ball model was tuned to the performance of a ball with a stitched on cover so the contribution of the cover and stitches were taken into account in the model.

The ball, consisting of 10240 8-node solid elements, was manually meshed by Duris. A viscoelastic material model (*MAT_006) was used for these elements and is based on the Power Law viscoelastic model. Recalling that the time-dependent shear modulus, G(t),

$$G(t) = G_{\infty} + (G_0 - G_{\infty})e^{(-\beta t)} \tag{3.6}$$

is a function of the long term shear modulus, G_{∞}, the short term shear modulus, G_0, and the decay constant, β, Duris showed that by adjusting one or more of these material properties allowed the ball to be tuned for dynamic COR and stiffness at a given impact speed. This tuning method was the method used here. The default "constant stress solid element" formulation was used as well for these elements.

The ball tuning was carried out by simulating the dynamic stiffness experiment. The only difference here was that the impact speed within the finite element simulation was determined by equation 3.5. The speeds at which the test bats were chosen to be impacted were 90, 100, 110, 120, and 130 mph, so an equivalent dynamic stiffness impact speed was needed for the

simulations and tuning of the ball. The ball deformation would be different at these various speeds, thus the ball model needed to be tuned for each impact speed.

The average weight of the balls used in the dynamic stiffness experiments was 6.745 oz. The specific weight of the ball was calculated based on the dimensions of the sphere and this average weight. Additionally, six test bats were chosen and their average MOI was determined to be 7028.73 oz-in^2. Preliminary finite element modeling of the bat-ball collision showed that the sweet spot, or location of highest rebound speed, was at 19 inches from the pivot point, thus, r was chosen to be 19 inches. With these parameters known, the equivalent dynamic stiffness test speeds were calculated. For the bat impact speeds, v_r, of 130, 120, 110, 100, and 90 mph, the resulting dynamic stiffness test speeds, v_f, are 112.0, 103.4, 94.8, 86.2, and 77.6 mph respectively.

The dynamic stiffness finite element model consisted of the ball model impacting a cylinder the same shape and size as the one used for the experiments, but because of symmetry, only one half of the ball and cylinder was modeled, as pictured in Figure 3.8, to reduce computation time. It was necessary to only model a quarter of the ball and cylinder because they are both symmetric on two planes, but the computation time for one simulation using half the ball and cylinder was approximately two minutes, so applying a second symmetry plane wasn't necessary.

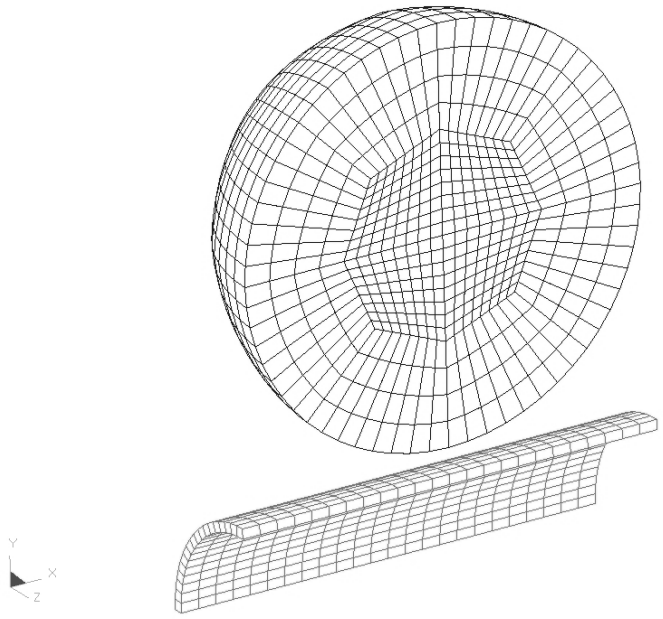

Figure 3.8 - Ball and cylinder model used to simulate the dynamic stiffness test.

The simulation was run for 0.002 s with an output frequency of 0.0001 Hz (*CONTROL _TIMESTEP), which allowed the ball to impact and rebound off of the rigid cylinder and reach a steady-state rebound speed. To simplify the extraction of the speed of the ball and the force exerted on the center element of the cylinder, the data was output to the *DATABASE_NODOUT and *DATABASE_RCFORC ASCII files, respectively. By utilizing these outputs, the time history for the selected nodes and elements was calculated and stored for a shorter output frequency of 0.00001 Hz. Typical time history plots reported to these ASCII files can be seen below in Figures 3.9 and 3.10.

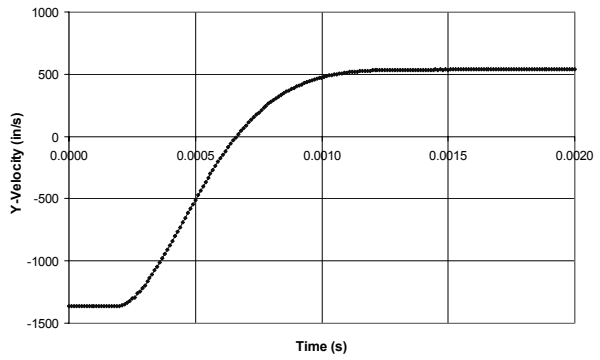

Figure 3.9 - NODOUT time history plot.

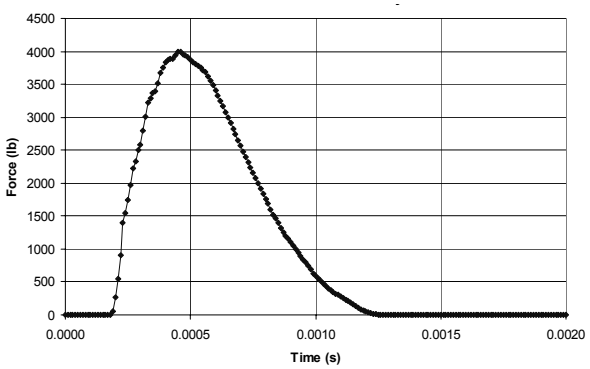

Figure 3.10 - RCFORC time history plot

The impact cylinder was modeled using thick shell elements (*ELEMENT_TSHELL) and the properties of steel were used. Although only an outer shell was modeled for the cylinder, all nodes were fixed to simulate the experimental boundary conditions. The appropriate boundary conditions were applied to both the ball and the cylinder to take into account the symmetry conditions. A contact (*CONTACT_SURFACE_TO_SURFACE) between the ball and the cylinder was defined with the upper half of the cylinder defined as the master segment and the lower half of the ball defined as the slave segment. LS-DYNA utilizes a contact algorithm and applies it when the two defined segments intersect one another. It is suggested that the master segment be part of the larger or stationary part, and the slave segment be part of the smaller or initially moving part. For these simulations, since an initial velocity was applied to the ball model, it was given the slave segment, and the cylinder, being rigid, was given the master segment.

The ball was assigned an initial velocity of v_f, and the calculated mass specific weight. Initial viscoelastic properties of bulk modulus K, short term shear modulus G_0, long term shear modulus G_∞, and decay constant β were also entered. Utilizing the experimental data for dynamic COR and stiffness, the simulations were run and the resulting rebound speed of the ball

and impact force was extracted using the eta/FEMB post-processing software. The rebound speed of the ball was taken from the speed of the center node of the ball model, and the impact force was taken from the force imparted on the surface of the cylinder which was in contact with the ball. The rebound velocity of the ball was taken from the center node of the ball to take into account any vibrations within the ball post-impact. These vibrations oscillate about the center of mass of the ball, hence the center node was chosen for the velocity output. The resulting dynamic COR and stiffness values were calculated for every simulation and compared to the experimental values for the appropriate rigid cylinder impact speed, v_f.

Using Duris' thesis work [3.6] for direction on what properties of the viscoelastic ball model changed what performance value, dynamic stiffness or COR, one or more of these properties was adjusted and the finite element simulation was run again. In an iterative fashion, small adjustments were made until the model produced the proper dynamic stiffness and COR for the appropriate impact speed. The viscoelastic properties used to achieve the proper results for the four impact speeds, and the target dynamic COR and stiffness can be seen in Table 3.1 below. For a complete list of all the iterations used to find these values, please see Appendix one, Table A1.1.

Table 3.1 - Viscoelastic material properties for the tuned ball models (Worth ball).

							Experimental/Target		FE Simulation	
v_f (mph)	v_r (mph)	Specific weight (lb·s^2/in)	Bulk Modulus (psi)	G_0 (psi)	G_∞ (psi)	β (Hz)	DYN. COR (-)	DYN Stiffness (lb/in)	DYN. COR (-)	DYN Stiffness (lb/in)
90	77.6	0.000038	8.0x10^5	28000	1590	66000	0.392	7831	0.393	7827
100	86.2	0.000038	8.0x10^5	28000	1520	64000	0.383	8020	0.377	8026
110	94.8	0.000038	8.0x10^5	28000	1480	68000	0.375	8195	0.371	8228
120	103.4	0.000038	7.0x10^5	28000	1400	71000	0.366	8357	0.365	8390
130	112.0	0.000038	7.0x10^5	28000	1300	74000	0.357	8509	0.354	8519

Although the calculated dynamic COR and stiffness values from the finite element simulations didn't match the experimental values perfectly, they were all close to or within one standard deviation range of experimental scatter. Figures 3.11 and 3.12 show a comparison between the finite element model results and the averaged experimental values for dynamic COR and stiffness. Additionally, the standard deviation was calculated for the experimental results at a given speed, and this data is represented in these Figures as error bars.

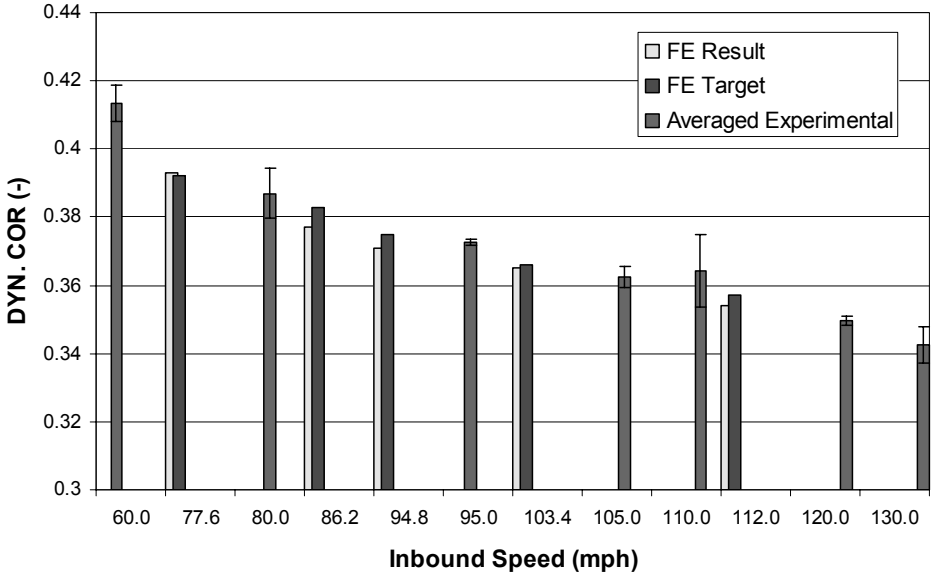

Figure 3.11 - Dynamic COR comparison showing finite element results and experimental scatter.

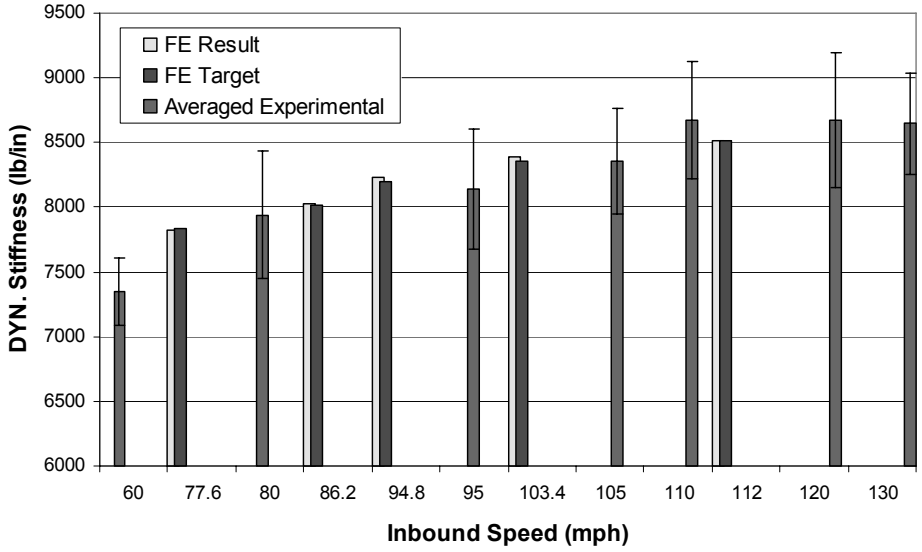

Figure 3.12 - Dynamic stiffness comparison showing finite element results and experimental scatter.

3.4 Summary

Experimental characterization of a slow-pitch softball was performed over a range of speeds using multiple balls and a high-speed ball cannon. The balls were fired at a rigid cylinder supported by four load cells. The subsequent impact force and rebound speed was recorded. The dynamic COR and stiffness for these impacts was calculated and recorded. A relationship was developed to correlate the speed of impact against a rigid cylinder to that of a hollow cylinder that was free to recoil, i.e. a hollow bat. This relationship was used to determine the speed at which the finite element model of the ball was to have its performance "tuned".

A finite element model of the ball was developed and its material formulation was based on the Power Law viscoelastic material model. Utilizing the developed speed correlation, the ball model was used to simulate the dynamic stiffness experiment and its properties were adjusted to achieve the correct performance. The method used to tune the ball model was successfully able to correlate the resulting finite element dynamic stiffness and COR values to that of the experiment.

This preliminary ball model development and tuning was critical to the work that will be described in the next chapter concerning the bat-ball modeling. Because the durability of the bat is directly related to the hardness of the ball, this characterization of the ball was necessary prior to performing any finite element modeling of the bat-ball collision.

REFERENCES

3.1 ASTM F 2219-05. *Standard Test Methods for Measuring High-Speed Bat Performance*. West Conshohocken, Pa. 2005.

3.2 Duris, J. *Experimental and numerical characterization of softballs*. Unpublished MS Thesis, Washington State University, December 2004.

3.3 Smith, L., J. Duris, and A. Nathan. *The Dependence of Bat Performance on Ball Properties.* Unpublished.

3.4 Suchy, J. Hillerich & Bradsbury (Louisville Slugger). *Private Communication*. December, 2005.

3.5 ASTM F 1887-02. *Standard Test Method for Measuring the Coefficient of Restitution of Baseballs and Softballs*. West Conshohocken, Pa. 2003.

3.6 Duris, J. *Experimental and numerical characterization of softballs.* Unpublished MS Thesis, Washington State University, December 2004.

3.7 *LS-DYNA keyword user's manual*. Version 970. Livermore Software Technology Corporation. April 2003.

3.8 *eta/FEMB-PC User's Manual*. Version 28. Engineering Technology Associates, Inc. October 2003.

3.9 ASTM F 1888-02. *Test method for compression displacement of baseballs and softballs.* West Conshohoken. Pa. 2003.

CHAPTER FOUR

- BAT MODELING AND EXPERIMENTAL COMPARISON -

4.1 Introduction

The bat-ball impacts presented in the previous chapter were performed at a speed that was low enough that it would not cause any permanent deformation in the barrel of the bat. The impacts presented in the following chapter were at speeds high enough that permanent deformation was expected. The numerical modeling builds on what was discussed in Chapter Three with the inclusion of plasticity material models within the finite element simulations, and the exploration of the effects of strain rate.

4.2 High speed ball cannon and test equipment

The same ball cannon as described in the previous chapter was used for the bat testing. The only difference in the experimental setup was that the dynamic ball stiffness setup and mounting bracket was replaced with a pivot fixture in which the bat was mounted and bolted to the end mill base. This pivot assembly, as seen in Figure 4.1, allows the bat to be positioned at the end of the light box and lets the bat swing freely after impact. The end mill base was computer controlled so that the height and impact location could be changed simply by making adjustments within the LabVIEW program.

Figure 4.1 - Bat pivot fixture.

4.3 Experimental test bats

4.3.1 Make and model

The bats used in this work were Louisville Slugger model SB806 single wall aluminum slow pitch bats, pictured in Figure 4.2. The advertised weight and length for these was 34 inches and 28 ounces, respectively. Upon receiving them, the grips and end caps were removed. The plastic end caps were removed to simplify the finite element models of the bat, as well as reduce the computation time of the simulations. The caps were removed simply by applying heat to them with a blowtorch until they were soft enough to be removed with pliers.

Because the focus of this work was on durability and not necessarily performance, the effects of the end cap were assumed negligible and not considered.

Figure 4.2 - Louisville Slugger "Gamer" model SB806

A sample of six bats was chosen, and with their end caps removed, the bats were then measured for length, weight, balance point, and moment of inertia (MOI). These measurements were taken in accordance with ASTM standard F2219 [4.5] and the resulting data for each bat can be seen below in Table 4.1.

Table 4.1 - Sample experimental test bat measurements.

Bat #	Measured Length (in)	Total Weight (oz)	Balance Point (in)	MOI (oz-in^2)
1	33.52	27.3	18.94	7036
2	33.52	27.2	18.96	7031
3	33.51	27.1	18.96	7008
4	33.52	27.2	18.94	7027
5	33.52	27.2	18.96	7040
6	33.54	27.3	18.94	7030
Average	33.52	27.2	18.95	7029
Std. Dev.	0.01	0.1	0.01	10

4.3.2 Bat material and nominal material properties

The SB806 model bats were made from 7046-T6 aluminum. The approximate material properties provided by Louisville Slugger [4.1] are as follows; yield strength of 60 ksi, ultimate tensile strength of 65 ksi, Young's/elastic modulus of 10.4 Msi, specific weight of 0.101879 lb/in^3, and a Poisson ratio of 0.30.

4.4 Bat modeling

As was done with the ball modeling and tuning, LS-DYNA was used for all the bat modeling and collision simulations. To properly model the bat, an accurate wall thickness profile was needed. Initially, a few measurements were taken using an ultrasonic thickness gage at incremental distances along the length of a bat. To verify these readings, the same bat was cut in half lengthwise and the thickness was measured at the same locations using calipers. Upon comparing the thickness data from the two methods, it was obvious that the ultrasonic gage

measurements were unreliable. Repeated measurements at the same location were very inconsistent and varied by up to about 5%. These inconsistencies were likely due to the flat surface of the measuring tip used. The bat was obviously round, so holding the flat surface of the measuring tip stationary against the bat surface was difficult. The caliper method was chosen to measure the profile and the bat was measured at one inch increments along the length. Additionally, the outer diameter was measured at these same locations, as well as the diameter of the knob. These measurements were then translated into x and y coordinates for use in the pre-processor model. A list of these profile coordinates can be seen in Appendix Two.

The profile coordinates could be entered directly into the pre-processor and the points connected by lines, but for this work, the points were entered into AutoCAD (Autodesk, San Rafael, CA) and a spline curve was fit between points to provide a smooth profile. The profile, both inner and outer, was then exported to a .DXF format file. This .DXF file was then imported into the eta/FEMB pre-processor. With the inner and outer profiles of the bat in place, the bat model could then be developed.

4.4.1 Thick shell element model geometry

An element that lent itself well to this type of geometry was the 8-node thick shell element (*ELEMENT_TSHELL). The thick shell element had three translational degrees of freedom per node, these nodes being located at the corners of the element. To perform in a shell-like behavior, a reference surface is constructed midway between the upper and lower surfaces of the element and a local coordinate system is implemented for use in the computations [4.2].

With a hollow geometry and a thin, or relatively thin, wall thickness, the implementation of this element allowed the bat to be modeled with only one element thru the thickness. In addition

to being designed for this type of geometry, it allowed for reduced computation time because of the reduced number of elements.

To model the bat using this element, the inner and outer profiles were rotated five degrees about the centerline of the bat and the ends of the profiles were connected by lines. To define the region to be meshed, the lower/inner surface was defined by four lines and the upper/outer surface of the bat was again defined by the other four lines. With the thick shell element, the order in which the lines are selected determines which surface of the element is the upper and lower [4.2]. For the bat model, it was important to define them in such a manner that the upper surface was at the exterior of the bat. The outward normal direction is dictated by the location of the upper surface of the element and with parts that come into contact with one another, it is ideal to have the outward normal directions pointed at one another.

The bat profile was discretized into four regions so as to dictate the element length and orthogonality to the surface profiles. For example, the straight section of the barrel was meshed and the element length was held to 0.25 inches. This ensured that the elements kept their rectangular shape. If the entire profile was meshed as a single section, the pre-processor allowed the elements to become skewed longitudinally along the length of the bat because of how the bat diameter changes. The element length was held to, or closely to, 0.25 inches for the other sections of the bat.

There were a total of 130 elements running the length of the profile. This total number of longitudinal elements was chosen in reference to the convergence study Cruz performed with 8-node solid elements [4.3]. He concluded that a model with 102 elements longitudinally was sufficient for the modal analysis work he performed. The computation time for his work was on the order of seven hours, but for this work it was considerably less, approximately one to two

hours, so 130 longitudinal elements was chosen. The shorter computation time may be attributed to increased computing power or the fact that these models were bat-ball collisions, not modal analysis.

With the length of the bat meshed, the elements were copied and rotated another 35 times to produce the final bat profile, as seen in Figure 4.3. (Because of symmetry, only 180 degrees of the bat was modeled) The resulting model had a total of 4680 thick shell elements.

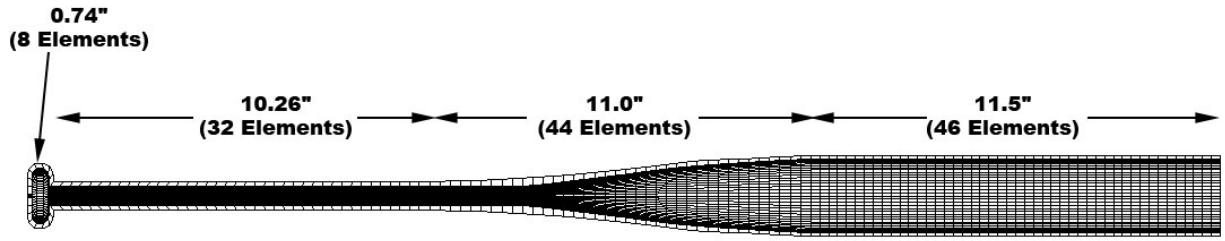

Figure 4.3 - Revolved mesh of thick shell model.

4.4.2 Solid element model geometry.

A second type of bat model was explored using 8-node solid elements (*ELEMENT_SOLID). The reason for the inclusion of this element type was to see if the results would correlate better with the experimental values as compared to the thick shell models. Additionally, Cruz [4.3] was successful employing these elements for performing modal analysis, so it was suggested that an attempt be made to use them for this work.

The same bat profile was used for the work performed with this element as was used for the thick shell element. It was known from Cruz's work that the computation time using the 8-node solid element was considerable, so a compromise was made where only a region of this bat model was meshed with solid elements. A six inch region centered at the 19 inch impact location (25 inches from the knob end), was meshed with the solid elements and the remainder of

the bat was modeled using thick shell elements in the same fashion as the model that uses them exclusively. Again, the thick shell element length was held to, or close to 0.25 inches. In the event of plasticity in this model, the six inch region modeled with solid elements would provide more than enough area such that all the plasticity that would occur would take place within this region.

The solid element is much more sensitive to aspect ratio. Too high of an aspect ratio and the element will not perform correctly. Additionally, a mesh with only one element thru the thickness would not be able to accurately describe the bending response that takes place during the impact [4.4], so the impact region that used these elements was modeled with multiple elements thru the thickness. Models with two, three, and four elements thru the thickness were investigated. These can be seen in Figures 4.4, 4.5, and 4.6. The aspect ratio of these solid elements was also held to 3:1 or less (longitudinal length to thickness). With this region being held to exactly six inches, the element length was dictated by the number of elements thru the thickness and the target aspect ratio of 3:1 or less. For each of these models, they consisted of 3816 thick shell elements and 3168, 7020, and 12528 solid elements for the two, three, and four element models, respectively. As with the thick shell model, all of these models were meshed taking into account symmetry and used 36 elements circumferentially.

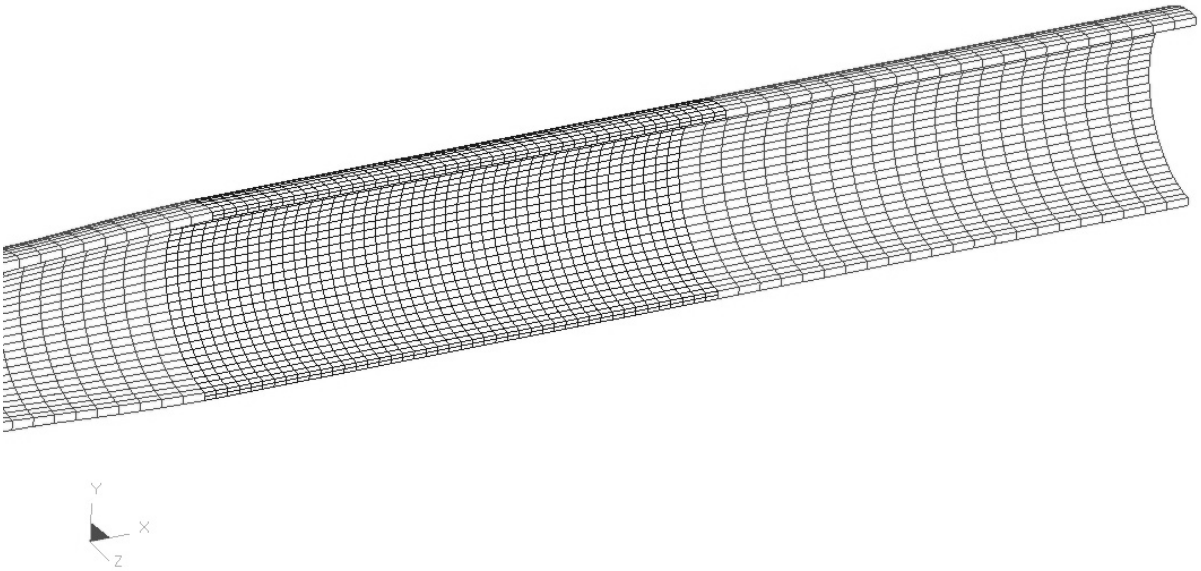

Figure 4.4 - Solid element model with 2 elements thru the wall thickness.

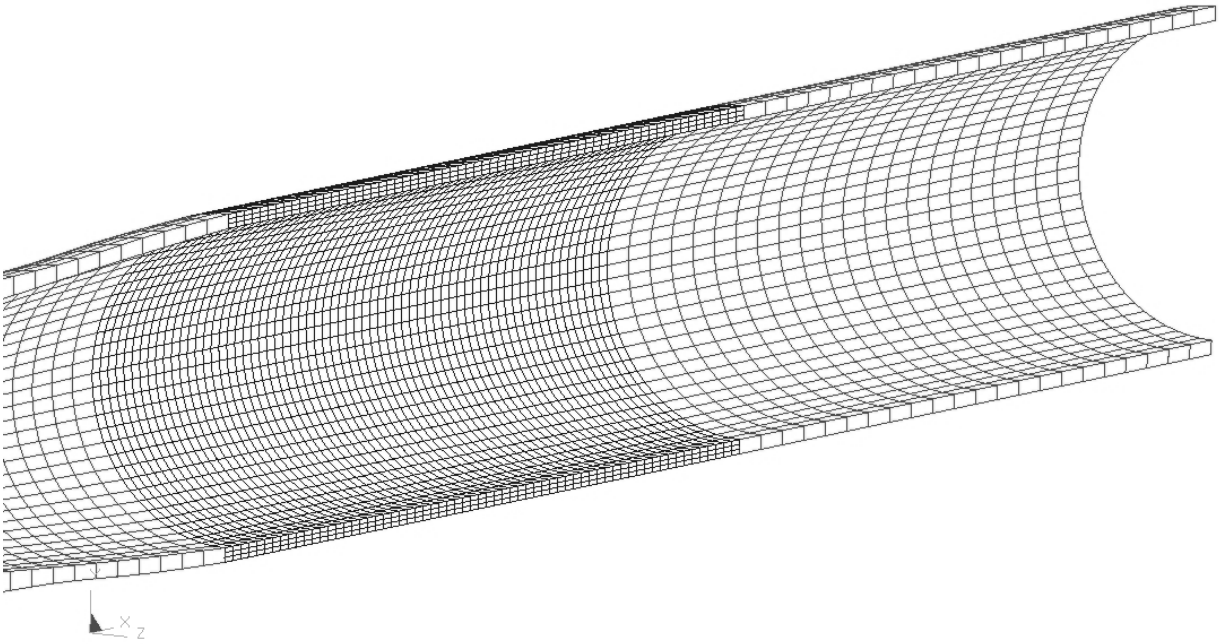

Figure 4.5 - Solid element model with 3 elements thru the wall thickness.

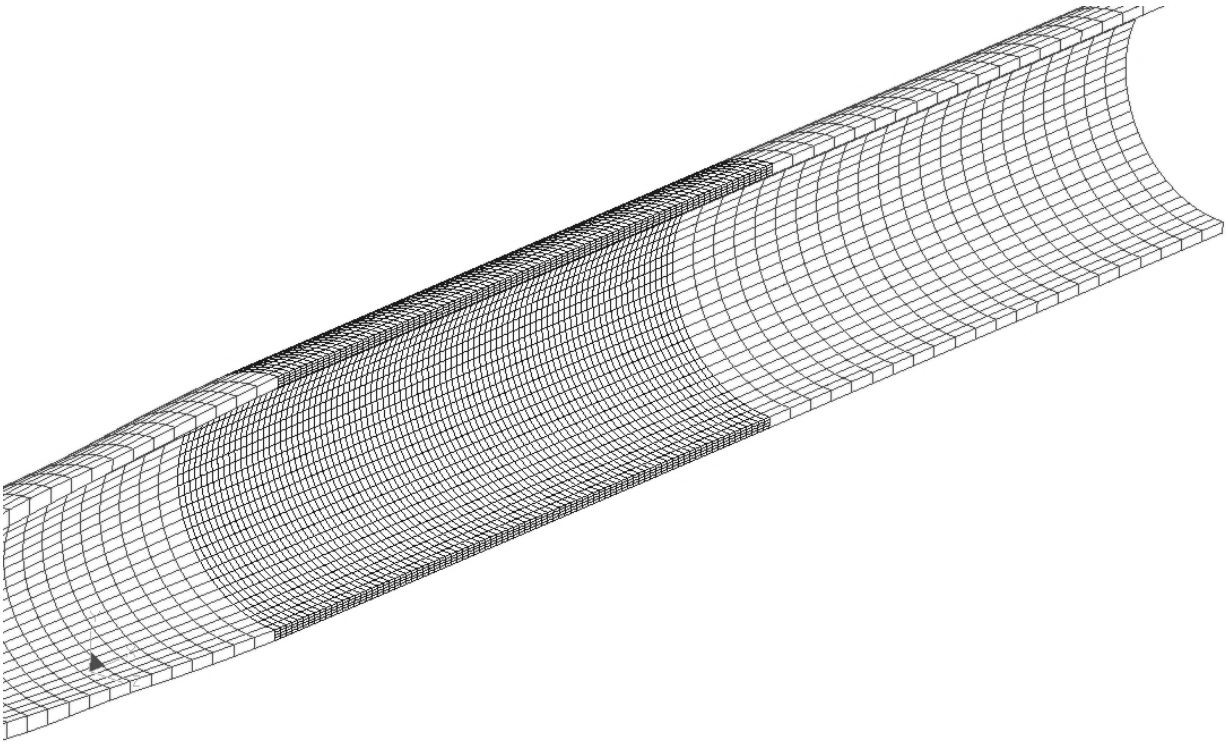

Figure 4.6 - Solid element model with 4 elements thru the wall thickness.

4.4.3 Inclusion of the ball model.

The viscoelastic ball model developed in the previous chapter was included in the bat model by importing the appropriate pre-processor file. The only difference here is that the Diamond brand ball was used. The properties of this ball were determined in the same fashion as was done for the Worth brand ball, and the material properties used to achieve the correct performance can be seen in appendix one, Table A1.2. The location of the ball was changed by moving all the nodes within the ball. Again, it is worth noting that the symmetrical condition was taken advantage of and only half of the ball was imported.

The appropriate material properties of the ball were applied according to the impact speed, and the ball was given the desired initial velocity by using the *INITIAL_VELOCITY card. The

initial velocity is applied to the nodes, so a node set was defined for the ball model, and every node within the ball was given the same initial velocity.

4.4.4 Application of boundary conditions.

The only boundary conditions that were applied to the bat-ball models were that of the symmetry condition and the pivot location. For the symmetry condition, every node either in the bat or ball that fell on the symmetry plane had a translational degree of freedom fixed such that the node could not deviate away from the symmetry plane at any time during the simulation. Both the solid and thick shell elements used in the bat models consisted of 8 nodes per element (located at the corners of the element) so it was necessary only to restrict the appropriate translational degree of freedom of the nodes that fell on the symmetry plane.

The simulation was meant to match the bat testing method set forth in ASTM F 2219 [4.5], so a pivot point six inches from the knob end of the bat was selected. This boundary condition was accomplished in the finite element model by restricting the translational degrees of freedom of the two nodes that fell on the six inch location. Only two nodes were needed to define the axis of rotation.

For both the symmetry and pivot boundary condition, the *BOUNDARY_SPC_SET_ID card was used.

4.4.5 Calibration of finite element model to the actual bat and ball.

For every model that was run in LS-DYNA, a d3hsp file was output that contained data pertaining to every part that was within the simulation. The data in the d3hsp that was of interest for calibration purposes was the calculated mass properties for every part. This data, consisting of the total mass, location of the center of gravity, and inertia tensor, was used to calculate the mass of the bat and ball, the center of gravity (CG) of the bat, and the ball mass. These

calculated values were then compared to experimental values. For the thick shell model and the model with solid elements, the calculated bat mass, center of gravity, and MOI were close initially, but with small adjustments to the material specific weight they were fine tuned even further. A comparison between model values and experimental values can be seen in Tables 4.2 and 4.3.

Table 4.2 - Thick shell model calibration comparison.

	FE Model	Experimental	% Difference
Ball Mass (oz)	6.745	6.745	0
Bat Mass (oz)	27.47	27.20	0.98
Bat CG (in)	18.84	18.95	-0.58
Bat MOI (oz-in^2)	7031	7028	0.04

Table 4.3 - Solid element model calibration comparison.[1]

	FE Model	Experimental	% Difference
Ball Mass (oz)	6.745	6.745	0
Bat Mass (oz)	27.45	27.20	0.91
Bat CG (in)	18.85	18.95	-0.53
Bat MOI (oz-in^2)	6977	7028	-0.73

The material specific weight used to produce these model values for the bat was then held constant for every subsequent bat-ball collision model, regardless of the plasticity model used. The aluminum densities used were 0.000249 and 0.000257 lb·s^2/in for the thick shell and solid models, respectively. The MOI calculated for the thick shell model most closely matched the experimental average, but to achieve such a result the specific weight had to be decreased 5.7% from the nominal value, whereas the solid element bat model deviated slightly more from the experimental value but the specific weight was only decreased 2.7 % from the nominal value.

[1] The bat models with two, three, and four solid elements thru the wall thickness produced the same bat mass, CG, and MOI.

4.5 Low speed impact strain comparison

To further verify the ball tuning procedure and bat model calibration, a low speed impact strain comparison was performed. This comparison consisted of instrumenting a bat with multiple strain gages and impacting it at a low enough speed that no plasticity would occur. The subsequent strains were then measured for that impact and compared to the results produced by the numerical model using the thick-shell bat model. Flexural, hoop, and impact strains were measured and compared. The flexural strain was measured at a location on the taper of the bat, the hoop strain was measured on the barrel, and the impact strain was measured at a location inside the barrel directly behind the impact location.

The impact speed for this study was 78.5 mph. The bat-ball collision for the impact at this speed was modeled as being elastic because the impact speed was so low.

4.5.1 Strain gage data collection

Because of the significance of strain in this work, it was important to be able to actually measure strain in a bat due to a ball impact prior to doing any finite element modeling for comparison and correlation. The equipment used in this work to measure strain consisted of multiple rosette strain gages, a strain gage conditioner, and a data acquisition board connected to the desktop computer that operates the ball cannon. The strain gages used were Vishay Micro-Measurements stacked rosette #C2A-13-062WW-350, with the gages oriented in a 0, 45, 90 degree orientation as can bee seen in Figure 4.7. This gage was chosen because it was designed for use with aluminum alloys and the stacked orientation would take into account any misalignment when the gage was applied.

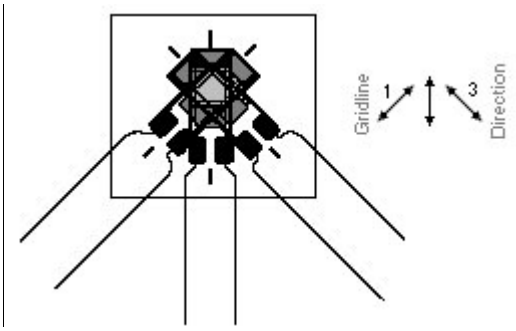

Figure 4.7 - Stacked rosette strain gage.

The strain gage conditioner used was a Vishay Micro-Measurements model 2160 with four independent channels. With one strain gage occupying each channel in the conditioner, this meant that the strains from only one rosette could be recorded at a time without the addition of more conditioners. The fourth channel in the conditioner was not used.

The analog data from the strain gages was taken through a data acquisition board and reported through LabVIEW on the same computer used to operate the ball cannon. 0.046 seconds of data was taken at a rate of 65000 Hz which equated to 3000 scans or data points. This duration of time/number of data points was more than sufficient to capture the strains the bat receives upon impact with the ball as well as the oscillations it undergoes post-impact.

4.5.2 Instrumented bat

The strains of particular interest to this work were at the point of impact from the ball. This was the first location selected for instrumentation, but the flexural strain and hoop strain were also of interest, so those were chosen as well. The exact location of where the strain gages were applied can be seen in Figure 4.8.

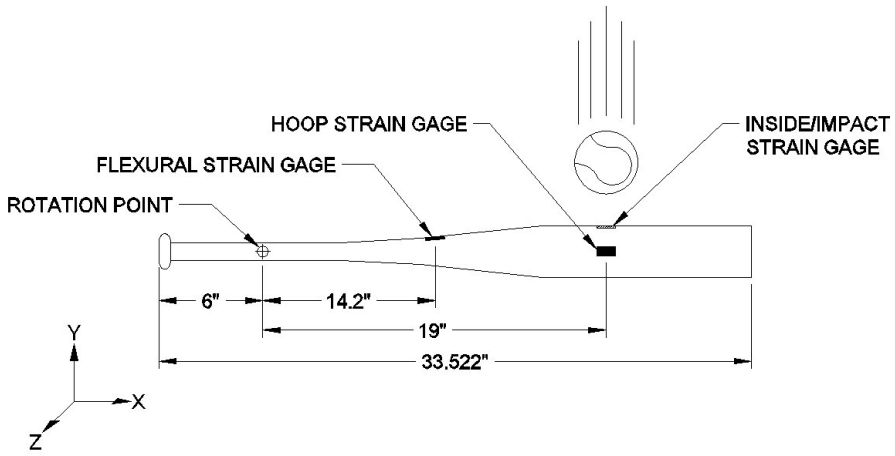

Figure 4.8 - Strain gage location on/in instrumented bat

The application of the strain gages on the outside of the bat was done following the instructions from the manufacturer and did not pose any problems as far as alignment went. The gage located in the barrel at the impact location was more difficult to apply and there were alignment concerns. As mentioned previously, the stacked gage orientation was meant to take into account any misalignment during application, but the goal was still to align them such that one of the gages was aligned with the axis of interest. For the inside rosette gage, the center/45° gage was ideally aligned with the longitudinal axis of the bat.

To accomplish the task of placing the inside strain gage, a rubber applicator was cut to the proper length and the strain gage was glued to it using rubber cement. The applicator was indexed off the end of the barrel and placed down the inside of the bat as seen in Figure 4.9. The rubber cement allowed the applicator to be pulled away after the epoxy adhesive (M-Bond AE-10 resin and curing agent, Vishay Micro-Measurements, Raleigh N.C.) had cured leaving only the rosette gage and wires intact within the barrel

The recommended pressure to adhere the strain gage was 5-20 psi. To apply this pressure during curing on the gage inside the barrel, a long latex balloon was used. The pressure within

the balloon was governed to about 15 psi for the duration of the curing by a regulator attached to a portable air tank, as seen in Figure 4.10.

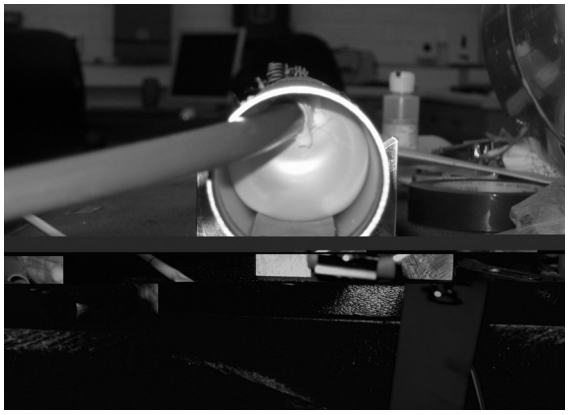

Figure 4.9 - Inside strain gage applicator.

Figure 4.10 - Air tank and regulator used for application.

All of the wires from the inside strain gage rosette were taped down using electrical tape to prevent them from breaking loose from the gage during impact. The instrumented bat was then re-measured for mass, center of gravity, and MOI. These values were then used for model calibration purposes. Figure 4.11 shows the inside gage adhered and the wires secured.

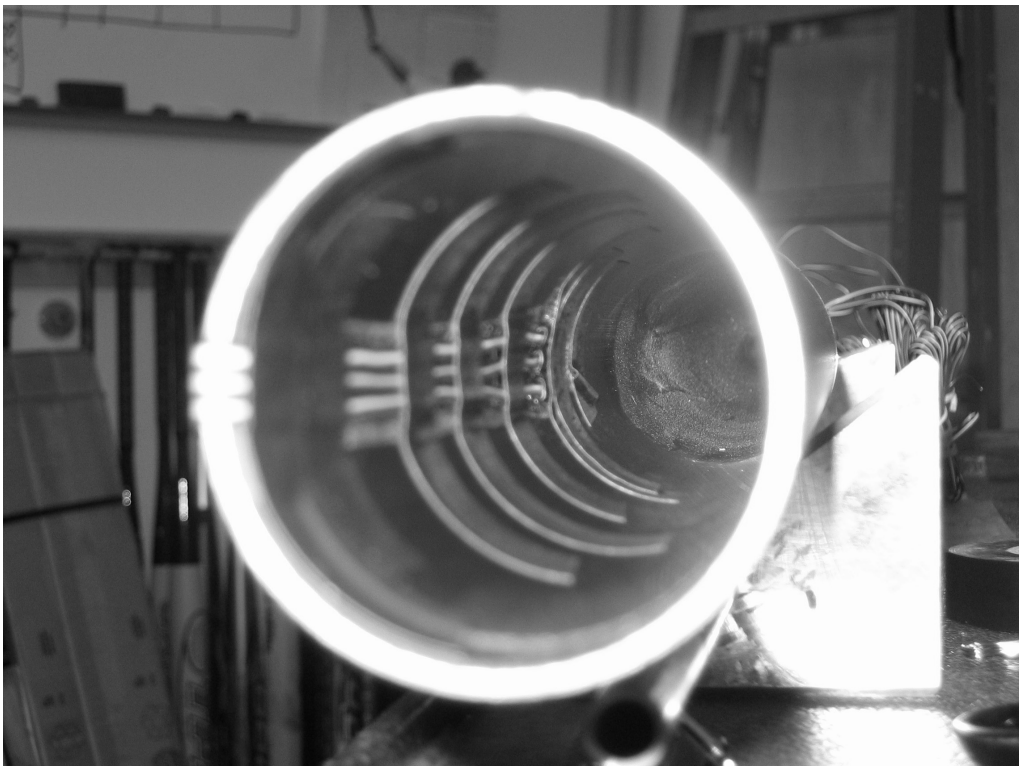

Figure 4.11 - Inside gage and wires adhered to the inside of the bat.

4.5.3 Experimental setup

The experimental setup used to impact this instrumented bat was no different than that outlined in section 4.1 for the rest of the test bats. The cabling for all of the gages was taped to the outside of the bat and it ran back close to the pivot clamp where it was suspended to allow the bat to swing without any added resistance from the wires. These cables were then routed to a terminal block where the connections to the strain gage conditioner were made. The mounted bat and the routed cables can be seen in Figure 4.12.

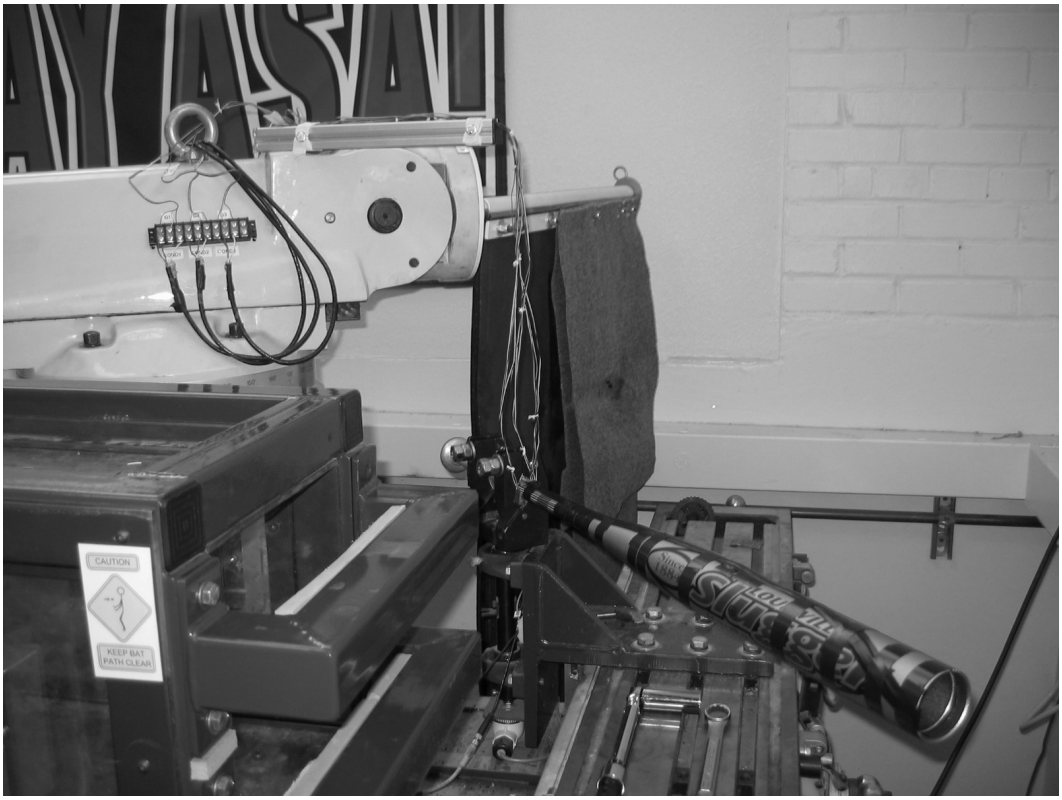

Figure 4.12 - Instrumented bat mounted and connected to terminal block.

The ball used for this testing was the Diamond Flyer model 12RSC 44 mentioned in the previous chapter.

4.5.4 Numerical strain output

For the instrumented bat experimental testing, the numerical data that was recorded was the time and the micro-strain value for each of the gages in the selected rosette. This set of data was recorded for each of the 3000 scans.

As for the finite element models, the strains were output for the appropriate element by matching their location and surface to that of the gage on the instrumented bat. The numerical data that LS-DYNA output using the *DATABASE_HISTORY_ELOUT card was the strain in global coordinates for every time step for the duration of the simulation.

To compare the experimental and numerical strains, the appropriate maximum or minimum principal and axial strains were calculated for every time step. For the experimental data, the first step was to transform the strain readings into normal strain components so they could be used for comparison to that of the model. The strain transformation [4.6] used was as follows in equation 4.1,

$$\begin{pmatrix} \varepsilon_x \\ \varepsilon_y \\ \gamma_{xy} \end{pmatrix} = \begin{bmatrix} \cos^2\theta_1 & \sin^2\theta_1 & \sin\theta_1\cos\theta_1 \\ \cos^2\theta_2 & \sin^2\theta_2 & \sin\theta_2\cos\theta_2 \\ \cos^2\theta_3 & \sin^2\theta_3 & \sin\theta_3\cos\theta_3 \end{bmatrix}^{-1} \begin{pmatrix} \varepsilon_1 \\ \varepsilon_2 \\ \varepsilon_3 \end{pmatrix} \tag{4.1}$$

where ε_1, ε_2, ε_3, were the strains measured by the first, second, and third strain gages of the rosette, respectively, θ_1, θ_2, θ_3, were the strain gage angles with respect to an alignment axis on the bat, and ε_x, ε_y, γ_{xy}, were the normal and shearing strains with respect to the alignment axis. Solving the three equations simultaneously in equation 4.1, the normal and shearing strains could be found and the maximum and/or minimum principal strains could then be calculated using equation 4.2,

$$\varepsilon_{\max,\min} = \frac{\varepsilon_x + \varepsilon_y}{2} \pm \sqrt{\left(\frac{\varepsilon_x - \varepsilon_y}{2}\right)^2 + \left(\frac{\gamma_{xy}}{2}\right)^2} \tag{4.2}$$

where ε_{max} and ε_{min} are the maximum and minimum principal strains, respectively.

4.5.5 Strain results and comparison to numerical simulation.

Although the models used for this comparison were elastic in nature, there were a few variables within the pre-processor material cards that needed to be finalized prior to running. Both models used thick shell elements and for their formulation it was suggested that five integration points be used thru the element thickness [4.4]. The default number of integration points is two. A brief study using two, three, five, and seven integration points showed that the model deformations converged to the same value with the use of five integration points thru the

thickness and there was no appreciable difference in the results using seven integration points. Also, the shear factor used for this element property was set to 5/6, as recommended by the LS-DYNA user's manual [4.7], and the default element formulation, one point reduced integration, was used to reduce computation time

As for the models that used solid elements, the only variable in the element property was the element formulation. The default element formulation, constant stress solid element, was used for accuracy and computational time reasons [4.8].

For the flexural strain comparison, the gage was on the outside of the bat and care was taken to align one of the gages with the centerline of the bat, so it was appropriate to compare the axial strains generated by this rosette to that of the numerical simulation. These results can be seen below in Figure 4.13.

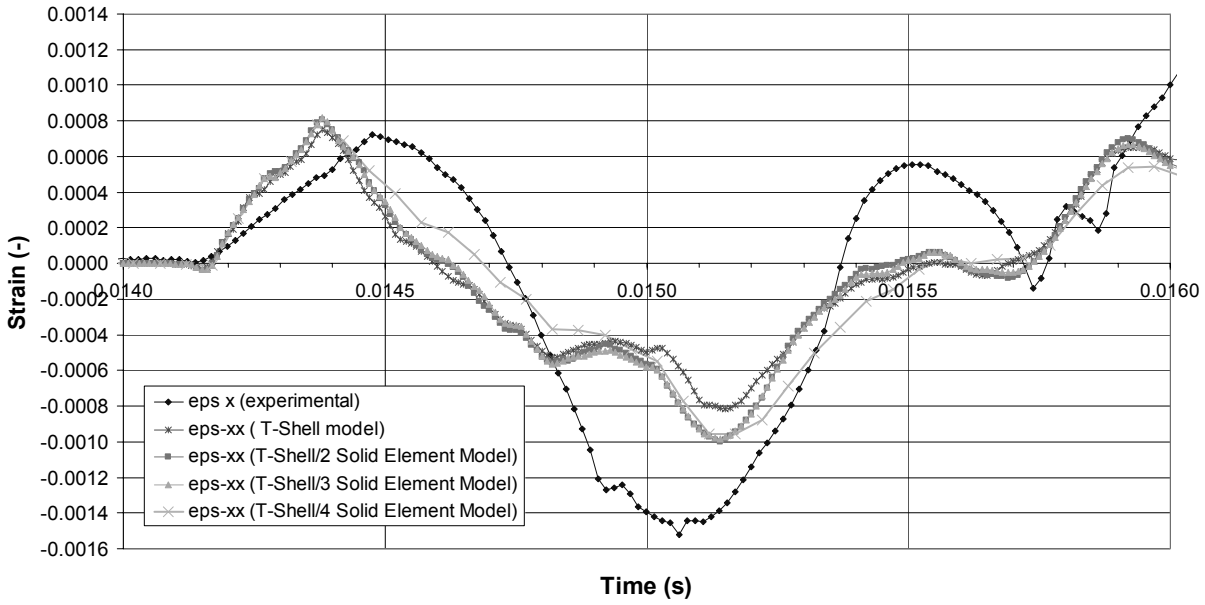

Figure 4.13 - Flexural strain comparison for a low speed impact at 19 inches.

The data that was of most interest for the flexural strain comparison was the peak strain value during impact. The duration of impact is shown in Figure 4.13 as the first half oscillation where the strain was climbing almost linearly and then reached a peak and declined rapidly. The

data following this first peak represents post impact free vibrations. Ideally, the peak strain value and time would be the same for the model and simulation, but the data generated here showed that the finite element simulations produced a slightly higher flexural strain and that it occurred shortly before when the experimental data said it should happen. The reason for this may be that the MOI of the bat pivot clamp was not accounted for within the numerical models. The MOI of this fixture was approximately 192 oz-in^2. A comparison of the peak strain values is shown below in Table 4.4.

Table 4.4 - Peak flexural strains for a low speed impact at 19 inches.

	Strain (-)	Difference (%)
eps-xx (experimental)	0.000723	-
eps-xx (T-Shell Model)	0.000750	3.56
eps-xx (T-Shell/2 Solid Element Model)	0.000805	10.14
eps-xx (T-Shell/3 Solid Element Model)	0.000816	11.37
eps-xx (T-Shell/4 Solid Element Model)	0.000776	6.84

The same comparison was made for the hoop strain generated during impact as well and the resulting experimental and simulation data can be seen in Figure 4.14.

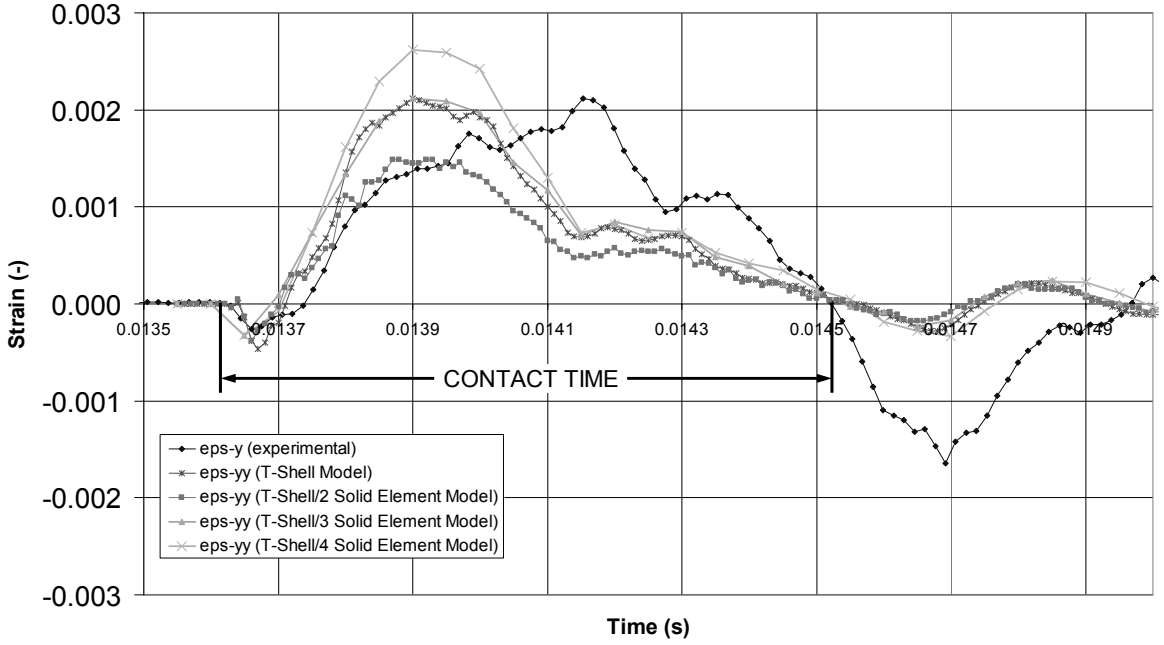

Figure 4.14 - Hoop strain comparison for low speed impact at 19 inches.

Here again, the peak strain values generated by the simulation during impact were expected to have the same magnitude and occur at the same time as that of the experiment, but the model's strain response demonstrated the same phase shift as was generated for the flexural strains. The peak hoop strains from the models were not as consistent from model to model as the flexural strain results were. A peak hoop strain comparison can be seen in Table 4.5.

Table 4.5 - Peak hoop strains for a low speed impact at 19 inches.

	Strain (-)	Difference (%)
eps-y (experimental)	0.002115	-
eps-yy (T-Shell Model)	0.002119	0.20
eps-yy (T-Shell/2 Solid Element Model)	0.001490	-41.94
eps-yy (T-Shell/3 Solid Element Model)	0.002119	0.21
eps-yy (T-Shell/4 Solid Element Model)	0.002620	19.29

Finally, the strains measured inside the barrel directly behind the impact location were compared to the finite element simulations. For this comparison, the minimum values of the first oscillation were of interest and compared. All of the finite element simulations demonstrated positive, or tensile, strains immediately upon impact, whereas the experimental strains were slightly negative, or compressive, for the same duration of time. Other than this initial discrepancy, the experimental and numerical values follow the same trend. As can be seen in Figure 4.15, the numerical models again exhibited a slight phase shift in reference to the experimental response.

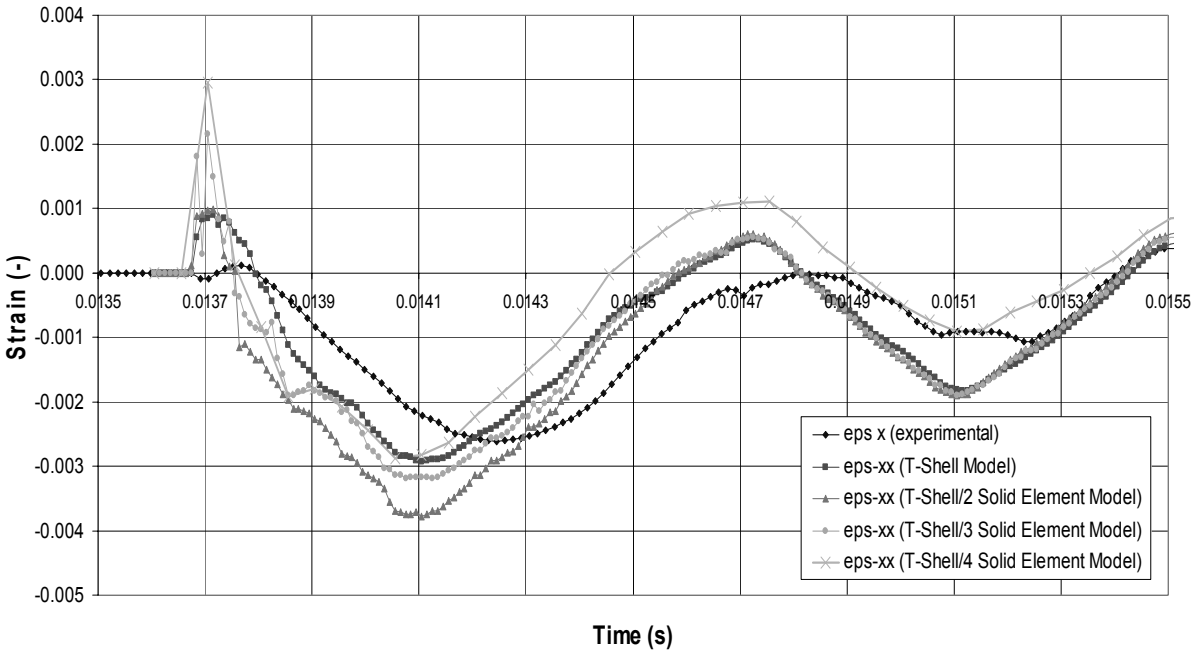

Figure 4.15 - Inside/Impact strain comparison for a low speed impact at 19 inches.

All of the finite element models showed an initial positive strain upon impact, whereas the experimental results showed little or no positive initial strain. Intuition would say that one would expect this positive strain because of the bending behavior and location of the strain measurement, but the experimental results showed otherwise. Regardless, the minimum impact strains were compared, as can be seen in Table 4.6.

Table 4.6 - Minimum impact/inside strains for a low speed impact at 19 inches.

	Strain (-)	Difference (%)
eps-xx (experimental)	-0.00261	-
eps-xx (T-Shell Model)	-0.00292	10.72
eps-xx (T-Shell/2 Solid Element Model)	-0.00377	30.93
eps-xx (T-Shell/3 Solid Element Model)	-0.00320	18.42
eps-xx (T-Shell/4 Solid Element Model)	-0.00288	9.49

As with the hoop strain comparison, there was more variation from model to model for these results than for the flexural strain comparison.

As mentioned before, there was some uncertainty as to how well the gage inside the bat was aligned to the centerline of the bat, so the minimum principal strains were calculated from the data generated by the rosette and compared to those generated by the different models. Shortly after doing the experimental testing, it was realized that one of the gages was not working properly and was reporting erratic data. Fortunately it was not the gage that was meant for axial alignment. After reviewing the data generated by the various models and comparing it to the axial strain data only, as seen in Figure 4.15, it was concluded that the rosette was aligned well and there would be little effect on the principal strains due to the lack of data from the faulty gage. With the rosette aligned properly, this data could be recreated even though the gage was not working. The strains generated for this gage should be equivalent to that of the gage it was symmetric to, the 90° gage. The calculated minimum principal strains for the inside/impact gage are shown in Figure 4.16.

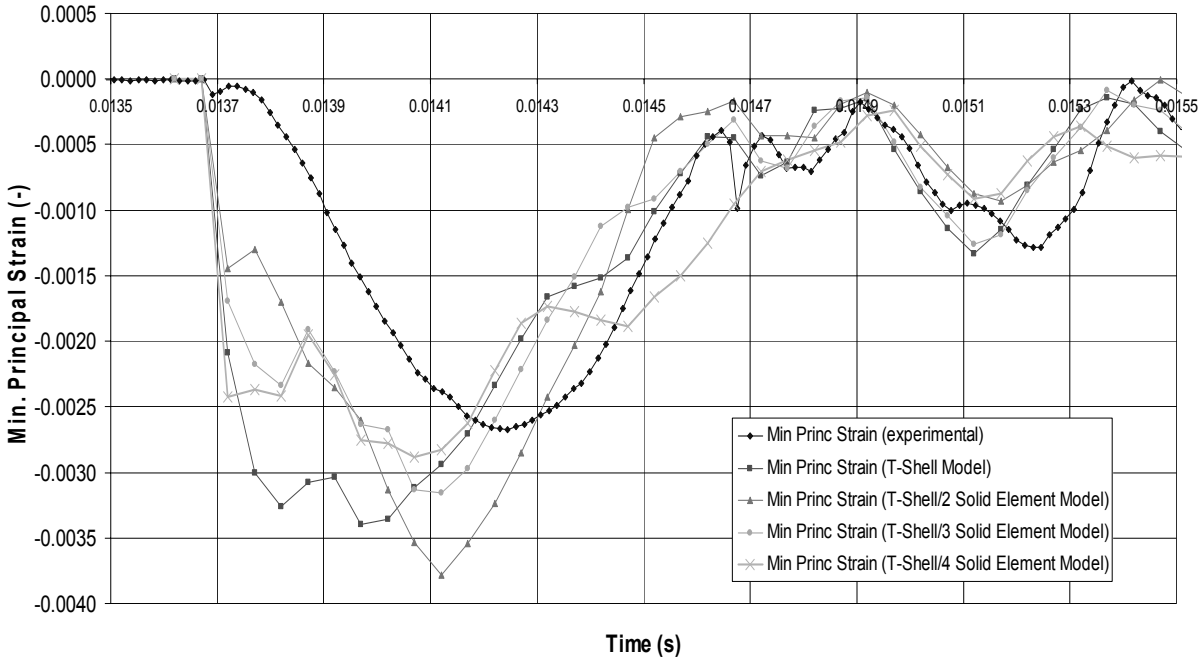

Figure 4.16 - Inside/Impact minimum principal strain comparison for a low speed impact at 19 inches.

Table 4.7 shows a comparison between the minimum principal strains for the experimental and numerical results.

Table 4.7 - Minimum principal strains for a low speed impact at 19 inches.

	Strain (-)	Difference (%)
Min Princ. Strain (experimental)	-0.00267	-
Min Princ. Strain (T-Shell Model)	-0.00340	21.40
Min Princ. Strain (T-Shell/2 Solid Element Model)	-0.00378	29.30
Min Princ. Strain (T-Shell/3 Solid Element Model)	-0.00315	15.25
Min Princ. Strain (T-Shell/4 Solid Element Model)	-0.00288	7.21

The principal strain comparison for the flexural and hoop gages can be seen in Appendix Three, Figure A3.1 and A3.1, respectively. Because their alignment could be seen during application, the principal strain comparison was not shown here.

4.6 High speed deformation comparison without accounting for strain rate.

4.6.1 Deformation comparison method.

For the high speed experimentation it was imperative to get a precise deformation measurement for comparative purposes. Prior to actually impacting the bat with a ball, an aerosol foot spray powder was used to lightly coat the area of the bat where the ball was to impact. This coating of powder allowed for a profile of the ball to be left on the bat after impact as seen in Figure 4.17.

Figure 4.17 - Ball impact profile

With the impact profile visible, it was then outlined with a permanent marker and the spray powder was then wiped off. Using these marks as a reference, the test bats were then mounted in a lathe and measured. By having the bat placed in a lathe with both ends centered in their respective fixture, it allowed for the use of a dial indicator mounted on the tool carriage. Mounting the dial indicator on the tool carriage allowed for easy movement along the length and circumference of the bat, while ensuring that the origin or set point would remain constant. A test bat mounted in the lathe for measurement can be seen in Figure 4.18.

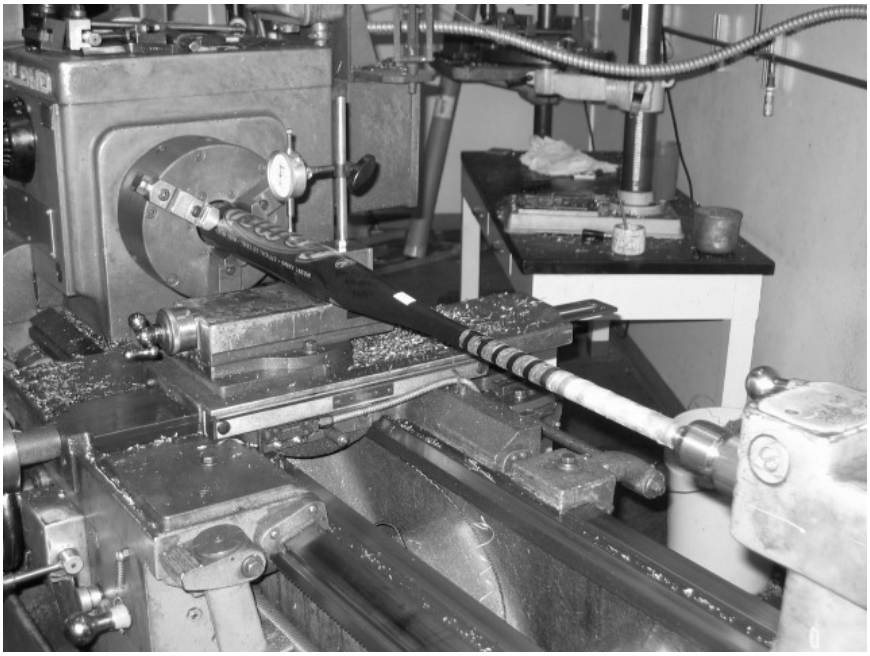

Figure 4.18 - Test bat mounted in lathe for measurement.

With the bat fixed in the lathe, the dial indicator was first used to scan the bat both longitudinally and circumferentially to locate the centerline of the bat and then to find the lowest point in the dent profile. The dial indicator was then zeroed and measurements were taken at ½ inch increments in both directions longitudinally along the bat for 3.5 inches. This was done for each of the bats impacted using the ball cannon. The dial indicator measurements can be seen in Figure 4.19.

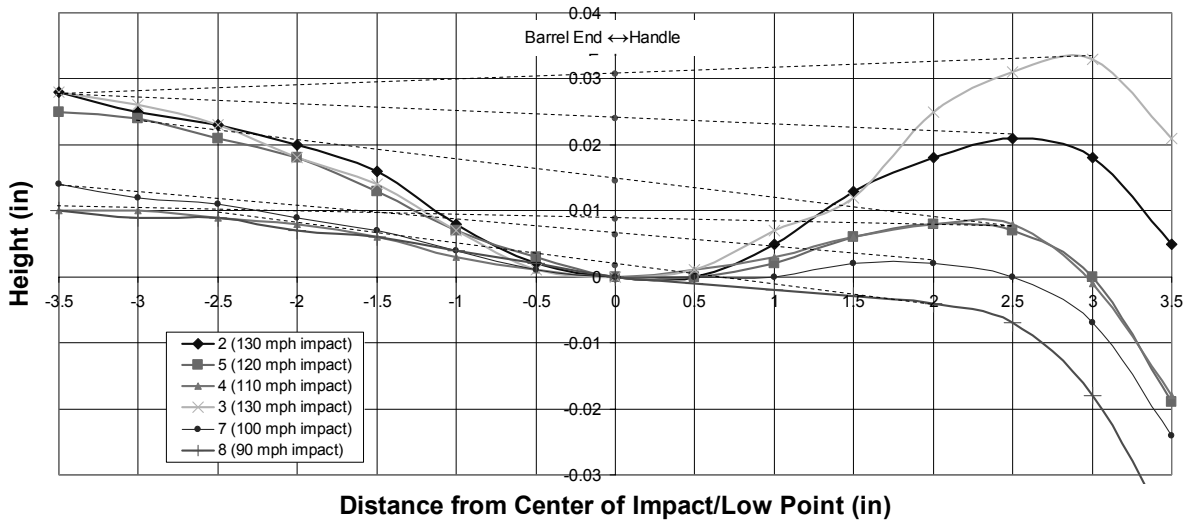

Figure 4.19 - Deformation measurements in test bats.

The maximum deformation was determined from the above measurements by calculating a y-intercept value for a straight line connected to the highest points on either side of the dent. This was done to take into account any possible manufacturing variations in the diameter of the bat. The calculated deformations can be seen in Table 4.8[2].

Table 4.8 - Calculated experimental bat deformations.

Bat #	Point/Slope Deformations (in)
2 (130 mph impact)	0.024
5 (120 mph impact)	0.015
4 (110 mph impact)	0.009
3 (130 mph impact)	0.031
7 (100 mph impact)	0.006
8 (90 mph impact)	0.002

The deformation that was generated in the numerical simulations was determined by measuring the outer diameter of the bat at the point of impact. This was done in the post-processor by utilizing the measurement command and selecting the node that was closest to the point of impact and the node that was on the opposite side of the bat. Because the bat was free

[2] Preliminary modeling showed poor correlation to the dent produced at 130 mph, so a second bat was impacted to verify the results of the first bat tested at 130 mph.

to vibrate post impact, the plotted diameter measurements showed that the bat was still undergoing hoop oscillations and there wasn't a constant diameter measurement. These oscillations were averaged out from the point at which the bat diameter exhibited this oscillatory motion to the end of the simulation. Figure 4.20 shows a sample plot of the diameter readings generated by the post processor and where the oscillations were averaged out.

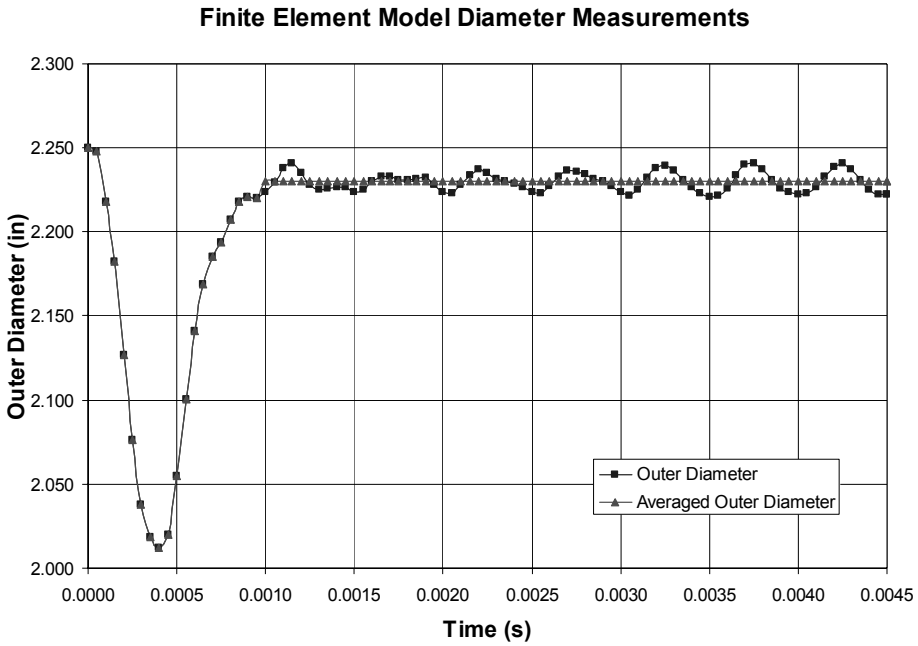

Figure 4.20 - Sample diameter readings taken from a finite element model.

4.6.2 Power Law isotropic hardening model comparison.

The first plasticity model chosen for comparison was the Power Law isotropic hardening model. To implement this model in LS-DYNA, the *MAT_POWER_LAW_PLASTICITY material card was used. The strength coefficient K, and the strain hardening exponent n, which are used in the flow curve to describe the behavior of the material in the plastic region, were determined from tensile test data provided by Louisville Slugger for the 7046 aluminum alloy and were calculated to be 82657 psi and 0.0684, respectively. Additionally, a yield stress and

elastic modulus were calculated from this tensile test data using a 0.2% offset, and were determined to be 58 ksi and 10.4 Msi respectively. The elastic modulus matched the nominal value provided, but the calculated yield stress was 2 ksi less than the nominal yield stress. Because the calculated yield stress was taken directly from the tensile test data that was going to be used to determine the Power Law hardening coefficients, it was used as the yield stress in all of the finite element models that utilized this material card. The tensile test data and the region used to calculate the Power Law hardening coefficients can be seen in Figure 4.21.

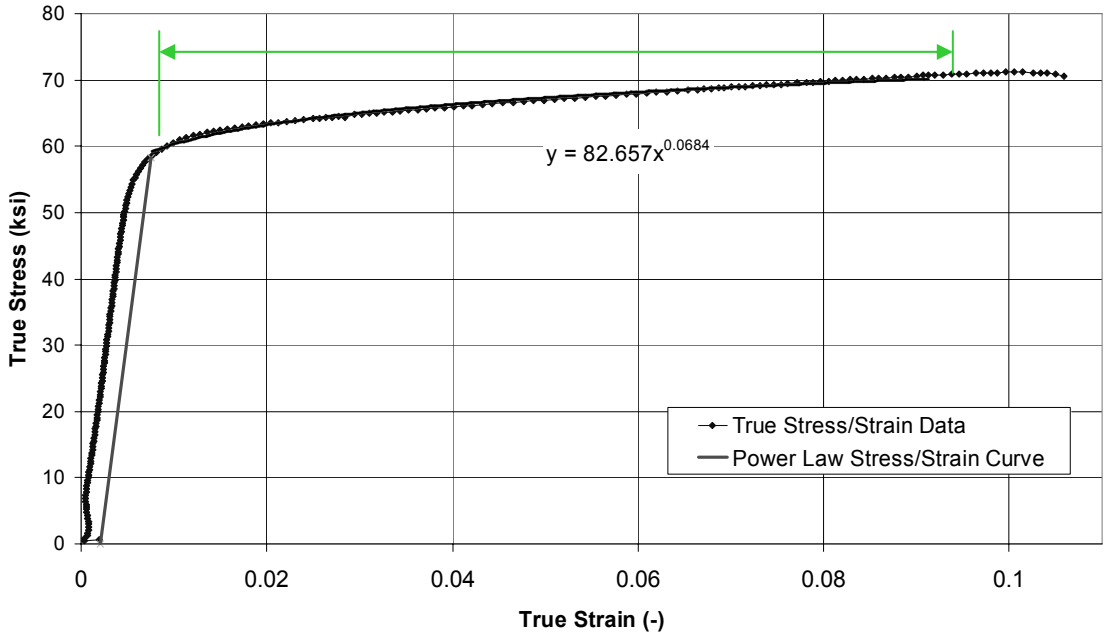

Figure 4.21 - True stress/strain data for 7046 aluminum and fit used for Power Law hardening.

The finite element models that were run using this material card were run at the highest impact speed of 130 mph.

The first model that was run was the thick shell model. As with the low speed impact model, five integration points thru the element thickness, a shear factor of 5/6, single point reduced integration, and Gauss quadrature was used for all of the elements. The deformation that resulted from this model was 0.25 inches as can be seen in Figure 4.22. Recalling that the

experimental deformations were 0.024 and 0.031 inches, it was suggested that the element mesh be refined in the region of impact to see if that would make a difference. So, the mesh was refined and the element length was held to 0.125 inches, doubling the number of elements in the impact region, and the model was run again. The resulting dent was still too deep and on the order of 0.25 inches as well.

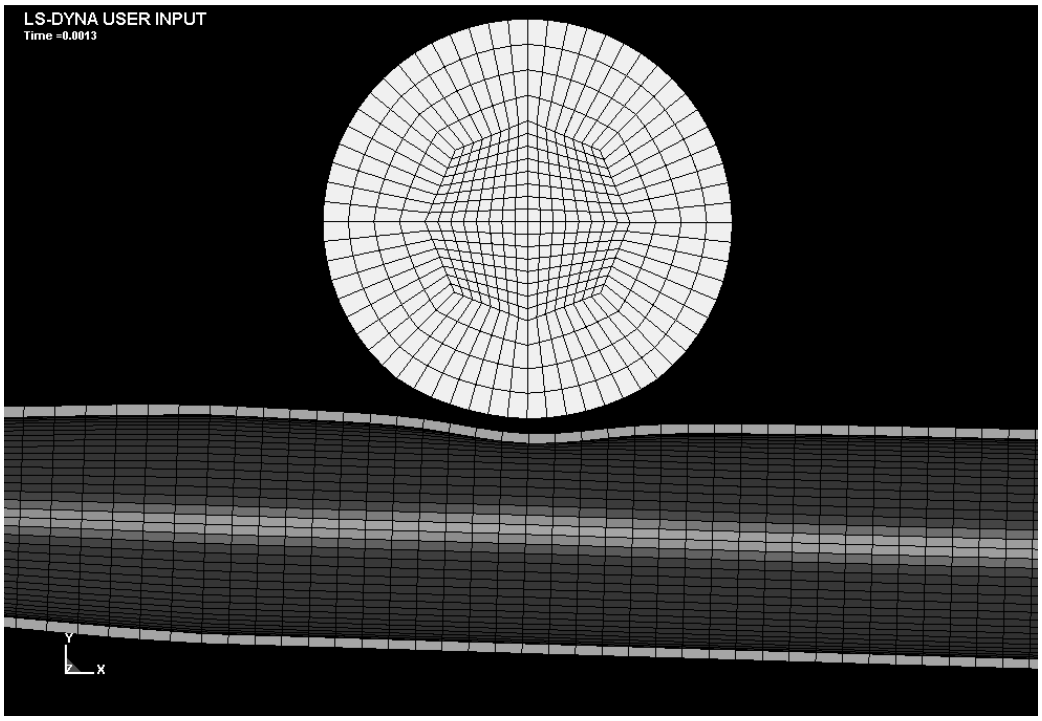

Figure 4.22 - Thick shell model deformation at 130 mph using Power Law hardening.

Since the deformation was too deep by a factor of about 10, and mesh refinement didn't make a noticeable difference, the solid element models were then used. As with the low speed testing, the solid elements used in the models with two, three, and four elements thru the wall thickness were held to a 3:1 aspect ratio and the default "constant stress solid element" formulation was used. The thick shell elements that made up the rest of the bat were given the same properties those described for the thick shell model. These models were run at 130 mph as well, and the resulting deformations can be seen in Table 4.9.

Table 4.9 - Solid element model deformations at 130 mph using Power Law hardening.

# Elements Thru Wall Thickness	Deformation (in)
2	0.070
3	0.280
4	0.260

There was a drastic improvement shown with the use of two solid elements thru the thickness, but when the models were run with three and four elements, the deformations were approximately the same as those for the thick shell model. Figure 4.23 shows this deformation for a four solid element model. Even though the deformation was now considerably closer for the two element model, it was high by at least a factor of 2.5.

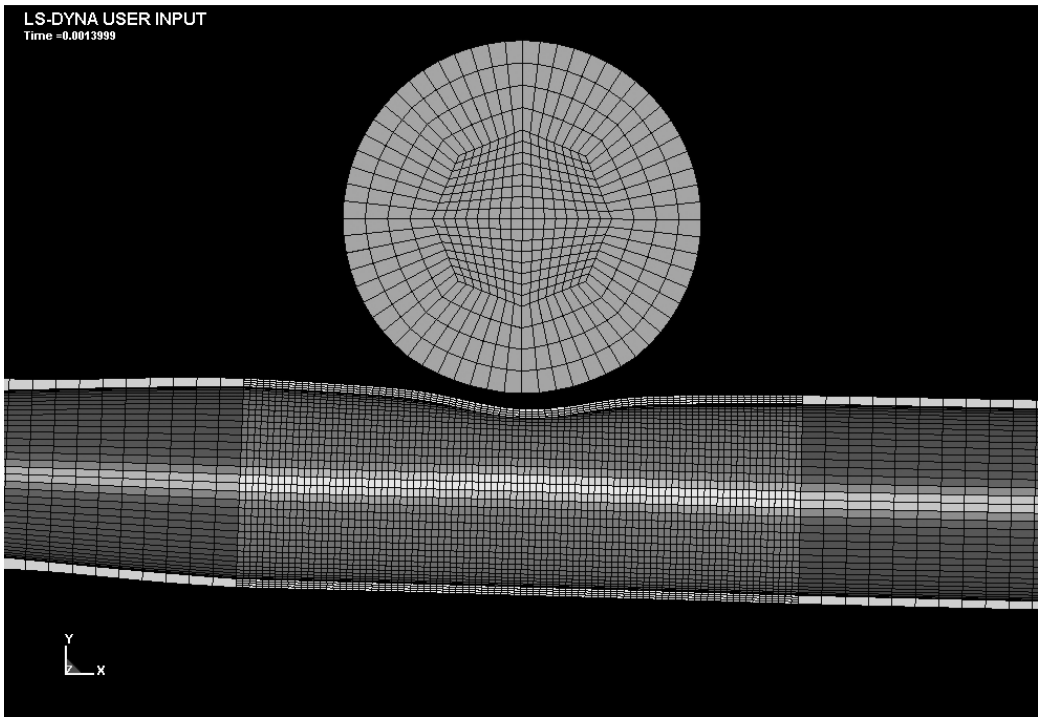

Figure 4.23 - Four solid element model deformation from a 130 mph impact using Power Law hardening.

4.6.3 Isotropic/kinematic hardening model comparison.

The second type of hardening law used to model the bat was one that was capable of implementing kinematic hardening as well. The LS-DYNA material card used for this material model was *MAT_PLASTIC_KINEMATIC. The use of this material card requires the input of a tangent modulus, a yield stress, a Young's/elastic modulus, and a hardening parameter, β. The hardening parameter can vary between 0 and 1, where 0 was a fully kinematic hardening model, and 1 was a fully isotropic hardening model.

This material model essentially modeled the stress-strain curve as being bilinear with the Young's modulus describing the behavior in the elastic region, and the tangent modulus describing the material behavior in the plastic region. Both the Young's/elastic and tangent modulii were again determined from the stress-strain data provided by Louisville Slugger, as well as the yield stress.

The tangent modulus is the slope of the line from the yield stress to the ultimate tensile stress on the true stress-strain curve. (The same region used to determine the Power Law hardening coefficients) A straight line was fit to this data and a tangent modulus of 116369 psi was calculated. The Young's/elastic modulus used was 10.4 Msi, the same value used for the Power Law hardening model. Because of the bilinear nature of the stress-strain curve used in this material model, if the same yield stress of 58 ksi was used for this model, the tangent modulus would be parallel to the true stress-strain data but would fall below the curve. So, to assure that the tangent modulus was falling on the tensile test data, a new yield stress was calculated by determining where the Young's/elastic modulus and tangent modulus would intersect. This yielding point was calculated to be 61165 psi. The tensile test data and the

bilinear representation of the stress-strain curve used for this material card can be seen in Figure 4.24.

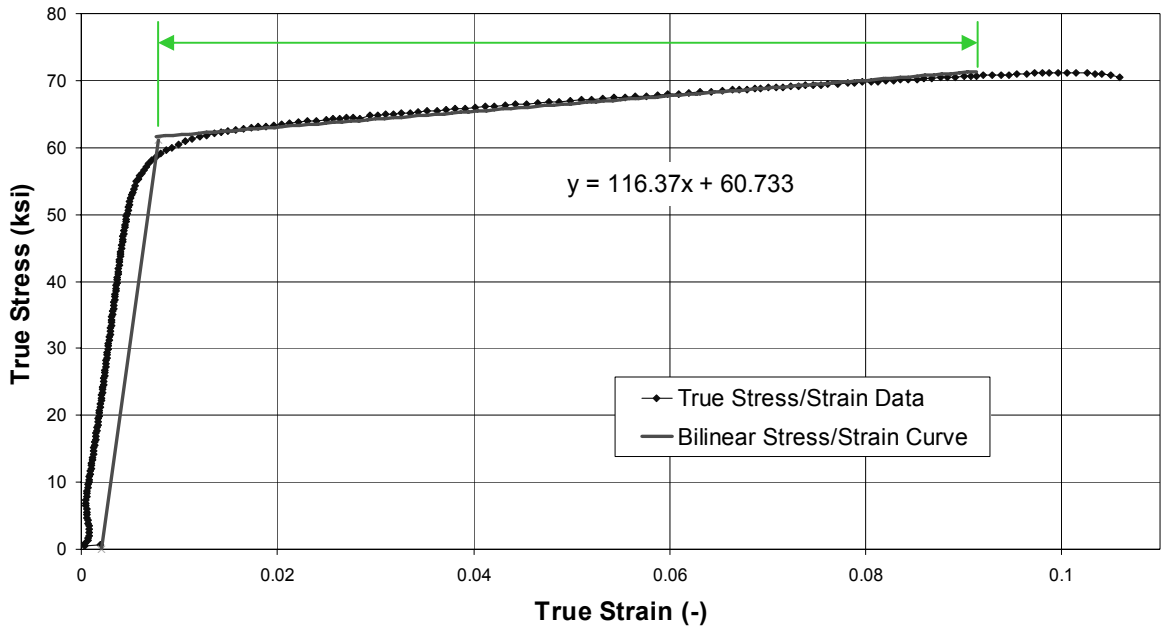

Figure 4.24 - True stress/strain data for 7046 aluminum and fit used for Isotropic/Kinematic hardening.

The same models were run again at 130 mph using this material card, but β was varied to see if it would have any effect on the resulting deformations. Three values of β were chosen, 1, 0.5, and 0. The predicted deformations for the thick shell model solid element models are shown in Table 4.10.

Table 4.10 - Model deformations at 130 mph for Isotropic/Kinematic hardening.

Model Type	B = 1	β = 0.5	β = 0
Thick Shell	0.242	0.231	0.238
2 Solid Elements	0.066	0.067	0.070
3 Solid Elements	0.275	0.275	0.273
4 Solid Elements	0.256	0.258	0.253

The results generated using this hardening model showed similar results when compared to those generated using the Power Law hardening model. It was expected that the deformations

for the fully isotropic model ($\beta = 1$) be similar to those generated by the Power Law hardening model, which they were, but of particular interest was the fact that there was very little difference between the fully isotropic and fully kinematic model results.

Regardless of the hardening law, the element type, or the number of elements thru the thickness, the predicted deformations were much greater than the measured values and it was obvious that something else was needed in the finite element models to increase their accuracy. It is worth noting that the material card *MAT_PIECEWISE_LINEAR_PLASTICITY was used as well to see if it would produce better results. This material card used actual true stress-strain data input by the user to define a piecewise stress-strain curve. The deformation it produced for a 130 mph impact was approximately 0.130 inches. The computation time using this material model increased depending on the options selected within the element formulation card but still produced the same approximate deformations, so it was not used again.

4.7 High speed deformation comparison taking into account strain rate.

It was suggested [4.8] that the lack of correlation of the models may be due to the fact that there was nothing included that took into account the hardening effects that high strain rates can have. At high enough strain rates, the material actually strengthens and exhibits behavior as if its yield strength has increased.

After reviewing the previous models and watching the strain rates calculated by the post-processor during impact, it was concluded that rate effects needed to be included. For the four solid element model using the Power Law hardening rule, at the instant of impact, the strain rate was approximately 36 s^{-1}.

4.7.1 Strain rate model used

Both the *MAT_PLASTIC_KINEMATIC and *MAT_POWER_LAW_PLASTICITY material cards used in the previous sections have the ability to include strain rate effects as well as hardening. The strain rate model that both these cards employ is the Cowper and Symonds model [4.7]. This model essentially scales the yield strength as a function of strain rate. This scaling factor is given as,

$$1+\left(\frac{\dot{\varepsilon}}{C}\right)^{\frac{1}{P}} \tag{4.3}$$

where $\dot{\varepsilon}$ is the strain rate, and C and P are scaling coefficients.

A previous work by Stranart [4.9] used values of 1300 and 5 for C and P, respectively, in his work involving modeling of hole expansion in 7075-T65 aluminum. No data could be found for use with the 7046 aluminum and this strain rate model, so the scaling coefficients used by Stranart were used here as well. Given the strain rate of 36 s^{-1} and yield strength of 58 ksi, these coefficients would produce a scaling factor of 1.49, significantly increasing the yield strength at that instant in the model. So, the effect of this additional model was expected to be dramatic.

4.7.2 Power Law isotropic hardening with Cowper-Symonds rate model comparison.

The material card chosen for the implementation of the Cowper and Symonds model was *MAT_POWER_LAW_PLASTICITY. This was chosen because the true stress-strain curve is better represented in the plastic region by the flow curve rather than a tangent modulus, and because there was no significant difference between the results generated by either material card without the strain rate effect. A sample of pre-processor code that utilizes the Cowper-Symonds strain rate model can be seen in Appendix Four.

The same four models were again run using an impact speed of 130 mph, the only difference being that the values of *C* and *P* were now input. The resulting deformations from these models can be seen in Table 4.11.

Table 4.11 - Model deformations at 130 mph including rate effects.

Model Type	Deformation (in)
Thick Shell	0.047
2 Solid Elements	0.020
3 Solid Elements	0.020
4 Solid Elements	0.020

The inclusion of strain rate effects had a dramatic effect on the results produced by the thick shell model. Just by implementing the Cowper and Symonds model, the deformation was reduced from 0.25 to 0.047 inches. Although it was an improvement, the deformation was still higher that the experimentally measured values.

The most significant result produced with the inclusion of the strain rate model was the fact that the two, three, and four solid element models produced the same deformation, and that deformation was very close to the measured value of 0.024 inches. Since all three of these models produced the same deformation, any one of them could be considered the converged model, but it would have to be based on something other than deformation alone. After reviewing the low speed impact strain response data and comparing the rebound velocities from the model and experiment, it was concluded that the four solid element model was the most accurate model used. (The calculated BBS for the low speed impact finite element model was 90.81 mph, and the experimental BBS was 90.04 mph.) Additional models were run with five and six elements thru the wall thickness and had comparable results, so the four element model was not only considered the most accurate, but the converged model as well. The deformation profile for the four element model was compared with a 130 mph impact and can be seen in

Figure 4.25. As expected, the profile generated by the finite element simulation was more symmetric about the center of the dent than the experimental result. This may be further indication of manufacturing variations in the diameter of the test bats.

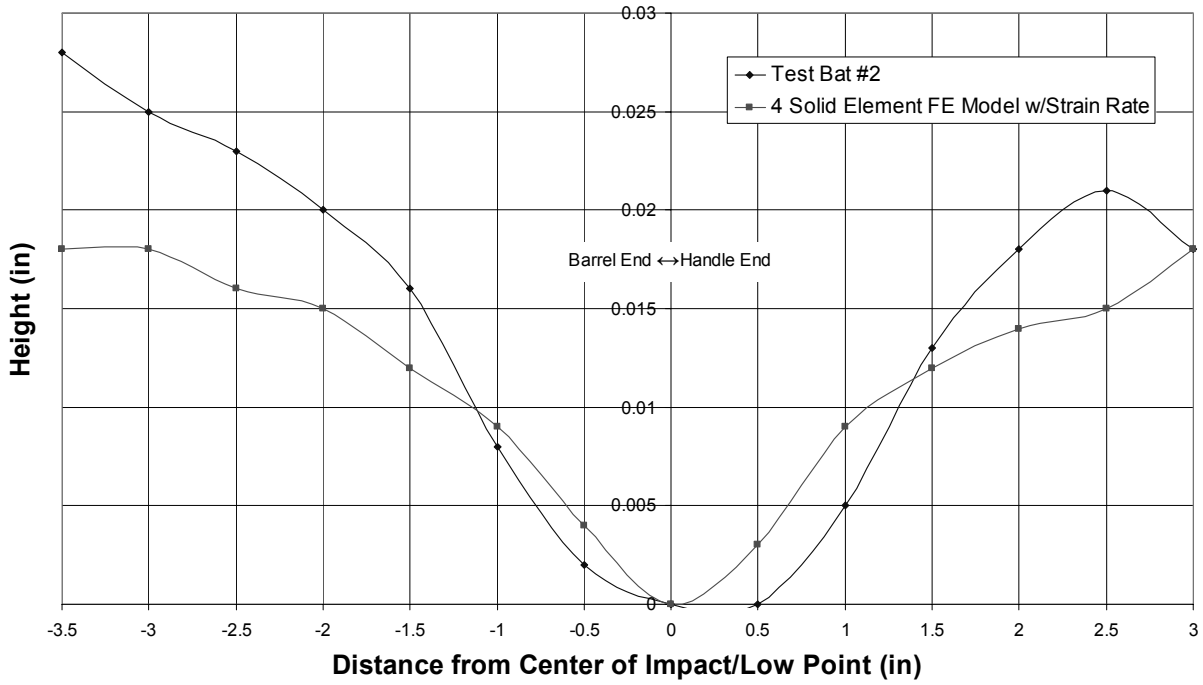

Figure 4.25 - Dent profile comparison for a 130 mph impact.

With a model that showed good correlation based on deformation, strain response, and performance at 130 mph, it was then used at 90, 100, 110, and 120 mph for comparison as well. This comparison can be seen in Table 4.12.

Table 4.12 - Deformation comparison using 4 solid element model.

Impact Speed (mph)	4 Solid Element Model (in)	Experimental (in)	Difference (in)
90	0.004	0.002	0.002
100	0.006	0.006	0
110	0.010	0.009	0.001
120	0.014	0.015	-0.001

Again, the models run at these various speeds showed good correlation and the results differed by no more than 0.002 inches from the experimental values. With the 90 mph relative

impact speed, the deformation was so small that it would be undetectable without the use of some precise measuring tool. So, it was shown here that the bat can dent from one impact with a relative impact speed of 90 mph, but it may only become noticeable to the player after multiple impacts at the same location on the bat.

4.8 Summary

Multiple finite element models were developed for this research using different element types and material hardening models. A bat model was developed that could accurately describe the deformation produced during impact with a softball. Based on the measured deformation, low speed strain response, and ball rebound velocity, a bat model consisting of four solid elements thru the thickness in the impact region was concluded to be the most sufficient of the models used.

Strain rate effects were explored in addition to hardening laws and they had a significant effect on the resulting deformations. A rather simple strain rate model was implemented in the finite element models which scales the yield strength of the material as a function of strain rate.

In addition, not only was it shown that the finite element models correlated well over a range of speeds, the relative impact speed at which a bat began to dent was shown to be 90 mph.

REFERENCES

4.1 Suchy, J. Hillerich & Bradsbury (Louisville Slugger). *Private Communication*. December, 2005.

4.2 *LS-DYNA Theoretical Manual*. Version 970. Livermore Software Technology Corporation. April 2003.

4.3 Cruz, C.M. *Characterizing Softball Bat Modifications and Their Resulting Performance Effects*. Unpublished MS Thesis, Washington State University, May 2005.

4.4 Cofer, W. Washington State University. *Private Communication.* May, 2006.

4.5 ASTM F 2219-05. *Standard Test Methods for Measuring High-Speed Bat Performance*. West Conshohocken, Pa. 2005.

4.6 Beer, Johnston, DeWolf. Mechanics of Materials. Third Edition. McGraw-Hill: San Francisco. 2001. ISBN: 0-07-365935-5

4.7 *LS-DYNA Keyword User's Manual*. Version 970. Livermore Software Technology Corporation. April 2003.

4.8 Customer Service Representative. Livermore Software Technology Corporation (LSTC). *Private Communication*. May, 2006.

4.9 Stranart, J.C. *Mechanically Induced Residual Stresses: Modeling and Characterization*. Ph.D. Thesis, University of Toronto, 2000.

CHAPTER FIVE

- SUMMARY -

5.1 Review

The work presented here set out to accurately model and predict the plastic deformation a single wall aluminum bat undergoes during an impact with a softball at various relative impact speeds.

5.2 Ball characterization and modeling

A speed correlation was successfully developed to compare the deformation of a polyurethane core softball impacting a solid rigid cylinder, and a hollow cylinder that was free to recoil. Utilizing a high speed ball cannon, dynamic stiffness experimentation was performed over a range of impact speeds and the dynamic stiffness and COR for a specific make and model of ball was calculated. A viscoelastic ball model was developed in the finite element modeling program, LS-DYNA, and the material properties of the ball were adjusted so as to "tune" the ball to these experimental results at the desired impact speed. This method of tuning the performance of the ball model proved to be very successful, and was necessary prior to doing any bat-ball collision modeling.

5.3 Bat modeling and experimental comparison

Again using LS-DYNA, a single wall aluminum bat was successfully modeled using one or two different element types. These models were successfully calibrated to the bat they were modeled after based on their weight, length, MOI, and center of gravity. For all of the models generated, they were within 1% of all of these calibration variables.

A low speed impact strain experiment was performed to further verify the ball tuning procedure and bat calibration. An identical bat was instrumented at three different locations with

strain gages and impacted at a speed too low to dent the bat. The strain response at these three different locations was compared to the various bat model types.

Identical bats were then impacted at higher speeds and their deformations were measured and compared to the numerical simulations. Multiple element formulations and meshes were used and compared. A simple strain rate formulation was used to take into account the high strain rate effects that took place during impact. The inclusion of strain rate effects had a dramatic effect on the resulting deformation, most noticeably with the thick shell model. Although there was significant improvement with the results generated for the thick shell model, the deformations were still too high as compared to the experimental values. The same strain rate model was then used for the solid element models and good correlation was achieved. Based on the measured deformations, preliminary performance numbers, and the low speed impact strain results, the most accurate solid element bat model was chosen out of the three models considered. The selected model consisted of both thick shell elements and solid elements, with four solid elements thru the wall thickness in the impact region. The deformations produced by this bat model were within ± 0.004 inches of the experimental value for every impact speed.

5.4 Future work

The work performed here was successful at predicting not only performance, but more importantly durability. In the course of this investigation, there were multiple issues that were brought up but were unable to be answered in the scope of this work.

It was shown that strain rate effects had a significant impact on the resulting model deformations, but one item that was never addressed was temperature effects. For high strain rates, greater than one strain/s, adiabatic heating occurs within the material and increases the

amount of plasticity/deformation [5.1]. Recalling that the calculated effective strain rate at the instant of impact for a relative speed of 130 mph was over 1100 strain/s, this may explain why the predicted deformation of 0.020 inches was less than the experimental values of 0.024 and 0.031 inches. The magnitude of the temperature effect at this strain rate was unknown, but impacts at lower relative impact speeds showed better correlation presumably because of the lower strain rates and thus lower temperature effects.

A material model within LS-DYNA that may suit this work well and account for temperature effects is material model #51, *MAT_BAMMAN. This material model assumes adiabatic temperature change at high strain rate deformations and makes the assumption that 90-95% of the plastic work is dissipated as heat [5.2]. Determining the information necessary to implement this material model was outside the scope of this work. Another material model, based on the Johnson-Cook constitutive model, is material model #15, *MAT_JOHNSON_COOK. This model can be used for problems where the strain rates vary over a large range and adiabatic temperature increases due to plastic heating cause material softening [5.2]. This model appeared much simpler than material model #51.

Single wall aluminum bats tend to be lower performing as compared to a multi-wall bat and aren't used nearly as much, so it would seem natural to continue this research in the area of multi-wall bats.

REFERENCES

5.1 Field, D. Washington State University. *Private Communication.* June, 2006.

5.2 *LS-DYNA Theoretical Manual*. Version 970. Livermore Software Technology Corporation. April 2003.

APPENDIX ONE

Viscoelastic ball property variations (Worth ball)

Table A1.1 - Ball tuning data for the Worth softball.

Ball Speed (mph)	Specific weight ($lb \cdot s^2/in$)	Mass (oz)	Bulk Modulus (psi)	G_0 (psi)	G_∞ (psi)	β (Hz)	COR	Y-Force (lb)	DYN Stiffness (lb/in)	Note
77.6	0.000038	6.745	8.0x10^5	28000	1520	66000	0.385	3942	7630	
77.6	0.000038	6.745	8.0x10^5	28000	1500	66000	0.382	3929	7579	
77.6	0.000038	6.745	8.0x10^5	28000	1540	66000	0.387	3955	7680	
77.6	0.000038	6.745	8.0x10^5	28000	1530	66000	0.386	3949	7654	
77.6	**0.000038**	**6.745**	**8.0x10^5**	**28000**	**1590**	**66000**	**0.393**	**3993**	**7827**	
77.6	0.000038	6.745	8.0x10^5	28000	1580	66000	0.392	3984	7790	
86.2	0.000038	6.745	8.0x10^5	28000	1480	68000	0.378	4415	7758	
86.2	0.000038	6.745	8.0x10^5	28000	1480	67000	0.375	4437	7835	
86.2	0.000038	6.745	8.0x10^5	28000	1480	70000	0.386	4373	7611	
86.2	0.000038	6.745	8.0x10^5	28000	1480	72000	0.393	4351	7535	
86.2	0.000038	6.745	8.0x10^5	28000	1480	62000	0.351	4557	8265	
86.2	0.000038	6.745	8.0x10^5	28000	1480	60000	0.349	4608	8450	
86.2	0.000038	6.745	8.0x10^5	28000	1500	66000	0.374	4475	7970	
86.2	**0.000038**	**6.745**	**8.0x10^5**	**28000**	**1520**	**66000**	**0.377**	**4491**	**8026**	
86.2	0.000038	6.745	8.0x10^5	28000	1520	65000	0.373	4514	8109	
86.2	0.000038	6.745	8.0x10^5	28000	1520	64000	0.369	4538	8195	
94.8	0.000038	6.745	2.0x10^7	28000	1700	68000	0.371	5281	9175	Nodal Penetrations
94.8	0.000038	6.745	3.0x10^7	28000	1800	68000	0.379	5381	9525	Nodal Penetrations
94.8	0.000038	6.745	1.5x10^7	28000	1600	68000	0.363	5176	8812	Nodal Penetrations
94.8	0.000038	6.745	1.5x10^7	28000	1650	68000	0.369	5218	8957	Nodal Penetrations
94.8	0.000038	6.745	1.0x10^7	28000	1500	68000	0.355	5060	8421	Nodal Penetrations
94.8	0.000038	6.745	1.0x10^7	28000	1400	68000	0.342	4969	8120	Nodal Penetrations
94.8	0.000038	6.745	7.5x10^6	28000	1400	68000	0.344	4961	8094	
94.8	0.000038	6.745	7.5x10^6	28000	1450	68000	0.351	5001	8227	
94.8	0.000038	6.745	4.0x10^6	28000	1500	68000	0.355	4959	8088	
94.8	0.000038	6.745	4.0x10^6	28000	1400	68000	0.349	4915	7947	
94.8	0.000038	6.745	3.0x10^6	28000	1500	68000	0.364	5007	8247	
94.8	0.000038	6.745	4.0x10^6	28000	1500	68000	0.361	5002	8229	
94.8	0.000038	6.745	2.0x10^6	28000	1500	68000	0.367	5007	8247	
94.8	0.000038	6.745	1.8x10^6	28000	1480	68000	0.365	5002	8229	
94.8	0.000038	6.745	1.0x10^6	28000	1470	68000	0.368	4876	7820	
94.8	0.000038	6.745	1.0x10^6	28000	1480	68000	0.369	4986	8176	
94.8	**0.000038**	**6.745**	**8.0x10^5**	**28000**	**1480**	**68000**	**0.371**	**5001**	**8228**	
94.8	0.000038	6.745	9.0x10^5	28000	1480	68000	0.37	5013	8265	
103.4	0.000038	6.745	8.0x10^5	28000	1480	68000	0.364	5627	8752	
103.4	0.000038	6.745	8.0x10^7	28000	1350	68000	0.367	5649	8819	
103.4	0.000038	6.745	8.0x10^5	28000	1350	68000	0.347	5479	8296	
103.4	0.000038	6.745	7.0x10^5	28000	1350	68000	0.347	5509	8389	

103.4	0.000038	6.745	6.0x10^5	28000	1350	68000	0.349	5520	8422	
103.4	0.000038	6.745	5.0x10^5	28000	1350	68000	0.35	5538	8477	
103.4	0.000038	6.745	3.0x10^5	28000	1300	68000	0.348	5504	8371	
103.4	0.000038	6.745	2.0x10^5	28000	1300	68000	0.353	5543	8493	
103.4	0.000038	6.745	7.0x10^5	28000	1350	65000	0.337	5559	8540	
103.4	0.000038	6.745	7.0x10^5	28000	1450	65000	0.351	5654	8836	
103.4	0.000038	6.745	7.0x10^5	28000	1350	71000	0.358	5457	8230	
103.4	0.000038	6.745	7.0x10^5	28000	1500	71000	0.377	5613	8709	
103.4	**0.000038**	**6.745**	**7.0x10^5**	**28000**	**1400**	**71000**	**0.365**	**5510**	**8390**	
103.4	0.000038	6.745	7.0x10^5	28000	1450	71000	0.371	5562	8550	

112.0	0.000038	6.745	7.0x10^5	28000	1800	71000	0.406	6619	10318	
112.0	0.000038	6.745	7.0x10^5	28000	1900	71000	0.417	6742	10703	
112.0	0.000038	6.745	7.0x10^5	28000	1200	71000	0.33	5945	8323	
112.0	0.000038	6.745	7.0x10^5	28000	1300	71000	0.344	6068	8671	
112.0	0.000038	6.745	7.0x10^5	28000	1200	74000	0.339	5888	8166	
112.0	0.000038	6.745	7.0x10^5	28000	1350	78000	0.337	6008	8500	
112.0	0.000038	6.745	7.0x10^5	28000	1250	78000	0.359	5879	8140	
112.0	0.000038	6.745	7.0x10^5	28000	1350	78000	0.373	6008	8502	
112.0	0.000038	6.745	7.0x10^5	28000	1300	76000	0.36	5979	8419	
112.0	0.000038	6.745	7.0x10^5	28000	1350	76000	0.367	6043	8599	
112.0	0.000038	6.745	7.0x10^5	28000	1300	75000	0.357	5998	8472	
112.0	**0.000038**	**6.745**	**7.0x10^5**	**28000**	**1300**	**74000**	**0.354**	**6015**	**8519**	

Viscoelastic ball property variations (Diamond ball)

Table A1.2 - Ball tuning data for the Diamond softball.

64.1	0.0000397	7	1.0x10^7	20000	1000	68000	0.397	2670	4942	
64.1	0.0000397	7	1.0x10^7	10000	1000	68000	0.570	2634	4807	
64.1	0.0000397	7	1.0x10^7	20000	1300	68000	0.446	2928	5942	
64.1	0.0000397	7	1.0x10^7	20000	1000	50000	0.504	2559	4539	
64.1	0.0000397	7	1.0x10^7	20000	1300	75000	0.469	2893	5801	
64.1	0.0000397	7	1.0x10^7	20000	1000	75000	0.591	2636	4816	
64.1	0.0000397	7	2.0x10^7	20000	1000	68000	0.392	2692	5023	
64.1	0.0000397	7	10000	10000	1300	23200	0.471	3196	7079	
64.1	0.0000397	7	2.0x10^7	20000	1300	68000	0.438	2915	5889	
64.1	0.0000397	7	10000	10000	1000	23200	0.410	3010	6279	
64.1	0.0000397	7	2.0x10^7	20000	1000	23200	0.174	3854	10295	
64.1	0.0000397	7	10000	15000	1000	23200	0.324	3352	7787	
64.1	0.0000397	7	10000	12500	1000	23200	0.359	3208	7133	
64.1	0.0000397	7	9000	12500	1000	23200	0.367	3177	6996	
64.1	0.0000397	7	10000	11250	1200	23200	0.426	3220	7188	
64.1	0.0000397	7	10000	11250	1000	26000	0.402	3002	6247	
64.1	0.0000397	7	11000	11250	1200	23200	0.421	3239	7273	
64.1	0.0000397	7	12000	11250	1200	23200	0.417	3227	7219	
64.1	0.0000397	7	13000	11250	1200	23200	0.413	3198	7088	
64.1	0.0000397	7	13000	12250	1200	23200	0.392	3261	7370	
64.1	0.0000397	7	12500	12250	1200	23200	0.395	3261	7370	
64.1	0.0000397	7	12500	12750	1200	23200	0.385	3296	7529	
64.1	0.0000397	7	12250	12250	1200	23200	0.395	3259	7361	Nodal Penetrations
64.1	0.0000397	7	12000	12250	1200	23200	0.396	3286	7484	Nodal Penetrations
64.1	0.0000397	7	2.0x10^7	25000	1200	68000	0.368	2858	5660	
64.1	0.0000397	7	2.0x10^7	25000	1100	68000	0.353	2772	5324	
64.1	0.0000397	7	2.0x10^7	25000	1400	68000	0.395	2999	6232	
64.1	0.0000397	7	2.0x10^7	23000	1400	68000	0.417	2987	6185	
64.1	0.0000397	7	2.0x10^7	25000	1700	68000	0.430	3192	7060	
64.1	0.0000397	7	2.1x10^7	25000	1700	68000	0.430	3202	7104	
64.1	0.0000397	7	3.0x10^7	25000	1700	68000	0.426	3175	6985	
64.1	0.0000397	7	2.0x10^7	27000	1600	68000	0.400	3139	6828	
64.1	0.0000397	7	2.0x10^7	27000	1700	68000	0.411	3204	7114	
64.1	**0.0000397**	**7**	**2.0x10^7**	**28000**	**1700**	**68000**	**0.402**	**3212**	**7149**	

Where "nodal penetrations" is indicated in the note column signifies that that combination of material properties caused nodes in the ball model to penetrate the outer surface of the thick shell elements used to model the impact cylinder. This phenomenon appeared to be related only to the combination of properties used.

APPENDIX TWO

Coordinate values used to model Louisville Slugger model SB806 softball bat.

Table A2.1 - Bat profile coordinate values.

Outside Profile (in)		Inside Profile (in)	
x	y	x	y
0	0.625	0.130	0.0625
0	0.664	0.130	0.648
0.710	0.673	0.582	0.649
0.741	0.404	0.627	0.264
11.0	0.404	11.0	0.264
12.0	0.416	12.0	0.259
13.0	0.448	13.0	0.271
14.0	0.507	14.0	0.278
15.0	0.579	15.0	0.385
16.0	0.664	16.0	0.505
17.0	0.766	17.0	0.633
18.0	0.884	18.0	0.763
19.0	0.966	19.0	0.856
20.0	1.028	20.0	0.924
21.0	1.087	21.0	0.984
22.0	1.125	22.0	1.032
33.5	1.125	33.5	33.5

APPENDIX THREE

Principal strain data for the flexural and hoop strain gage rosettes

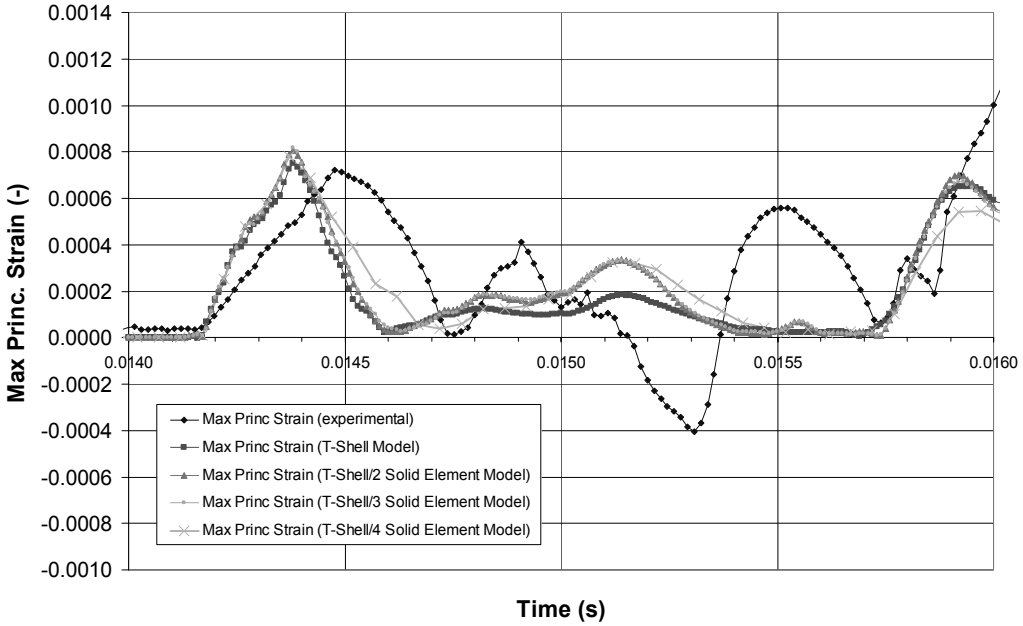

Figure A3.1 - Maximum principal flexural strain response for a low speed impact at 19 inches.

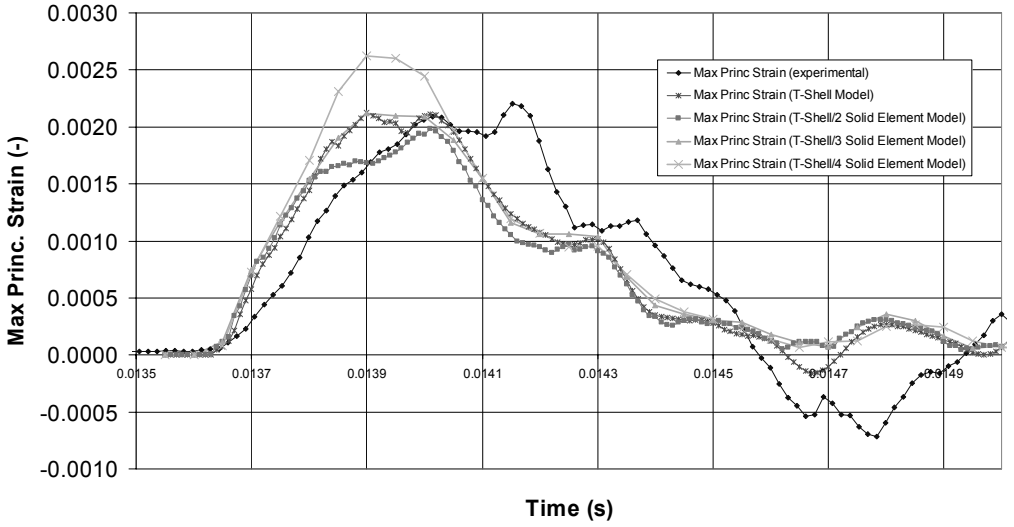

Figure A3.2 -Maximum principal hoop strain response for a low speed impact at 19 inches.

APPENDIX FOUR

Sample pre-processor input code used for modeling in LS-DYNA

Below is a portion of code used to model a 130 mph impact using the four solid element model with the inclusion of strain rate effects. Notes have been entered in italics where relevant.

```
$---+----1----+----2----+----3----+----4----+----5----+----6----+----7----+----8
$ LS-DYNA(970) DECK WRITTEN BY : eta/FEMB-PC version 28.0
$ TEMPLATE #: 20040810
$  ENGINEER :
$   PROJECT :
$     UNITS : IN, LB*SEC^2/IN, SEC, LB
$      TIME : 01:48:29 PM
$      DATE : Monday, June 05, 2006
$---+----1----+----2----+----3----+----4----+----5----+----6----+----7----+----8
*KEYWORD
$---+----1----+----2----+----3----+----4----+----5----+----6----+----7----+----8
*TITLE
LS-DYNA USER INPUT
$---+----1----+----2----+----3----+----4----+----5----+----6----+----7----+----8
$                                                                               $
$                                 CONTROL CARD                                  $
$                                                                               $
$---+----1----+----2----+----3----+----4----+----5----+----6----+----7----+----8
*CONTROL_TERMINATION
$   ENDTIM    ENDCYC     DTMIN    ENDENG    ENDMAS
    0.0045         0  0.000050       0.0       0.0
*CONTROL_TIMESTEP
$   DTINIT    TSSFAC      ISDO    TSLIMT     DT2MS      LCTM     ERODE     MS1ST
  0.000050      0.90         0       0.0       0.0         0         0         0
$   DT2MSF   DT2MSLC

$---+----1----+----2----+----3----+----4----+----5----+----6----+----7----+----8
$                                                                               $
$                           DATABASE CONTROL FOR ASCII                          $
$                                                                               $
$---+----1----+----2----+----3----+----4----+----5----+----6----+----7----+----8
*DATABASE_ELOUT
$       DT    BINARY
  0.000050         3
*DATABASE_NODOUT
$       DT    BINARY
  0.000050         3
*DATABASE_RCFORC
$       DT    BINARY
  0.000050         3
$---+----1----+----2----+----3----+----4----+----5----+----6----+----7----+----8
$                                                                               $
$                          DATABASE CONTROL FOR BINARY                          $
$                                                                               $
$---+----1----+----2----+----3----+----4----+----5----+----6----+----7----+----8
*DATABASE_BINARY_D3PLOT
$  DT/CYCL      LCDT      BEAM     NPLTC
  0.000050         0         0         0
$    IOOPT
         0
$---+----1----+----2----+----3----+----4----+----5----+----6----+----7----+----8
$                                                                               $
$                             DATABASE EXTENT CARDS                             $
$                                                                               $
$---+----1----+----2----+----3----+----4----+----5----+----6----+----7----+----8
*DATABASE_EXTENT_BINARY
$^EXTENT_1
$    NEIPH     NEIPS    MAXINT    STRFLG    SIGFLG    EPSFLG    RLTFLG    ENGFLG
         0         0         3         1         1         1         1         1
$   CMPFLG    IEVERP    BEAMIP     DCOMP      SHGE     STSSZ    N3THDT
         0         0         0         0         0         0         2
$  NINTSLD
         1
$---+----1----+----2----+----3----+----4----+----5----+----6----+----7----+----8
$                                                                               $
$                             DATABASE FORMAT CARDS                             $
$                                                                               $
$---+----1----+----2----+----3----+----4----+----5----+----6----+----7----+----8
```

```
*DATABASE_FORMAT
$    IFORM   IBINARY
         0         0
$---+----1----+----2----+----3----+----4----+----5----+----6----+----7----+----8

$                            DATABASE HISTORY CARDS
$
$---+----1----+----2----+----3----+----4----+----5----+----6----+----7----+----8
*DATABASE_HISTORY_NODE
$^HISTORY_2
$     NID1      NID2      NID3      NID4      NID5      NID6      NID7      NID8
      9589     11747     14584     14582
*DATABASE_HISTORY_SOLID
$^HISTORY_2
$     SID1      SID2      SID3      SID4      SID5      SID6      SID7      SID8
      9240      9241      9242      8979      8980      8981
$---+----1----+----2----+----3----+----4----+----5----+----6----+----7----+----8
$                                                                              $
$                                  PART CARDS                                  $
$                                                                              $
$---+----1----+----2----+----3----+----4----+----5----+----6----+----7----+----8
*PART
BAT
$      PID     SECID       MID     EOSID      HGID      GRAV    ADPOPT      TMID
         3         3         1         0         0         0         0         0
*PART
BALL
$      PID     SECID       MID     EOSID      HGID      GRAV    ADPOPT      TMID
         1         2         2         0         0         0         0         0
*PART
IMPACT SHELL
$      PID     SECID       MID     EOSID      HGID      GRAV    ADPOPT      TMID
         2         4         1         0         0         0         0         0
$---+----1----+----2----+----3----+----4----+----5----+----6----+----7----+----8
$                                                                              $
$                                SECTION CARDS                                 $
$                                                                              $
$---+----1----+----2----+----3----+----4----+----5----+----6----+----7----+----8
*SECTION_SOLID_TITLE
P-2
$    SECID    ELFORM       AET
         2         1         0
*SECTION_TSHELL_TITLE
P-3
$    SECID    ELFORM      SHRF       NIP     PROPT   QR/IRID     ICOMP
         3         1   0.83333         5       1.0         0         0
*SECTION_SOLID_TITLE
P-4
$    SECID    ELFORM       AET
         4         1         0
$---+----1----+----2----+----3----+----4----+----5----+----6----+----7----+----8
$                                                                              $
$                                MATERIAL CARDS                                $
$                                                                              $
$---+----1----+----2----+----3----+----4----+----5----+----6----+----7----+----8
*MAT_POWER_LAW_PLASTICITY_TITLE
M-1
$      MID        RO         E        PR         K         N       SRC       SRP
         1  0.0002571.0400E+07      0.30   82657.0    0.0684    1300.0       5.0
$     SIGY        VP
   58211.0       0.0
*MAT_VISCOELASTIC_TITLE
M-2
$      MID        RO      BULK        G0        GI      BETA
         2  0.000038  700000.0   28000.0    1300.0   74000.0
$---+----1----+----2----+----3----+----4----+----5----+----6----+----7----+----8
$                                                                              $
$                             SEGMENT SET CARDS                                $
$                                                                              $
$---+----1----+----2----+----3----+----4----+----5----+----6----+----7----+----8
*SET_SEGMENT_TITLE
```

Master and slave segment list is located here.

```
$---+----1----+----2----+----3----+----4----+----5----+----6----+----7----+----8
$                                                                             $
$                                NODE SET CARDS                               $
$                                                                             $
$---+----1----+----2----+----3----+----4----+----5----+----6----+----7----+----8
*SET_NODE_LIST_TITLE
```

Nodes and node set lists are located here.

```
$---+----1----+----2----+----3----+----4----+----5----+----6----+----7----+----8
$                                                                             $
$                             BOUNDARY SPC CARDS                              $
$                                                                             $
$---+----1----+----2----+----3----+----4----+----5----+----6----+----7----+----8
*BOUNDARY_SPC_SET_ID
$       ID
         1
$     NSID       CID      DOFX      DOFY      DOFZ     DOFRX     DOFRY     DOFRZ
         2         0         1         1         0         0         0         0
         2
         3         0         0         0         1         0         0         0
$---+----1----+----2----+----3----+----4----+----5----+----6----+----7----+----8
$                                                                             $
$                           INITIAL VELOCITY CARDS                            $
$                                                                             $
$---+----1----+----2----+----3----+----4----+----5----+----6----+----7----+----8
*INITIAL_VELOCITY
$     NSID    NSIDEX     BOXID    IRIGID
         1         0         0
$       VX        VY        VZ       VXR       VYR       VZR
      0.0  -2288.0       0.0       0.0       0.0       0.0
$---+----1----+----2----+----3----+----4----+----5----+----6----+----7----+----8
$                                                                             $
$                                CONTACT CARDS                                $
$                                                                             $
$---+----1----+----2----+----3----+----4----+----5----+----6----+----7----+----8
*CONTACT_SURFACE_TO_SURFACE
$^CONTACT1
$     SSID      MSID     SSTYP     MSTYP    SBOXID    MBOXID       SPR       MPR
         1         2         0         0         0         0         0         0
$       FS        FD        DC        VC       VDC    PENCHK        BT        DT
      0.0       0.0       0.0       0.0       0.0         0  0.01.0000E+20
$      SFS       SFM       SST       MST      SFST      SFMT       FSF       VSF
      1.0       1.0       0.0       0.0       1.0       1.0       1.0       1.0
$---+----1----+----2----+----3----+----4----+----5----+----6----+----7----+----8
$                                                                             $
$                               NODE INFORMATION                              $
$                                                                             $
$---+----1----+----2----+----3----+----4----+----5----+----6----+----7----+----8
*NODE
```

Node numbers and coordinates are listed here.

```
$---+----1----+----2----+----3----+----4----+----5----+----6----+----7----+----8
$                                                                             $
$                             ELEMENTS INFORMATION                            $
$                                                                             $
$---+----1----+----2----+----3----+----4----+----5----+----6----+----7----+----8
$---+----1----+----2----+----3----+----4----+----5----+----6----+----7----+----8
$                                                                             $
$                                SOLID ELEMENTS                               $
$                                                                             $
$---+----1----+----2----+----3----+----4----+----5----+----6----+----7----+----8
*ELEMENT_SOLID
```

Elements are grouped by type and their respective nodes are listed here.

```
$---+----1----+----2----+----3----+----4----+----5----+----6----+----7----+----8
*END
```